Defence Research and Development Canada
Recherche et développement pour la défense Canada

LTE Handheld Synthetic Array

Interim Report I

John Nielsen

Defence R&D Canada – Ottawa

Canada

Contract Report
DRDC Ottawa CR 2012-141
December 2012

LTE Handheld Synthetic Array

Interim Report I

John Nielsen

Prepared By:
John Nielsen
Department of Electrical Engineering
The University of Calgary
2500 University Dr., NW
Calgary, AB T2N1N4

Contract Project Manager: John Nielsen, 403-210-9704
PWGSC Contract Number: W7714-115915
CSA: Susan Watson, Defence Scientist, 613-998-2098

Defence R&D Canada – Ottawa

Contract Report
DRDC Ottawa CR 2012-141
December 2012

Scientific Authority

Original signed by Susan Watson

Susan Watson

Defence Scientist

Approved by

Original signed by Bill Katsube

Bill Katsube

Section Head, Communications and Navigation EW

Approved for release by

Original signed by Chris McMillan

Chris McMillan

Chief Scientist

This contractor report is related to intellectual property protected under Canadian patent CA2679673.

Abstract

In the LTE, a 4th-generation cellular communications standard, downlink synchronization signalling is provided via its access nodes (ANs). This downlink signalling could provide the opportunity for the user equipment (UE) to self geo-locate with no assistance from network location processing or GPS. The proposed self geo-location approach is based on the particle filter; a general method Bayesian filtering used when the statistics of the movement model and observations are non-Gaussian. The novel aspect of the work is the creation of a synthetic array as the handset is moved, and the objective of the research is to combine the LTE downlink processing with the synthetic array processing in order to extract measurements which enhance the self-geolocation result. The performance enhancement that is afforded by the synthetic array processing relative to traditional geo-location methodology will be quantified.

Résumé

Dans le domaine de la technologie d'évolution à long terme (Long Term Evolution — LTE), soit une norme de communication cellulaire de 4e génération, la signalisation de synchronisation descendante est assurée par les nœuds d'accès. La signalisation descendante pourrait permettre l'autogéolocalisation d'un équipement utilisateur, sans l'appui d'un traitement de positionnement de réseau ou d'un système de positionnement à couverture mondiale (Global Positioning System — GPS). Dans le présent rapport, on propose une approche d'autogéolocalisation qui repose sur un filtre à particules et qui constitue une méthode de filtrage générale bayésienne utilisée lorsque les statistiques d'un modèle de déplacement et d'observations ne sont pas de type gaussien. Les travaux ont revêtis un nouvel aspect, à savoir une antenne dont le réseau synthétique se développe à mesure qu'un dispositif est déplacé, et visaient à combiner le traitement descendant de la LTE et celui de l'antenne réseau synthétique, afin d'extraire des mesures qui permettraient d'améliorer l'autogéolocalisation. Dans le présent rapport, on quantifie l'amélioration du rendement obtenue par un traitement d'antenne réseau synthétique par rapport à celle obtenue par géolocalisation classique.

This page intentionally left blank.

Executive summary

LTE Handheld Synthetic Array: Interim Report I

John Nielsen; DRDC Ottawa CR 2012-141; Defence R&D Canada – Ottawa; December 2012.

Introduction or background: In the LTE, a 4th-generation cellular communications standard, downlink synchronization signalling is provided via its access nodes (ANs). This downlink signalling could provide the opportunity for the user equipment (UE) to self geo-locate with no assistance from network location processing or GPS. The proposed self geo-location approach is based on the particle filter; a general method Bayesian filtering used when the statistics of the movement model and observations are non-Gaussian. The novel aspect of the work is the creation of a synthetic array as the handset is moved, and the objective of the research is to combine the LTE downlink processing with the synthetic array processing in order to extract measurements which enhance the self-geolocation result. The performance enhancement that is afforded by the SA processing relative to traditional geo-location methodology will be quantified. The approach taken to mitigate multipath fading will be to use the particle filter into two modes; one for line of sight signals and one for non-line of sight signals, where the multipath bias will be estimated and tracked. The trajectory of the user equipment (UE) will also be tracked according to a measurement model, with sensor measurement input from a small camera, MEMS-based accelerometers and gyro devices.

Results: The LTE downlink signalling is described, and the observables that might be of use for self geo-location are identified. A description of belief map Bayesian filtering is given, which will be the generic processing supporting self geo-location; more specifically, a particle filter approach is described that takes into account the synthetic array and computer vision aspects of the sensor. The performance of the particle filter is analyzed under various theoretical scenarios such as ideal deterministic motion in 1- and 2-dimensions. There is an analysis of the circumstances under which there will be sufficient information to perform self geo-location, given the possible lack of synchronization between access nodes and between the access nodes and the UE, and given the presence of multipath propagation channels from the AN to the UE. Finally, there is an overview of the experimental hardware design for implementation of the self geo-location system.

Significance: The algorithms and methodologies described here will be the drivers for the LTE synthetic array and self geo-location demonstrator. This background research is necessary to motivate the further development of the demonstrator, and to attempt to quantify its performance under various propagation conditions.

Future plans: In the next phase of work, the LTE synthetic array processing algorithms will be further defined. If there is a demonstrable improvement in self geo-location performance in typical wireless environments provided by the LTE synthetic array, the system will be implemented in hardware, and tested.

Sommaire

LTE Handheld Synthetic Array: Interim Report I

John Nielsen ; DRDC Ottawa CR 2012-141 ; R & D pour la défense Canada – Ottawa; décembre 2012.

Introduction ou contexte : Dans le domaine de la technologie d'évolution à long terme (Long Term Evolution — LTE), soit une norme de communication cellulaire de 4^{e} génération, la signalisation de synchronisation descendante est assurée par les nœuds d'accès. La signalisation descendante pourrait permettre l'autogéolocalisation d'un équipement utilisateur, sans l'appui d'un traitement de positionnement de réseau ou d'un système de positionnement à couverture mondiale (Global Positioning System — GPS). Dans le présent rapport, on propose une approche d'autogéolocalisation qui repose sur un filtre à particules et qui constitue une méthode de filtrage générale bayésienne utilisée lorsque les statistiques d'un modèle de déplacement et d'observations ne sont pas de type gaussien. Les travaux ont revêtis un nouvel aspect, à savoir une antenne dont le réseau synthétique se développe à mesure qu'un dispositif est déplacé, et visaient à combiner le traitement descendant de la LTE et celui de l'antenne réseau synthétique, afin d'extraire des mesures qui permettraient d'améliorer l'autogéolocalisation. Dans le présent rapport, on quantifie l'amélioration du rendement obtenue par un traitement d'antenne réseau synthétique par rapport à celle obtenue par géolocalisation classique. En vue d'atténuer l'affaiblissement multitrajets, on a adopté une approche qui exploite le filtre à particules en deux modes : l'un destiné aux signaux de visée directe et l'autre, aux signaux sans ligne de vue (dont les biais multitrajets ont été estimés et suivis). On a également suivi la trajectoire de l'équipement utilisateur conformément à un modèle de mesure, à l'aide de données de mesures de capteur fournies par une petite caméra, des accéléromètres reposant sur un système microélectromécanique et des dispositifs gyroscopiques.

Résultats : Dans le présent rapport, on brosse un tableau de la signalisation descendante de la LTE, des variables observables et exploitables aux fins de géolocalisation et du filtrage bayésien d'un graphe de croyance qui constituera le traitement général appuyant l'autogéolocalisation. On y décrit plus particulièrement une approche qui repose sur un filtre à particules et tient compte des aspects du capteur relatifs à l'antenne réseau synthétique et à la vision artificielle du capteur. On y analyse le rendement du filtre à particules selon divers scénarios hypothétiques, comme un déplacement déterministe idéal unidimensionnel et bidimensionnel. Le rapport comporte une analyse des circonstances qui fournissent suffisamment de données pour permettre l'autogéolocalisation, compte tenu du manque de synchronisation possible entre les nœuds d'accès et entre ceux-ci et un équipement utilisateur, ainsi que de la présence de canaux de propagation multitrajets entre les nœuds d'accès et un équipement utilisateur. Enfin, on y donne un aperçu du matériel expérimental destiné à la mise en œuvre du système d'autogéolocalisation.

Importance : Le démonstrateur de l'antenne réseau synthétique de LTE et de l'autogéolocalisation reposeront sur les algorithmes et les approches décrites dans le présent rapport. Les présentes recherches préliminaires permettront de perfectionner le démonstrateur et de tenter de quantifier son rendement dans différentes conditions de propagation.

Perspectives : Au cours de la prochaine étape des travaux, on définira davantage les algorithmes de traitement de l'antenne réseau synthétique. Si le système présente une amélioration mesurable du rendement de l'autogéolocalisation dans un environnement sans fil fourni par l'antenne réseau synthétique de LTE, il sera intégré à du matériel, puis mis à l'essai.

This page intentionally left blank.

Table of contents

List of figures

List of tables

1 Overview

This document is the first of two interim reports which outlines the research that was conducted during the first phase of the contract spanning January 2012 to March 2012. This first phase report was submitted in accordance with the deliverable due date of March 31, 2012.

In a recent issue of Bloomberg Businessweek (Jan 16, 2012) a technology article was featured that outlined the race to have "Google Maps" extended to indoor locations, malls, airports, arenas and so forth. Smartphone manufactures such as Apple, Nokia, Samsung and RIM and asic manufactures such as Qualcomm and Broadcom are scrambling to achieve processing that will provide sufficient resolution such that the detail of these available maps will be useful to the smartphone user. Such technology has obvious application for military based personal and asset location. Differences will be that the wireless signals of opportunity that can be used for such positioning are perhaps uncooperative with poorly defined source locations and no guarantee of being accurately synchronized. The overall objective of the research is the enhancement of signal processing algorithms for estimating the location of a mobile station (MS) or user equipment (UE) based on wireless signalling. The wireless signalling is assumed to be sourced from 4G Long Term Integration (LTE) access nodes (AN) which are primarily used for mobile data and voice communications. The downlink signalling is specifically exploited, as the desire is for the UE processing to be capable of stand alone "self geo-location" (SGL). This implies that the network location processing or assistance is not involved. Further it is not assumed that the UE be registered with the LTE network but rather that it exploits LTE downlink signals of opportunity for the location estimate. Hence the relevant signalling will come from the LTE downlink reference signals (RS) that are synchronised across the LTE network of AN's. The signal structure of the RS's are assumed to be known by the UE as well as the location of the AN's. In the optional third phase of this contract the network assisted location can potentially be addressed. However, the work proposed herein assumes that SGL implies specifically UE based location processing.

The processing and analysis used in this research will be based on the particle filter (PF) which is a very general method of Bayesian filtering that is particularly advantageous to use when arbitrary constraints are imposes with non-Gaussian dynamics and observations. This will aptly account for the smoothness in the UE trajectory that can be assumed. A novel element of the research is the exploitation of the synthetic array (SA) in which the UE captures a continuous snapshot of the LTE wireless signals as the handset is moved. If the evolving carrier phase of the LTE snapshot is available then various forms of beamforming processing are possible. If the carrier phase is more random then diversity gains are possible as developed in previous works. Regardless the concept of a continuous time snapshot is of value and will be exploited in the second phase of this contract. Diversity can be further enhanced by arbitrary changes in antenna orientation as the signal is being captured. Furthermore, in scenarios where the propagation is characterized by line of sight (LOS) conditions, then the SA processing provides a means of achieving coherent beamforming. Consequently the bearing angle of the LTE AN downlink signal can be estimated relative to the trajectory of the moving UE. Another possibility is the relative difference in the bearings of two AN's can be estimated which is of significance in terms of SGL estimation.

More specifically then, the objective of this research is to combine the LTE downlink processing of the UE with that of the SA processing for the purpose of extracting observables that enhance the performance of SGL. The SA specifically designed for the LTE downlink signalling will be denoted as the LTESA. Associated with the stated main objective is that of quantifying the performance enhancement of SGL that is afforded by the LTESA processing relative to the conventional SGL processing based on a stationary UE.

The research will be conducted in three phases as per the proposal which will be expanded in further detail in the following sections. Phase I will consist of a thorough analysis of the LTE standard such that the relevant attributes of the downlink signal that affect the SGL processing algorithm design and choices can be assessed. Phase II will involve the development of the LTESA processing algorithms for various propagation conditions and the experimental verification thereof. Phase III is an optional component of the research that will be completed if there is a demonstrable improvement of the SGL performance in typical wireless propagation environments provided by the LTESA.

The primary objective with this phase is to develop a sufficiently detailed background understanding of the LTE downlink signalling that is suitable for the UE SGL processing. Hence the various configurations of the RS (resource signal) formats need to be thoroughly understood.

An outline of the phase I interim report is as follows:

2 LTE downlink signalling – a description of the synchronized and deterministic downlink signalling will be described. The outcome of this section will be the observables that can be inferred from the LTE downlink signals from the AN's at the UE.

3. SGL methodologies – a description of the belief map Bayesian filtering will be given as a primary means of generating generic processing for supporting SGL. This is also useful for the eventual simulation and analysis of the SGL processing. A particle filter (PF) approach will be described in detail that accommodates all of the standard methods of SGL as well as incorporating the SA and computer vision (CV) as well. The PF will be expanded to include the processing of the synthetic array and the computer vision. This will form the basis of the thrust for phase II.

4. CV Observables – The short term trajectory estimation will be provided by the Computer Vision (CV) based observables. Such observables will be used the augment the LTE observables. As well a CV system is necessary to characterize the performance of the SA. The outcome of this section will be the augmentation of the PF with the CV observables.

5. Experimental HW design – Elements of the HW system for testing and processing development were completed during this phase. The bulk of the experimental work will occur in phase II.

2 LTE Downlink Signalling

In this section we intend to expound on the details of the downlink of an LTE system. That is the link between eNodeB to UE. For convenience we also denote the eNodeB as the access node or AN. LTE also known as *evolved universal terrestrial radio access* (E-UTRA), Super 3G (S3G) has differentiated itself from WCDMA by using Orthogonal Frequency Division Multiplexing (OFDM) as a way to transfer data for its downlink scheme and Single Carrier FDMA (Frequency Division Multiple Access) for its uplink scheme.

LTE is designed to transfer packets and should satisfy the following specifications.

100 Mbit/s for downlink and 50Mbit/s for uplink

Optimized operation for mobility of 0 to 15 Km/h and high performance between 15Km/h to 120 Km/h and connected at speeds above 120 Km/h till 350 Km/h.

Bandwidths of 1.5 to 20 MHz depending

Support of both FDD (Frequency Division Duplexing) and TDD (Time division Duplexing)

User latency of 5ms and control latency of 100 ms going from idle to active

Support for 20 users at 5MHz bandwidth and 400 users at higher bandwidths.

The difference between the LTE and prior standards is the reduction of latency and new modulation scheme that has improved the performance. LTE has reduced the interfaces between the core network and the base station which is also called eNodeB. In LTE eNodeB does the both jobs of mobility management and radio resource management which reduce the latency between these tasks. Figure 2-1 shows the structure of LTE architecture.

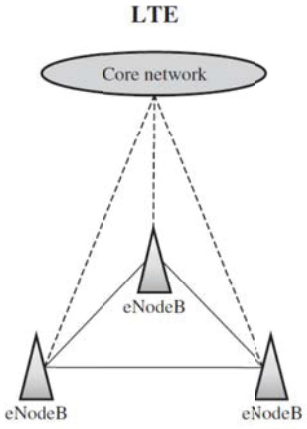

Figure 1: LTE architecture

LTE is divided into user plane protocols and control protocols which all reside between the eNodeB and the UE (user end) or as it called the mobile terminal (also User Equipment). These protocols are shown in figure 2-2.

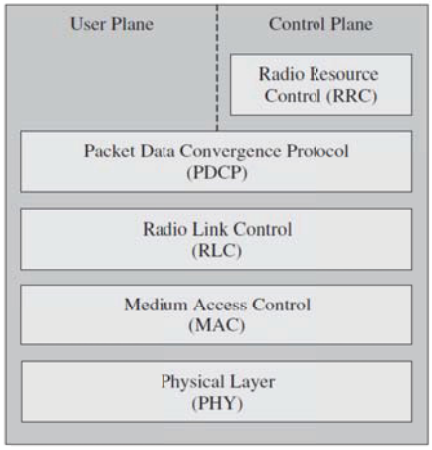

Figure 2: User plane and Control plane protocols

The protocol layer we are interested in is the Physical layer which is all the modulation; coding and antenna schemes are located. LTE uses OFDM with cyclic prefix. OFDM is a type of multi-carrier transmission where narrowband channels overlap each other but remain orthogonal due to their unique orthogonal basis function. Figure 2-3 shows an OFDM carrier division. Figure 2-4 shows LTE block diagram.

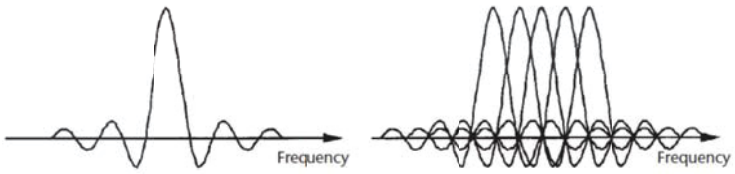

Figure 3: OFDM carrier spectrum

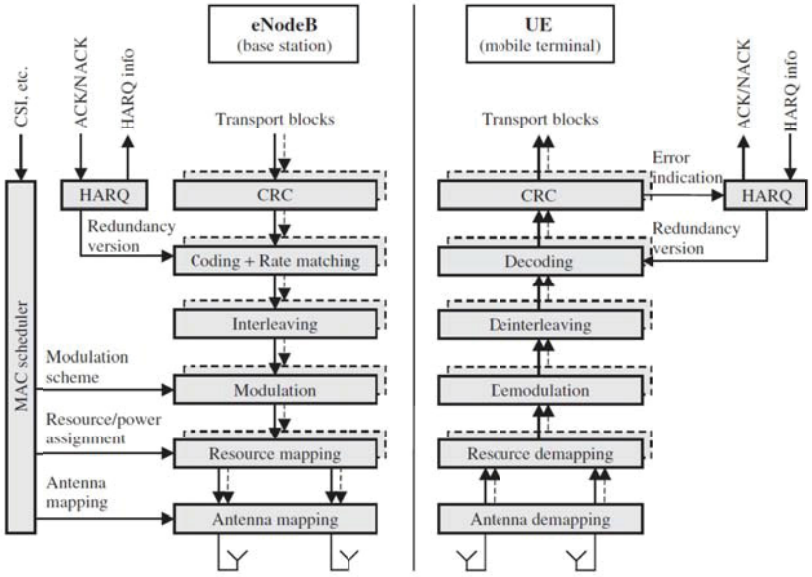

Figure 4: LTE Physical layer block diagram

The two important blocks that we are interested in are the resource mapping and the antenna port blocks. Resource mapping has the task to assign symbols to the carriers based on the quality of the particular channel. LTE transmission is based on radio frames. LTE has a 10 ms radio frame which is divided into 10 sub-frame and each 1 ms sub-frame is divide into 2 slots of 0.5 ms. Slot is the smallest unit of LTE radio structure with 0.5 ms time duration each slot contains 6 or 7 symbols for normal and extended cyclic prefix consequently. The length of cyclic prefix is related to the channel length and the symbol number. A larger CP is intended in rural areas and the shorter CP in urban areas where the channel length is smaller and higher throughput without a loss of signal orthogonality is required.

OFDM symbols have either normal or extended cyclic prefix. In case of a normal CP, the CP length is equal to 5.2 us for the first symbol and 4.7 us for the remaining symbols. A CP length of 17.7 us is used for the extended CP which as mentioned before is used in areas where there is a long delay spread. OFDM symbol duration without a guard interval has a duration of 66.7 us. Figure 2-5. Shows LTE radio frame and the mentioned timings.

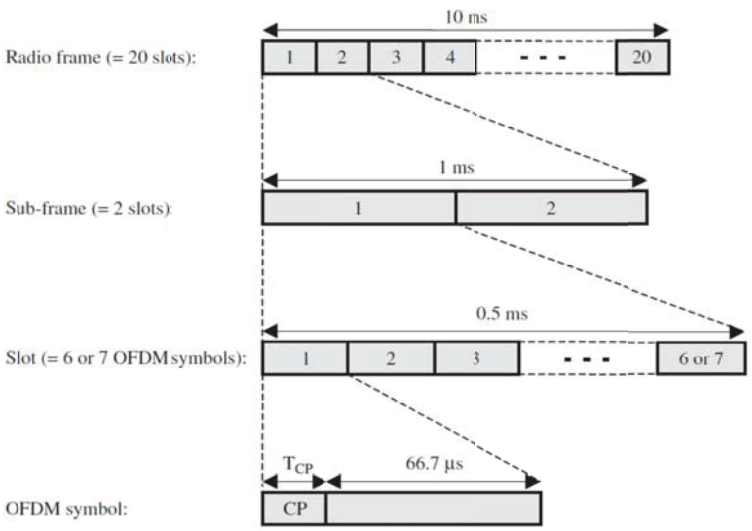

Figure 5: LTE radio frame

LTE supports channel bandwidth from 1.4 to 20 MHz and subsequently subcarrier sizes from 128 to 2048 carriers. Sampling time of it has been carefully placed at multiple of 3.84 MHz at 30.72 MHz for back compatibility with legacy standard like UMTS and EDGE.

The subcarrier frequency space is divided into smaller units named as resource block. Each resource block consists of 12 carriers and 2 slots which can virtually be shown in time and frequency domain. A resource block consists of 84 resource elements for normal cyclic prefix and 72 resource elements for extended cyclic prefix. A resource element is a symbol transmitted on a single carrier on an OFDM symbol. Carriers in a resource block are spaced 15 KHz apart, therefore an RB spans the bandwidth of 180 KHz.

In order to obtain channel information for coherent detection and synchronization some carrier-symbol cells of the resource block is dedicated to reference signals. These reference signals are either Pilots, which are known symbols transmitted at certain RE's or dedicated channels for synchronization such as PSS (primary sync. series) and SSS (secondary sync. series) channels. Pilots are inserted in the RB depending on what antenna port is being used. In a simple single antenna scheme pilots is placed in first and third last OFDM symbol. Pilots are placed 6 carriers apart in frequency domain and 3 symbols apart in time domain. The simplest channel estimator scheme needs to interpolate in time and frequency domain to obtain the channel response for the entire resource block. Obviously more sophisticated methods are used when mobility is involved.

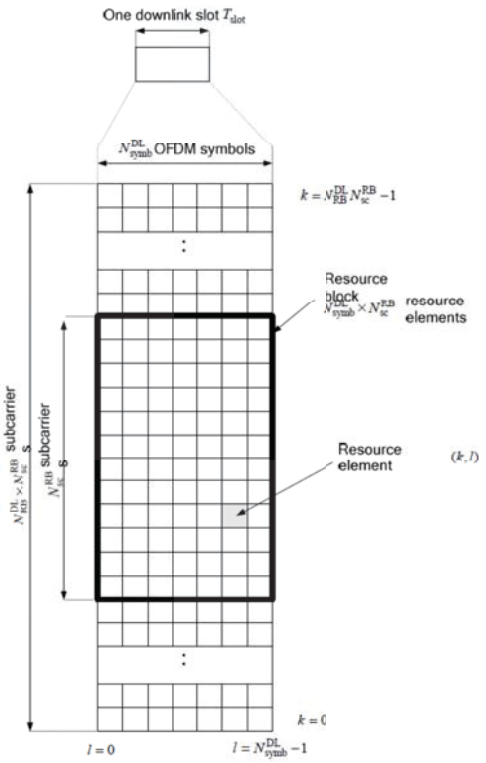

Figure 6: Resource block (RB) and Resource Element (RE)

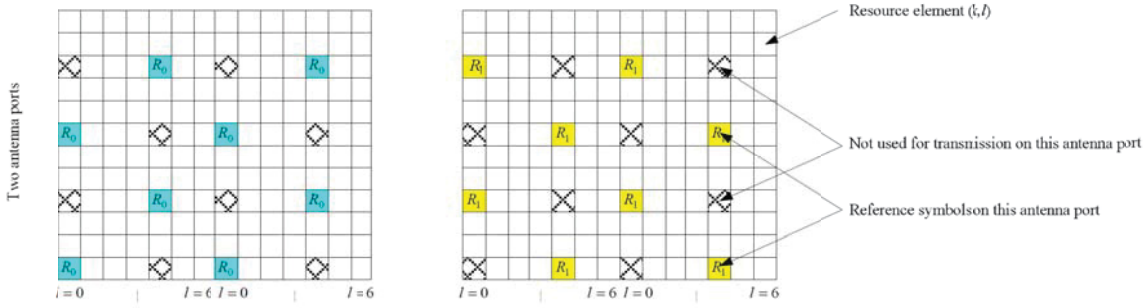

Figure 7: Resource element and pilot positioning in CP for two antenna ports

In a multiple antenna scheme pilots are positioned such that they are orthogonal to other antenna ports. A channel estimation algorithm requires calculating the channel information for each of the antennas separately. In a multiple antenna scheme, the resource elements occupied for the pilot in one antenna port is empty in another antenna port RE to avoid interference with each other. Figure 2-7. Show the pilot positioning for a normal CP scheme in two antenna ports. In the channel estimation section we will show how the pilots are used for estimating the channel

information. Before we proceed into detail physical layer algorithms we need to investigate the procedures in LTE to know how UE and base station communicate.

2.1 Important physical layer procedures

The most important procedures that UE uses to initiate a communication with the eNodeB are:

Cell search

Random Access procedures

2.1.1 Cell search

Cell search is the method that UE uses to find a suitable base station to communicate with. UE identifies the cell which is associated with the base station via detecting the primary and secondary synchronization signals that are transmitted from the base station on regular basis. When discussing the synchronization procedures we will examine the cell search procedure in more detail.

What important for us is that cell search procedure is also utilized to search neighbouring cells for handover procedures. Resource have to be allocated at specific time to minimize interference with cells own resources.

2.1.2 Random access procedures

UE requests resources from base station using the RA channels. This would be important as if utilized extra information would be available for the UE to estimate its position. In order to initiate such requests the user terminal needs to send known preambles which are the Zadoff-Chu sequences. These sequences have the characteristic that they build an orthogonal basis each and when transmitted together are separable. As long as they are not repeated by different users there would be no collision. When base station detects the preamble or in other words the RA procedure request, the terminal can send further information and initiate the channel. Random access channels can be a part of standalone locationing algorithm as it utilizes the eNodeB and UE alone.

2.2 LTE Physical layer characteristics

In order to conduct the experiments as realistic to the LTE physical characteristics we briefly outline the LTE characteristics.

2.2.1 Supported BW

LTE supports the following bandwidths. Each bandwidth then would have specific RB's that it can support which in turn dictates the number of maximum pilots available to each UE. Table 2-1. Shows the available bandwidth.

Channel bandwidth (MHz)	1.4	1.6	3	3.2	5	10	15	20
Number of resource blocks with FDD	6	N/A	15	N/A	25	50	75	100
Number of resource blocks with TDD	6	7	15	16	25	50	75	100

Table 1. Supported Bandwidths

2.2.2 LTE Duplex

LTE transmits in FDD or TDD full and half duplex method. E-UTRA TDD band 40 is the band that occupies the ISM band and could be utilized for tests. This band occupies 2300 to 2400 MHz.

2.2.3 LTE spectral mask

FCC guidelines for the LTE transmission masks are shown in Figure 8. It is suggested that tighter requirements be placed for locationing purposes to reduce interference from neighbouring cells. Possibly this should go with better pulse shaped OFDM transmitter and receivers for locationing purposes. This is feasible if non-commercial radio is intended.

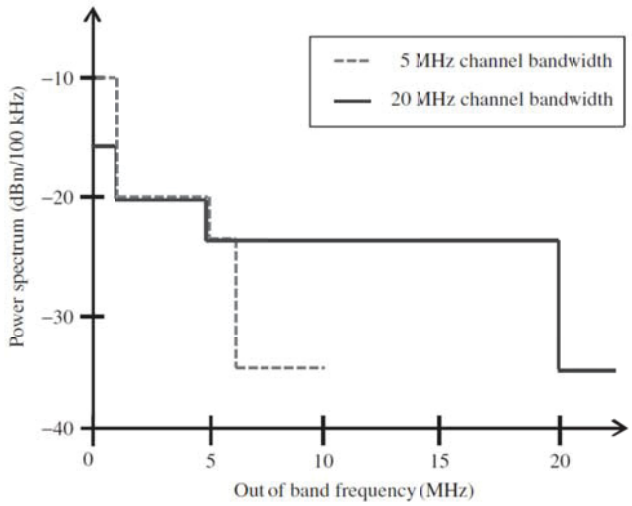

Figure 8: LTE TX spectral mask

OFDM have succeeded as a high data rate transmission scheme on the fact that it combines high data rates with low symbol period time. Unlike a single carrier transmission where data rate is inversely proportional to the symbol duration T_s, therefore susceptible to channel delay spread T_d, OFDM by transferring serial data symbols in parallel increases he symbol time in expense of slight frequency bandwidth increase.

In OFDM stream of data is first converted from serial to a parallel stream and then transmitted onto each carrier. The transformation of serial stream into N parallel data streams increases the symbol time, which is the time it takes for one symbol to transmit, by a factor of N. Figure 9. shows a typical OFDM transmission scheme.

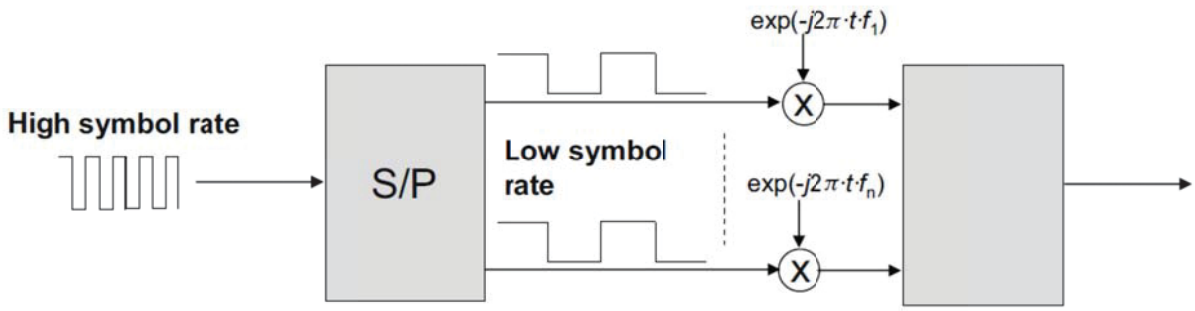

Figure 9: OFDM transmission

As seen in Figure 2-9 each symbol is transmitted via one carrier. In an OFDM system total number of carriers is always more than the transmitted symbols. Some of these extra carriers are used as guard bands and some used to transmit reference symbols. Figure 2-10 shows an OFDM transmitter and receiver.

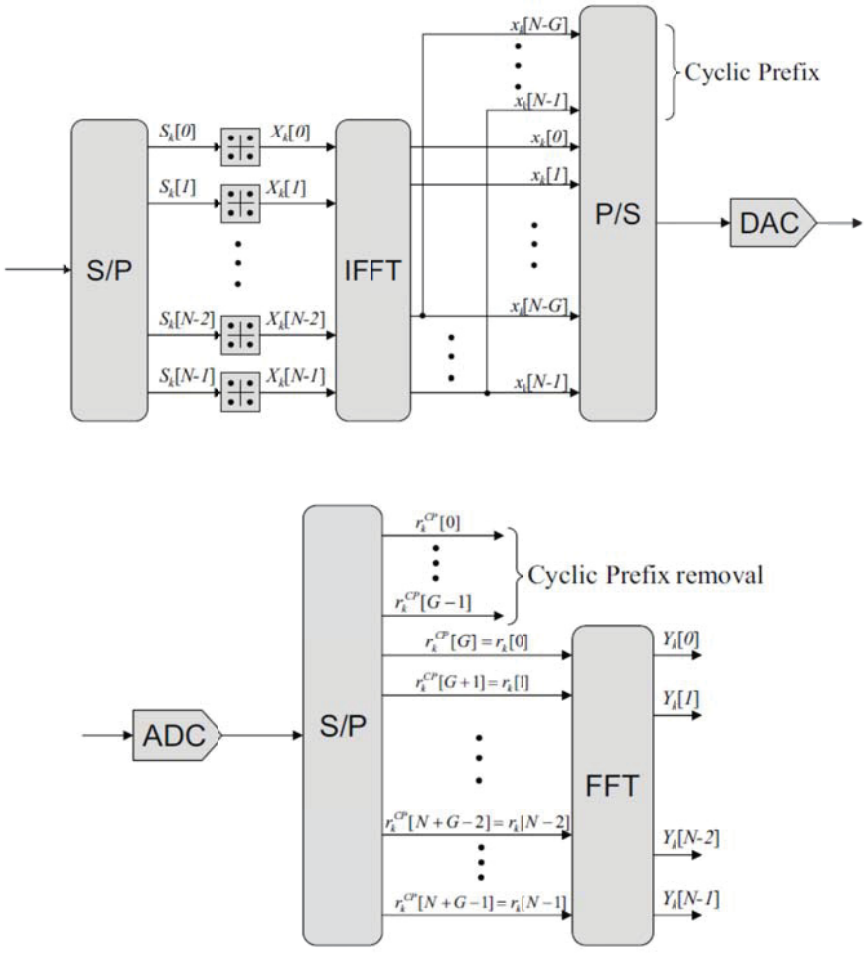

Figure 10: OFDM transmitter and receiver

One concept in modem design is the equalization and match filtering. OFDM modulation scheme has solved the match filter concept by using two orthogonal and matched basis function which is sine and cosine transformation. An iFFT and FFT is used as transmitter and receiver matched filters. In such scheme equalization of the signal is done in frequency domain, therefore prior to match filtering preserving the symbol energy in one FFT block is very important.

OFDM solves the channel effect and the ISI by introducing Cyclic Prefix and by simply copying the last L symbols to the beginning of the block and then transmitting through the channel. By doing so any channel with length less than L will have its effect preserved in the CP. In this way an FFT block becomes cyclo-stationary and it would be unimportant from which position the FFT block is taken as long as it contains the whole CP as a part of the block. By doing this basically the effect of the channel is reversed and OFDM blocks are capable of equalizing the channel very effectively with minimal resources provided that they are given the channel information in frequency domain. Figure 2-11. shows the position of CP in an FFT block. In this figure T_{cp} is the duration of the CP which depends on the channel it is going to be used. T_u is the actual symbol duration.

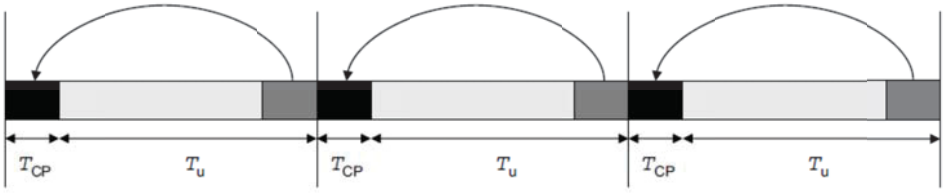

Figure 11: Cyclic Prefix in FFT block

At the receiver the beginning of the packet is found and from that position and FFT block is separated and an ISI free block is passed to the FFT which in turn transfers back the signal from what is known time domain to frequency domain.

2.3 LTE Downlink

Now that we have familiarized ourselves with OFDM, LTE basic facts and procedures we will discuss the LTE downlink specifically.

LTE resources

LTE Synchronization

LTE Channel estimation

We also discuss LTE preambles (Zadoff-Chu sequence) and their unique characteristics.

2.3.1 Synchronization in LTE down Link

No resource can be extracted including pilots if proper synchronization is not performed between eNodeB and UE. The following synchronization has to be performed:

Carrier frequency synchronization

Symbol and frame timing synchronization

Sampling clock synchronization

Without the above three synchronization no pilots can be extracted and no channel information could be calculated, therefore prior to channel estimation we are interested in how to make a good synchronization.

2.3.1.1 Cell search

UE (user equipment) needs to perform a cell search procedure to access an LTE cell. This involves detecting the Primary Synchronization Signal (PSS) and Secondary Synchronization Signal (SSS) which is broadcasted by the eNodeB at specific radio frame locations for this purpose.

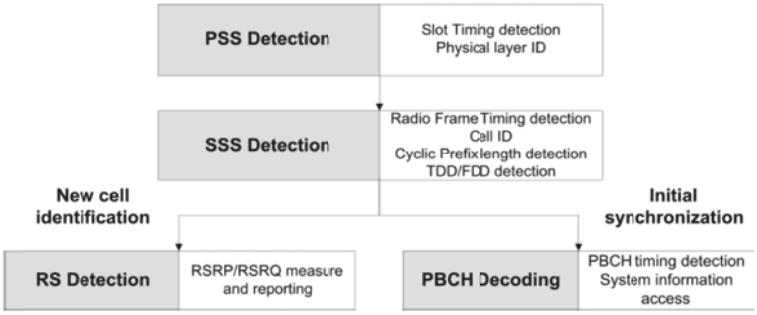

Figure 12: Cell search procedures

As seen from Figure 2-12, in order to examine the pilots for neighbouring cell and associated cells, SSS and PSS has to be performed in order. In a radio frame the PSS and SSS signal position is different for FDD or TDD transmission. Figure 13 shows the position of these signals in the radio frame for both types of frames. Prior to SSS detection the CP length is unknown so the synchronizer blindly should search for the SSS in the given locations. Totally 4 different positions has to be searched if both TDD and FDD is supported in an algorithm design. PSS signal always proceeds SSS either immediately (FDD) or after 3 symbols (TDD). The job of a locationing algorithm besides extracting information from the channel information is to provide better synchronization algorithms for neighbouring cells if it intends to use multiple cell information in its positioning algorithms.

We mentioned the position of the PSS and SSS signals in time domain which their position in the radio frames. Now we are interested in their position in frequency domain. As no bandwidth information is known prior to synchronization the PSS and SS are positioned in centre of the frequency band occupy 6 resource blocks (RB's) which is the minimum number to allocate. The PSS and SSS have 62 symbols which are all mapped to 62 central carriers in the 6 mentioned RB's. As mentioned before each RB has 12 subcarriers which mean from 72 subcarriers available only 62 carriers are used and the rest is not used. This means 5 RE at each end of the resource block is not used. Figure 14 shows the position of the RB's and the empty RE's at the lower end RB.

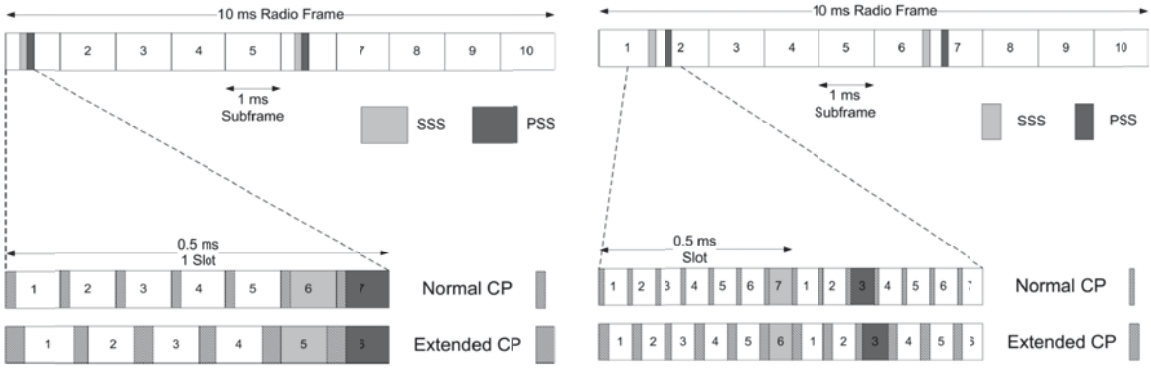

(a) (b)

Figure 13: (a) FDD frame, (b) TDD frame

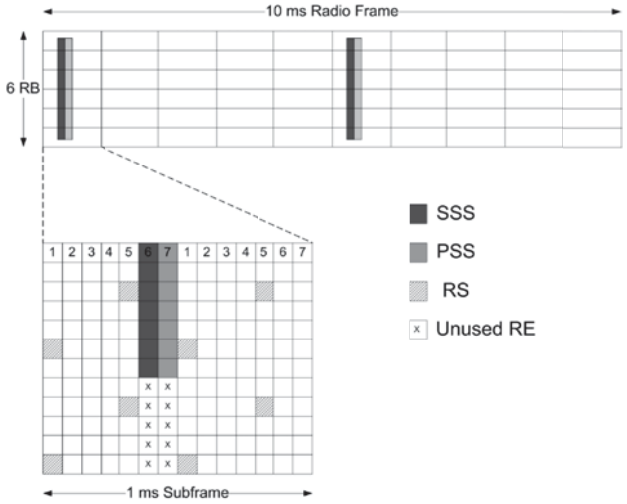

Figure 14: PSS and RSS position in RB's

2.3.1.2 Detection of PSS and SSS

PSS uses Zadoff-Chu (ZC) sequence. ZC sequences are Constant Amplitude Zero Auto correlation sequences. Unlike golden codes these codes are non-binary and suitable for IQ transmission. Equation 1 shows the odd length ZC sequence:

$$a_q(n) = e^{\left\{-j2\pi q\left(\frac{n(n+1)}{2}\right)+l.n\Big/N_{ZC}\right\}} \quad (1)$$

Where :

$q\epsilon\{1, \ldots, N_{ZC} - 1\}$ is the root index.

$n = \{0,1, \ldots, N_{ZC} - 1\}$

$l\epsilon$N where in LTE l = 0 is used.

$R_{kk(\tau)} = \sum_{n=0}^{N_{zc}-1} a_k(n)a_k^*(n+\tau) = \delta(\tau)$
(2)

Where R(.) is the autocorrelation function of a_k at position τ

The properties of these sequences are:

ZC sequences have constant amplitude in time and frequency domain.

ZC codes have ideal cyclic autocorrelation which enables the user to detect the codes even when they are delayed. If the code is designed to operate at delay N. The autocorrelation of a delayed sequence will generate a peak at the delayed time as long as the delay is shorter than the designed maximum delay of N samples.

Multiple orthogonal sequences can be generated from one sequence. The cross correlation of two sequences have a constant amplitude of $1/\sqrt{N_{ZC}}$ if and only if the difference of sequence indices are relatively prime toN_{ZC}. This means if N_{ZC} is chosen as a prime number $N_{ZC} - 1$ orthogonal sequences may be generated by just changing the indices of the sequence.

A DFT of the ZC sequence is a weighted cyclic shift ZC. This means ZC can be generated in frequency domain directly. Later some papers will be shown that use this property to generate ZC sequences efficiently.

2.3.1.3 PSS signal

As mentioned above the ZC codes can be generated in frequency domain directly. The frequency domain codes have the exact same characteristic as time domain ZC codes. A PSS signal uses this feature and transmits a 63 length ZC code on 63 carriers with middle code punctured to avoid dc subcarrier. LTE uses 3 PSS codes for 3 possible physical layer sections in a cell which means one PSS code for each group in the cell.

In equation (1) q is the root of the ZC sequence. PSS codes are defined if choosing $l = 0$ and q = 29, 34, 25. The chosen PSS signals have low sensitivity on frequency offset and can still be detected if there is a 7.5 KHz frequency drift. This is due to their almost flat frequency response.

A correlator will decide which code has been transmitted. The received signal is correlated against the existing codes and the position of the peak shows the offset of the signal.

2.3.1.4 SSS signal

SSS is signal is an M-sequence. It is constructed by interleaving two 31 length BPSK M-sequence codes known as SSC1 And SSC2. SSC1 and SSC2 are cyclic shifted versions of a 31 length M-sequence. The shift of each code is mentioned in 6.11.2.1-1 in technical specification 36.211 of 3GPP group. SSC2 is scrambled by a sequence depending on the SSC1 shift and SSC1 is scrambled based on the PSS signal index.

SSS detection is done after PSS detection and therefore the system has the channel information at this point. The system can either use a coherent detector or a non-coherent one which is based on the code correlation.

In coherent detection the performance depends on the presence of the interferer and the quality of the channel estimation, this is due to the fact that the interfere uses the same PSS signal therefore the SC1 and SC2 signals would be identical. In a non coherent detection the performance depends on the coherent bandwidth of the channel which should be greater than the 6 resource blocks being used by the SSS signal. This ensures that the SS signal would not be changing during the transmission.

2.3.2 Channel estimation

A locationing algorithm needs channel estimation. A coherent detector is used that can utilize the phase and amplitude of the received signal. A common way to estimate the channel information is to use a known signal such as a pilot. These known signals are called Reference Signals (RS's). One can realize an OFDMA signal as a three dimensional frame of time, frequency and space signal. RS signals are placed in the LTE frame at known time and frequency positions on an optional or chosen space which is the antenna port. The position in frequency is called subcarrier and the position in time is known as slots and the smallest element in this two dimensional domain is called the Resource Element (RE).

LTE downlink uses 5 different reference signals (RS) based on the LTE release number.

Common reference signal which are available to all UEs (*Pilots*)

Demodulation reference signal specific to the UE

Multimedia broadcast Single Frequency Network MBSFN specific reference signal

Positioning reference signal (Release 9 onwards)

Channel state Information reference signal (Release 10 LTE advanced)

Reference signals are transmitted from eNodeB. LTE introduces antenna ports as ports to transmit RS which can either be physical antenna or virtual ports. From UE point of view any measurement obtained from these antenna ports defines the characteristic of that port.

What we are going to first target for the channel estimation is the common reference signals or the cell specific signals. These RS signals are available to all UE's in the cell and it is a standard RS since release 8, these are the primary RS for channel estimation purposes.

In Figure 15 an R_0 indicates a RS for antenna port zero. The transmitted RS signal is a QPSK signal defined in equation (3).

$$r_{l,n_s} == \frac{1}{\sqrt{2}}[1 - 2c(2m)] + j\frac{1}{\sqrt{2}}[1 - 2c(2m+1)] \quad (3)$$

In equation (3), m is the reference signal index, n_s is the slot number and l is the symbol number. C(m) is taken from a length 31 gold sequence which is initialized based on the RS type. The initialization is done every OFDM symbol and the value depends on the cell identity, N_{ID}^{cell}. Each cell uses a cell specific frequency shift equal to $N_{ID}^{cell}\ mod\ 6$ which avoids frequency collisions between the RS signals from neighboring 6 cells. This is an important feature when using the channel estimation from neighboring cells to calculate the location.

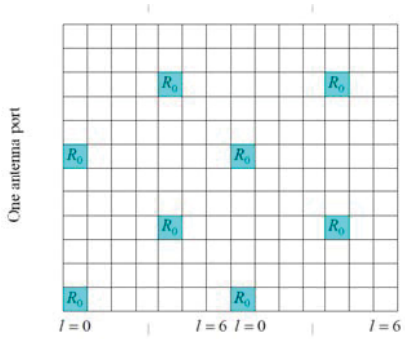

Figure 15: Cell specific RS for normal CP length

We would leave the rest of the RS signals for now till later phases of the project but before leaving this section we need to mention the next important RS which is the UE specific RS. UE-specific RS are used only between eNodeB and particular UE and are transmitted as of any other PDSCH (Physical Downlink Shared Channel) signal. The difference is that these RS signals are mapped to specific RB's that target the specific UE and therefore contain UE specific RS signals. This can be beam-forming signals or extra RS signals. We will go into details of these specific RS signals later.

We will consider the channel $h(\tau, t)$ to be the channel time varying complex signal at delay τ and time instant of t. In a discrete form this channel is modelled as $h[l, kT]$ with l as the delay at time sampling instant kT. We also consider the channel to be approximated by an FIR vector of:

$$h[k] = h[0, k], \ldots, h[L-1, k] \quad (4)$$

where L is the channel delay.

Practical channel estimation for LTE is done in frequency domain. If the received signal is:

$$y = h * x + n \quad (5)$$

The FFT of the received signal is:

$$Y = HX + N \quad (6)$$

Where X is the Nx1 FFT of the transmitted symbols and H is the LxN cyclic FFT of the channel information and N is a zero mean complex cyclic white noise with covariance of C. In order to obtain the channel matrix H it is sufficient to correlate the X with the known transmitted symbols and obtain H:

$$Y = H(X.X^H) + NX^H = H + z = \widehat{H} \quad (7)$$

If X is the reference symbols and has zero mean and unit energy then z is still a circular zero mean noise and the result would be the NxL estimated channel where L is the channel length.

As shown in Figure 15, the channel estimation would result in estimating the channel for locations in frequency-time lattice that the RS signal is present. In order to estimate the channel for the rest of the subcarriers approximate estimation of the channel at the frequency and time lattice is required. If the frequency and time is considered statistically independent then we can divide the estimation in 2 domains as a single domain linear estimation which in its simplest form will be interpolation.

More sophisticated approaches to obtain the two dimensional estimates would be LS least square and MMSE approach. Any approach in time domain has been proven to be impractical although from estimation point of view it would have resulted in more accurate unbiased estimations. Chapter 8.4 in [1] compares different channel estimation methods but the most practical channel estimation for an immobile user is the interpolation method described above.

2.3.3 Simulation Environment

The system requires TOA and channel estimation from multiple eNodeB's at the UE position. As mentioned in previous sections the synchronization methods provided in LTE system would provide the TOA of signals from different cells to the UE and the channel estimation methods described in previous section would provide the channel information needed. In order to set up such simulation environment a single antenna downlink scheme as shown in Figure 16 is provided:

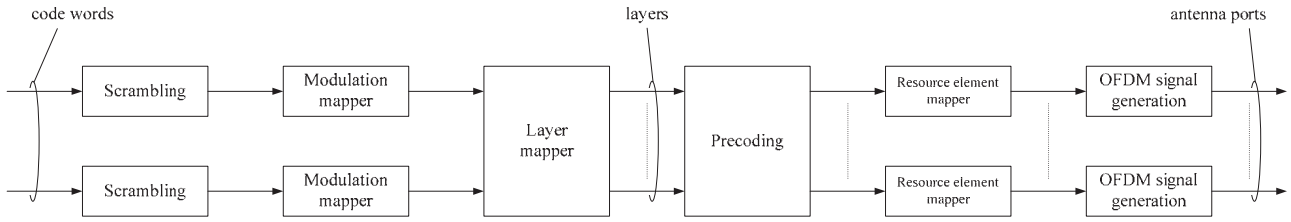

Figure 16: Downlink Physical Chain per eNodeB

The OFDM signal from different eNodeB goes through a Lagrange interpolator to change phase according to their distance to the UE and then multiplexed with other eNodeB's and passed through the channel. Figure 17 shows an alternative that the signal is individually passed through the channel and delay is performed on the signal after the channel.

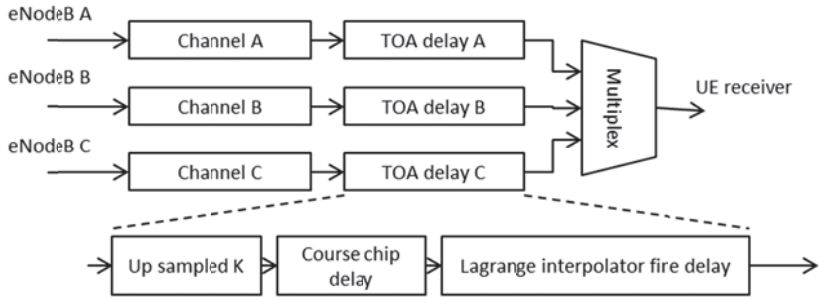

On the receiver the PSS and the SSS signal is extracted and the delay associate with the intended eNodeB is considered. The interpolated signal for each intended eNodeB is passed to their channel estimator and the channel is extracted for each eNodeB-UE path.

The LTE observables which are relevant are essentially the known synchronization signal segments that are part of the resource blocks. While it is a reasonable assumption that the LTE AN signals are frequency synchronized (which can be accurately obtained from GPS signals amongst other potential sources), it is not a reasonable assumption in many cases to assume that the AN's are accurately time synchronized. This depends as the network may be specifically calibrated for SGL purposes. Tight timing synchronization amongst the AN's is not necessary for optimum data communication functions nor is it necessary for facilitating network based location, hence there is little impetus for the service provided to accurately time synchronize the network. Consequently, the SGL processing developed will consider the two modes when the LTE network is tightly time synchronized and when it is not.

3 SGL Methods and Analysis

3.1 Objectives

There are a large number of processing methods for SGL that are applicable for the LTE downlink signalling which have been reviewed in the literature. The purpose here is not to provide an exhaustive treatment of such methods but rather to narrow down to specific focus of the research that will be conducted over these three contract phases. The basic assumptions are as follows:

1. LTE wireless signalling will be used for the observables

2. Only downlink LTE signals will be assumed. The UE is not registered with the network and hence uses the LTE downlink signals as signals of opportunity.

3. The LTE downlink signals from the various AN's may or may not be accurately time synchronized. Both modes will be considered.

4. The UE will perform all of the calculations involved with the SGL estimate

5. Multipath will be variable as indoor and dense development areas are of primary interest.

6. The UE is expected to be undergoing some arbitrary motion that varies in terms of smoothness.

The overall objective is to generate a belief map of the location of the UE as the trajectory unfolds. The belief map will provide a posterior estimate of the location of the UE that is iterated every time interval which is based on all available data up to the current time. For such estimation problems based on the aforementioned assumptions, it is generally not valid to assume Gaussian statistics. Consequently Kalman filter type parametric Bayesian filters are a typically a poor fit. Consequently, the particle filter (PF) will be used extensively for the simulation analysis as well as the basis of the processing. Having described the fundamentals of the PF and the application to SGL with LTE signalling, the various standard techniques of SGL will emerge naturally as will the development of the SA processing. SA processing is primarily a subject of investigation for phase II. The PF essentially provides an estimate of the posterior PDF based on the accumulation of UE movements and the measurements made. From this PDF, statistical parameters such as the posterior mean and variance can be computed directly. Hence determining the conditional mean which is equivalent to the MMSE estimate of the state variables and the covariance matrix can be done directly. Therefore measures of clairvoyant performance bounds can be determined. This would include numerical calculations of the CRLB.

Some further simplifying assumptions will be made initially that will be further addressed in the second phase. The main one is that the position of the AN's is known and that the AN's are precisely time synchronized. When the SA is accounted for in the second phase methods will be given that can accommodate non-synchronized AN's. However, it is necessary to have appreciable motion of the SA in order to overcome the unknown timing offsets of the AN's. The principle is that the UE undergoing a smooth trajectory will simultaneously estimate the clock

offsets. Further, the CV observables can be used in the PF for SGL temporary calibration of the AN network as the timing offsets will be determined jointly with the location estimate.

A related issue is that the clock of the UE will not be entirely stable but will vary. Hence a bias offset and drift offset of the UE clock is required. As will be developed, clock biases will be appropriated to each AN-UE link and treated as a state variable that is initially unknown. It is possible to even consider the case of simultaneously unsynchronized AN's and unknown positions of these. Also it is necessary to contend with the uncertainty of the UE clock instability.

Indoor environments are subject to severe multipath which significantly distorts wireless signals in the LTE frequency bands. Even though LTE has a large bandwidth in the excess of 10 MHz, this is typically not sufficient to provide adequate accuracy of time of flight measurements for indoor SGL. Multipath distortions it itself renders traditional methods of SGL virtually useless. Combatting the effects of multipath is the most significant challenge in providing adequately accurate SGL and hence new methods are required. Another significant issue is that the AN's are not necessarily synchronized. They may be frequency locked to a reference such as GPS but there is no guarantee that the AN's are individually synchronized. This implies that there is a random delay offset that must be considered with regards to each AN that cannot be considered to be a Gaussian random variable. This is why the underlying research of this contract is based on the Bayesian filtering of an assumed smooth UE trajectory. It is necessary to assume that the UE is moving and to combine multiple spatially separated LTE observations along the trajectory. This is combined with computer vision (CV) observables as well as observables from physically small MEMS based accelerometers and gyro devices. The primary role of the accelerometer will be that of estimating the tilt angle of the UE notwithstanding the issue that gravitational acceleration due to tilt is indistinguishable from motion acceleration. The CV will be assumed to consist of a very small webcam to a more elaborate (though integratable into a handset form factor) CV sensor using a diffraction grating laser source. An overall imposed constraint is that the UE needs to be self-contained and that the apparatus and processing required for the SGL function must be commensurate with the handheld form factor.

Initially pure LOS links will be assumed between the UE and the various AN's. However, these will be supplanted with NLOS multipath links which will be accounted for by assuming a time of flight (TOF) bias that varies with time. Hence it is not really a bias but more a slowly varying random variable representing the bias. This bias can switch quickly when moving from LOS to NLOS conditions. Boolean switch models and Markov models have been analysed for the fluctuating delay bias issue. Boolean multipath model switches are compatible with the PF however with the expense of an additional variable. An example of a scenario where the propagation changes from LOS to NLOS is shown in Figure 3.1. The concept would be that the processing would have to recognize that there has been a change in the propagation perhaps from the coherency of the carrier phase as the UE propagates. The PF could have an implementation where the Boolean state variable is changed based on measurements of coherency. An issue with this is that the velocity would have to be known to some extent.

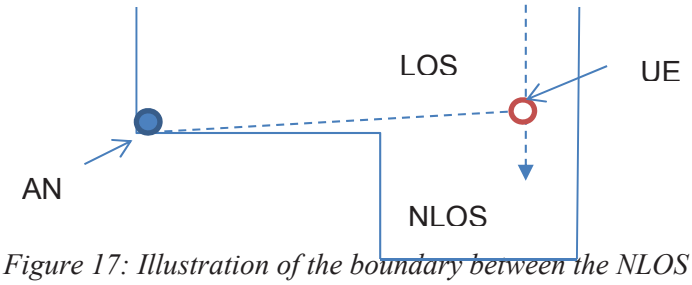

Figure 17: Illustration of the boundary between the NLOS and the LOS region. In theory, as the UE moved across this boundary, the bias model would switch from LOS to NLOS with appropriately selected delays

The question is how many signal samples are required to reliably make this switch. Also in the NLOS region there are several multipath models to choose from that are based on various delay profiles and fast fading models of the standard statistical kind represented by Ricean, Rayleigh, Nakigami and other distributions. All indoor propagation is very different that it is typically not useful to attempt to abstract a statistical model that the SGL method can be optimized for. Many samples are required to determine the statistical details of the NLOS propagation as well as the switch between LOS and NLOS models. Hence it may be better to assign a single delay bias that is a trackable state variable instead of attempting to collect enough samples to switch between propagation models. Having a continuously variable parameter for excess delay allows for a simpler more robust tracking system. Certainly this will be an area that is to be experimentally tested. Hence the approach taken here is one of generalization. Ultimately, any multipath model results in some form of fast fading with spatial distance as well as a varying delay of the time of flight. The approach assumed in the receiver processing is to take the first resolvable multipath component which will have a variable excess delay which is represented by a factor "b". The PF assumes b as a state variable that is allowed to change with time subject to some reasonable overarching statistical constraints. The receiver demodulates the resource blocks of the LTE signal which are narrow bandwidth coded signal bursts that are then Fourier transformed to obtain the channel time domain impulse response. The TOA estimate of a given LTE signal is then taken as the time of the leading edge of the transformed impulse response offset by the parameter "b" which is determined by the PF. The higher the aggregate bandwidth of the LTE downlink signal the sharper the leading edge transition of the estimated channel impulse response will be which will result in less variation of "b". In turn, this implies that the spread of the posterior pdf of the state variable belief is more confined resulting in an overall lower position variance. This will be verified by experimentation in phase II and phase III of this contract.

The trajectory of the UE itself is assumed to be fairly smooth based on a markov model that assumes white acceleration but integrated velocity and doubly integrated position. This approach provides a somewhat realistic representation of the UE special movements with modelling parameters that can be changed for various purposes. An advantage of assuming Markov models is that they are directly compatible with the PF. All of the unknown variables to be tracked including the location of the UE are represented in a state variable vector. Additional state variables are the UE velocity components, delay biases, clock drift parameters and potentially the location of the AN's if they are initially assumed to be unknown. A useful observation is that the multipath bias delay, the UE clock instability and the AN issue of synchronization are related. It is solved by augmenting the state variable vector with bias variables for each AN which

incorporates the UE clock instability. This is all wrapped up in the parameter denoted as "b". Typically there will be a "b" variable associated with each AN. A refinement would call for a measure of correlation between these random biases.

A Bayesian PF analysis will be used extensively to characterize changing belief map as data and sampling is continuously updated. Current belief of state variable vector (posterior pdf) will incorporate all information regarding the UE position and pose contained in the observations. PF is used as the observations can be highly varied with multimodal PDF's. All the traditional location methods will be contained in the state variable posterior pdf which is determined using the PF. The outcome will be an LTE model that is compatible with the PF analysis.

In phase II the synthetic array (SA) attributes will be combined with the PF processing to account for the information of the evolving state variables as the UE is arbitrarily moved. An obvious start is the independent measurements that can be taken that slowly build up the posterior pdf belief map. The added feature will be the addition of the first order Markoff motion model of the UE itself. To this stage measurements are based on TOA of the signal with possible compensation of the multipath bias. The carrier phase is ignored. An added possibility is to consider the RSS of the signal strength in addition. RSS and TOA can be construed as generally independent observations in a typical multipath environment. This implies that the noise associated with these measurements is independent. However, they are clearly related the state variables. Then we will consider carrier phase which is really only applicable when the multipath is suppressed (LOS or Ricean with a moderately high K factor). The SA can be used to estimate LOS conditions and powerfully exploit the localized relative carrier phase information if the trajectory is accurately known. A blind SA can be implemented if the trajectory is estimated jointly. However, we will consider the use of ancillary estimates of the trajectory based on the camera, accelerometers and the possible gyro.

Complementary experimental work will be done to collect measurement data to demonstrate the validity of the analysis and simulations done. The primary motivation of the experimental work is that the multipath delay bias conditions from simultaneous AN transmissions are not possible the adequately justify. Algorithm development and verification based on simulation analysis only tends to become insidiously self-referential. To avoid complications with LTE receiver processing requiring FPGA developments two types of modulations will be considered. The first is a step frequency modulation across the LTE band and the second modulation is a narrow pulse signal. This narrow pulse modulation is periodic which results in a number of simultaneous frequency components uniformly spaced across the LTE band of interest. If the spacing of the frequency harmonics are well within the coherence bandwidth of the propagation channel then the channel can be accurately characterized by the pulse modulated signal. This will then be equivalent to channel characterization by the downlink LTE signal.

Additional incidental side information needs to be accounted for in terms of assisting the SGL algorithm. But these are problematic as they involve some randomness. Of primary importance is the assumed smoothness of the UE trajectory which allows for significant filtering of the received data. It is the assumptions regarding the UE trajectory that allows for a set of consecutive samples to be combined greatly adding to the information available for positioning. However, the UE trajectory is still random which generates incremental innovations which must be accounted for in the position estimation. It is for this reason that Bayesian filters are used exclusively. Other possibilities are emissions from other UE's that are synchronized to the LTE

network but are at a location that is unknown to the UE. Furthermore, these temporary anchor nodes may themselves move randomly creating additional uncertainty. The task of the SGL is then to optimally use this set of disparate inputs for various scenarios. The key to accurate location estimation will be shown to be diversity of which the evolving trajectory of the UE plays a key role.

In the remainder of this chapter section, the PF will be built up from a description of the underlying theory of the Bayesian PF followed by problem scenarios of increasing complexity.

3.2 Outlines the PF as a nonparametric Bayesian filter that is suitable for the SGL problem

3.3 Gives the PF response to simple examples in LOS

3.4 Determines the issues with multipath which is modelled as a time varying bias.

3.5 PF is developed for the case of UE with clock instability

3.6 Development of the unsynchronized UE's

3.2 Nonparametric particle filter

The flexibility of the discrete time Bayesian filter (BF) is that it can take these arbitrary sets of observables into account. The outcome of the BF is the posterior PDF that accounts for all of the random motions of the UE and the set of measurements. Having the posterior PDF allows for optimal estimation of the state variables in the context of the smallest variance. Also the estimate can be unbiased. Hence not only do we have a measure of the performance of the estimation of the state variables but also a recipe for implementing the required optimal processing. If some rather restrictive conditions are met then the recursive Bayesian filter is analogous to the traditional Kalman Filter (KF). These conditions are:

1. prior PDF of UE state variables is jointly Gaussian

2. observations are jointly Gaussian and linearly related to the UE state variables

3. the random component of the UE trajectory update is jointly Gaussian

In many cases of practical interest, these restrictive conditions are sufficiently satisfied such that the KF is nearly optimum. Slight violations of the conditions can often be satisfactorily accommodated by the extended KF or scented KF. However, when larger deviations from these conditions are encountered, the variants of the KF give very sub-optimal and unpredictable performance. For this reason the particle filter (PF) is exclusively developed for the SGL processing.

To describe the PF start with the concept of the state vector at a given time t which is represented as x_t that contains the state variable of the location and pose of the UE. The notation used is adapted from [1] and [2]. Initially only location of the UE will be considered such that $x_t = \begin{bmatrix} x \\ y \end{bmatrix}$.

A convenient way of addressing a particular component of the vector is to use the notation of $x_t.x$ and $x_t.y$. A set of M particles is considered each associated with the set of state variables. The time sequence of specifically the m[th] particle is given as

$$x_{0:t}^{[m]} = x_0^{[m]}, x_1^{[m]}, ..., x_t^{[m]}$$

where m denotes the particle index and t the discrete time index. It is assumed that the initial distribution of particles corresponds to an initial statistical state. That is $x_0^{[m]}$ is given and corresponds to some initial belief of the state distribution. If there is no prior state knowledge then $x_0^{[m]}$ is a uniform distribution across the entire state space. The prior PDF is an expression of our ignorance of the state variables with the uniform distribution being commensurate with complete ignorance.

The state space vector can be a mix of continuous and discrete variables. For example consider a one dimensional SGL example where x_t represents the range which is a continuous variable. The makeup of the particles of $x_t^{[m]}$ are then M discrete samples of the pdf over a continuous range at the discrete time t. A grid based method on the other hand assumes that the states correspond to a finite set of discrete states. In the radar example we can approximate the continuous range as a set of discrete points in range. The assumed prior belief of the state is represented approximately by the set of M particles of $x_0^{[m]}$. The belief is represented by the density of particles over a continuous variable say range as in the current radar example. We wish to propagate this belief forward in time to the next time step occurring at T_s which is represented by the set of particles of $x_1^{[m]}$. Note that in the 1D SGL problem we are representing the continuous time stochastic differential equations with an approximate discrete time variant.

The particle filter method is a means of recursively updating the particles to represent the current belief of the state of the system. The particle filter mapping of $x_0^{[m]} \rightarrow x_1^{[m]}$ incorporates the deterministic and random components of the UE motion over the time interval of $(0, T_s]$. As well it incorporates the new measurement of z_1 made by the UE itself. In the KF , the two step processing first accounts for the target motion producing a prediction of the state and then corrects this prediction with the measurement made. In the PF the posterior pdf of the state is approximated by the distribution of M particles. The estimation of the UE state vector is then a mean of this posterior pdf which being conditioned on the measurements is the minimum variance estimate of the actual state. Hence in the PF the particles are simply averaged to determine the mean value which is then the current estimate of the state.

At the outcome of the time step t-1 we have $x_{0:t-1}^{[m]}$ for which we wish to generate $x_t^{[m]}$ and add it to the sequence for the m[th] particle. To do this consider the posterior distribution over the entire sequence (for all state sequences). That is we consider the joint belief over the entire state evolution over the interval of $(0, tT_s]$. This is represented as the conditional pdf of

$$bel(x_{0:t}) = p(x_{0:t} \mid u_{1:t}, z_{1:t})$$

Here $u_{1:t}$ is an abstract vector encapsulating all of the deterministic updates and $z_{1:t}$ likewise encapsulates all of the measurements or observations make, relevant to the state variables over the time intervals from 1 to t. We derive based on Bayes and Markov assumption

$$p(x_{0:t} \mid u_{1:t}, z_{1:t}) = \eta p(z_t \mid x_t) p(x_t \mid x_{t-1}, u_t) p(x_{0:t-1} \mid u_{1:t-1}, z_{1:t-1})$$

where η can be construed as a normalizing constant. This gives us an iterative approach as

$$bel(x_{0:t-1}) = p(x_{0:t-1} \mid u_{1:t-1}, z_{1:t-1})$$

such that

$$bel(x_{0:t}) = \eta p(z_t \mid x_t) p(x_t \mid x_{t-1}, u_t) bel(x_{0:t-1})$$

Consider what is implied by this recursive relation. We start with $p(x_0)$ as the pdf of the initial state at t=0. Then we have for the first update

$$p(x_1, x_0 \mid u_1, z_1) = \eta_0 p(z_1 \mid x_1) p(x_1 \mid x_0, u_1) p(x_0)$$

which is the joint pdf of x_0 and x_1 given the deterministic motion of u_1 and the observation of z_1. η_0 is the normalizing constant that is different for each iteration. It is useful to derive this expression directly from Bayes as

$$\begin{aligned} & p(x_1, x_0 \mid u_1, z_1) p(z_1 \mid u_1) = p(x_1, x_0, z_1 \mid u_1) \\ & = p(z_1 \mid x_1, x_0, u_1) p(x_1, x_0 \mid u_1) \\ & = p(z_1 \mid x_1) p(x_1 \mid x_0, u_1) p(x_0 \mid u_1) \\ & = p(z_1 \mid x_1) p(x_1 \mid x_0, u_1) p(x_0) \end{aligned}$$

Let $\eta_0 = 1 / p(z_1 \mid u_1)$ such that $p(x_1, x_0 \mid u_1, z_1) = \eta_0 p(z_1 \mid x_1) p(x_1 \mid x_0, u_1) p(x_0)$. Generally we do not bother with determining $p(z_1 \mid u_1)$ as it is not relevant to the state. Rather we normalize directly by ensuring that the total integration of $p(x_1, x_0 \mid u_1, z_1)$ accumulates to 1.

The second update is

$$p(x_0, x_1, x_2 \mid u_1, u_2, z_1, z_2) = \eta_1 p(z_2 \mid x_2) p(x_2 \mid x_1, u_2) p(x_0, x_1 \mid u_1, z_1)$$

We can also derive this from Bayes as

$$p(x_0, x_1, x_2 \mid u_1, u_2, z_1, z_2)\, p(z_2 \mid z_1, u_1, u_2) = p(x_0, x_1, x_2, z_2 \mid z_1, u_1, u_2)$$
$$= p(z_2 \mid x_0, x_1, x_2, z_1, u_1, u_2)\, p(x_0, x_1, x_2 \mid z_1, u_1, u_2)$$
$$= p(z_2 \mid x_2)\, p(x_2 \mid x_0, x_1, z_1, u_1, u_2)\, p(x_0, x_1 \mid z_1, u_1, u_2)$$
$$= p(z_2 \mid x_2)\, p(x_2 \mid x_1, u_2)\, p(x_0, x_1 \mid z_1, u_1)$$

Let

$$\eta_2 = p(z_2 \mid z_1, u_1, u_2) = p(z_2 \mid u_1, u_2)$$

and we get back to the recursion that we started with. We have a sequence of the m[th] particle from the initial time interval 0 to t-1 as an instance of the pdf associated with $bel(x_{0:t-1})$. That is $x_{0:t-1}^{[m]}$ can be construed as a sequence that is essentially drawn from the pdf corresponding to $bel(x_{0:t-1})$.

Instead of the sequence of states, we are interested in the current state in terms of the previous state. We can write this as

$$bel(x_t) = \eta\, p(z_t \mid x_t)\, p(x_t \mid x_{t-1}, u_t)\, bel(x_{t-1})$$

where it seems that we have heuristically marginalize away the prior states. Note that this is done by the PF as we consider the aggregate of the particles of the prior pdf to determine the posterior pdf. To see this consider the first iteration as

$$p(x_1 \mid u_1, z_1) = \int p(x_1, x_0 \mid u_1, z_1)\, dx_o = \eta_0 \int p(z_1 \mid x_1)\, p(x_1 \mid x_0, u_1)\, p(x_0)\, dx_o$$

The iteration of the PF for the first iteration is to take all of the particles of the initial distribution and map these into the posterior distribution. Hence the consideration of the aggregate of the particles effectively performs the marginal integration.

An important point is that like the KF, the PF is a recursive algorithm to determine the current posterior pdf based on observations to the current iteration and not the future measurements. That is

$$p(x_1, x_0 \mid u_1, z_1) \neq p(x_1, x_0 \mid u_1, u_2, ..., z_1, z_2, z_3, ...)$$

Note that for the KF, smoothing can be imbued into the evaluation of the current pdf by considering all of the measurements, future and past. Hence it is important to realize that the corresponding smoothing PF that uses all of the data is calculated differently. For the current purposes, the posterior pdf of the current state vector given past and present data is evaluated. In the propagation of the particles we are effectively updating the belief of the current or new state

of x_t. We are not changing the belief of the previous states. Hence $bel(x_t)$ implies the prior states although they are not explicit in the notation. Another way of stating this is that $bel(x_t)$ is a function of $\{u_{1:t}, z_{1:t}, x_0\}$ and not the estimates of the prior states.

Now we use the recursive relation to derive the new sample corresponding to the m[th] particle as per the SIR PF algorithm. Initially we have $p(x_0)$ as the prior probability of the state from which we draw a set of M particles. The distribution of these particles is equivalent to the initial belief of $bel(x_0)$. To move to the posterior belief after the first step is completed we need to evaluate

$$bel(x_1) = \eta p(z_1 \mid x_1) p(x_1 \mid x_0, u_1) bel(x_0)$$

This implies first drawing M samples of

$$x_1^{[m]} \sim p(x_1 \mid x_0^{[m]}, u_1)$$

Note that the m[th] particle of $x_0^{[m]}$ is used to generate a new particle of $x_1^{[m]}$ based on the assumed known state transition probability. Part of the model of the incremental UE motion is that there is some random error or uncertainty involved with the update. Next we assign a weight based on the measurement given as

$$w_1^{[m]} = p(z_1 \mid x_1^{[m]})$$

Assuming that the resampling is done at each step we then generate a set of new particles based on the proportional size of the weights. In this step particles are reassigned values. Note though that particles of new values are not created. Rather particles of low weight or importance have a high probability of being annihilated. Particles of high weight can attract several particles of the same value. The density of these new particles represents the belief of $bel(x_1)$. Note that the joint density of the two sets of particles of $x_{0:1}^{[m]}$ represents the joint belief of $bel(x_0, x_1)$.

The iteration of the PF for the interval t is therefore:

Initially we draw the particle as

$$x_u^{[m]} \sim p(x_t \mid x_{t-1}^{[m]}, u_t)$$

where $x_u^{[m]}$ denotes an intermediate particle that is the outcome of the motion update. The conditional pdf reflects the uncertainty of the control update. As the update is incremental, the particle drawing can usually be satisfactorily achieved with a simple approximate pdf. Next we need to incorporate the likelihood of the measurement that is represented by the likelihood of

$p\left(z_t \mid x_t^{[m]}\right)$. We can either carry this likelihood with the particle or we resample the particle. In the resampling process the new particle of $x_t^{[m]}$ is generated from a statistical observation sample based on the distribution of $p\left(z_t \mid x_t^{[m]}\right)$ and the prior distribution of the particles of $x_t^{[m]}$. That is an importance weight is assigned given as

$$w_t^{[m]} = p\left(z_t \mid x_t^{[m]}\right)$$

Resampling does not have to be done at every iteration. One could recursively update the weights as

$$w_t^{[m]} = p\left(z_t \mid x_t^{[m]}\right) w_{t-1}^{[m]}$$

As such the importance factor of the particle accumulates as the sequence is incremented.

If resampling is not done then the accumulated weight of the particle can become so low that it is negligible. This represents a waste of computation as particles of very low probability are carried forward. When resampling eventually occurs then the low probability particle is typically annihilated. This represents a potential loss of particle diversity as well as a loss of computational effort of tracking it. If the UE state update is deterministic then the loss of particle diversity is permanent which eventually leads to issues. In this case, there will eventually only be one surviving particle such that the posterior pdf is approximated as a delta function of zero variance. However, if the UE state update has a random component then the diversity is not lost as degenerate particles of the previous iteration are used as given parameters for the current iteration where new particles are drawn from $x_u^{[m]} \square\ p\left(x_t \mid x_{t-1}^{[m]}, u_t\right)$. There can still be a loss of diversity if the deviation of the distribution of $p\left(x_t \mid x_{t-1}^{[m]}, u_t\right)$ is small relative to the average distance between the particles themselves. In this case small isolated clusters of particles may result which is not an accurate representation of the posterior pdf. The remedy is to increase M. However this obviously increases the computational effort of the PF processing and performance evaluation. A general observation regarding the use of the PF is that it is necessary to assess the performance for each SGL application.

In the following subsections, various tracking problems will be considered from the simple 1D problem where x_t represents a single state to a more practical application where there are 6 to 10 state variables.

3.3 Analysis with PF for idealized conditions

3.3.1 Ideal Deterministic 1D motion with perfect LOS measurements

Consider a 1D problem where the UE is moving along the x axis. At every time step it makes an constant increment of Δx which is deterministic and known to the receiver. Hence we have

$$x_t.x = t\Delta x = x_{t-1}.x + \Delta x$$

An ideal perfect range measurement is done at every time increment which corresponds to a displacement measurement with a pdf of

$$p\left(z_t \mid x_{t-1}, u_t\right) = \delta\left(z_t - \left(x_{t-1}.x + u_t\right)\right)$$

Note the notation in that when a particle is given all of the state variables associated with the particle are assumed to be available. In this trivial case there is only one state variable. Now apply the PF to this trivial case. As the initial location at t=0 is exactly $x_0.x = x_0 = 0$ and that this is known deterministically by the receiver we have all M particles with

$$x_0^{[m]}.x = 0$$

Now we propagate forward such that

$$p\left(x_1.x \mid x_0, u_1\right) = \delta\left(x_1.x - \Delta x\right)$$

Now the measurement is exact such that

$$p\left(z_1 \mid x_1, u_1\right) = \delta\left(z_1 - \Delta x\right)$$

Next draw the M particles from

$$p\left(x_1^{[m]}.x \mid x_0^{[m]}, u_1\right) = \delta\left(x_1^{[m]}.x - \Delta x\right)$$

The weights are determined as

$$w_1^{[m]} = p\left(z_1 \mid x_1^{[m]}, u_1\right) = 1$$

Of course the weights do not matter in this trivial example as all of the particles have the same location. Note though what happens if the initial particles were drawn randomly from a continuous distribution of nonzero kernel width. The probability of a particle being exactly correct is zero and hence all the weights will be zero resulting in the PF failing.

3.3.2 Ideal Deterministic 1D motion with Gaussian LOS measurements

Consider now the same problem but with noisy measurements such that

$$p\left(z_t \mid x_t, u_t\right) = N\left(z_t, t\Delta x, \sigma_z^2\right)$$

In the first time increment we have

$$p(x_0.x) = \delta(x_0)$$
$$p(x_1.x \mid x_0, u_1) = \delta(x_1.x - \Delta x)$$

Such that

$$p\left(x_1^{[m]}.x \mid x_0^{[m]}, u_1\right) = \delta\left(x_1^{[m]}.x - \Delta x\right)$$

The weights are determined as

$$w_1^{[m]} = p\left(z_1 \mid x_1^{[m]}\right) = N\left(z_1, \Delta x, \sigma_z^2\right)$$

Again the weights do not matter as the particles are all the same. A trivial example but it does raise a point. The initial particles are all the same and they are updated in a deterministic fashion. Then the weights will all always be the same.

We can change the example such that the initial distribution of particles is uniformly distributed. Say

$$p(x_0.x) = \frac{1}{D}\pi\left(\frac{x_0.x}{D}\right)$$

where $\pi(x)$ is a unit width and unit height pulse function. Now each of these particles are translated in a uniform fashion as before maintaining the uniform distribution of particles. However, the conditional pdf of each particle is deterministic as

$$p\left(x_1^{[m]}.x \mid x_0^{[m]}, u_1\right) = \delta\left(x_1^{[m]}.x - \Delta x\right)$$

The measurements are noisy such that

$$p\left(z_t \mid x_t, u_t\right) = N\left(z_t, t\Delta x, \sigma_z^2\right)$$

The weights can therefore be calculated based on the Gaussian sample given as

$$w_1^{[m]} = N\left(z_1, x_1^{[m]}.x, \sigma_z^2\right)$$

It is interesting to note that for small t, the influence of the measurement of z_t is large. This is due to the spread of $x_0.x$ being larger than the deviation of the measurement of z_1. The particles are resampled resulting in a larger number of particles centred at the measurement of z_1. As the iterations progress, the particles become more clustered at the mean value of z_t which is the unbiased correct value of $t\Delta x$. As the deviation of the measurement z_t is now significantly

larger than the spread of $x_t.x$, then the measurement has little additional influence. However, this is due to the update being deterministic with no uncertainty. If there was an uncertainty, it would appear that the update uncertainty or randomness would tend to spread $x_t.x$ with each iteration while the measurement would tend to group them together. The re-sampling process continuously tends to annihilate particles of low probability and add new particles or re-incarnated particles at higher probabilities. The balance of the spreading and grouping eventually results in a steady state deviation. This is equivalent to the steady state solution of a Kalman Filter. Figure 3-1, 3-2 and 3-3 show distributions of the particles with $x_t.x$ for t=1,2 and 20. Figure 3-4 shows the distribution of weights at t=20. It is interesting to note that a portion of the particles will have very low weight and hence are of negligible significance. Too high a proportion of weights that are very low is an indication of the loss of particle diversity such that the PF or PF processing becomes inefficient. Graphs were generated from pf1.m in the appendix A.

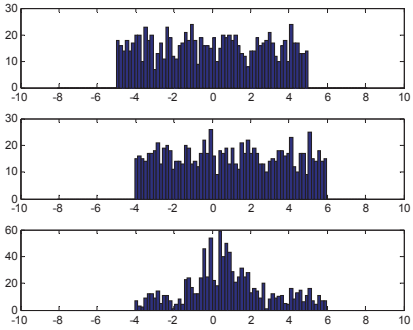

Figure 18: Plot of histograms of $x_0^{[m]}$, $x_u^{[m]}$ *and* $x_1^{[m]}$ *for* $\Delta x = 1$

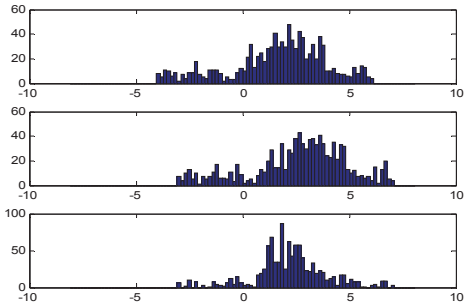

Figure 19: Plot of histograms of $x_1^{[m]}$, $x_u^{[m]}$ *and* $x_2^{[m]}$ *for* $\Delta x = 1$

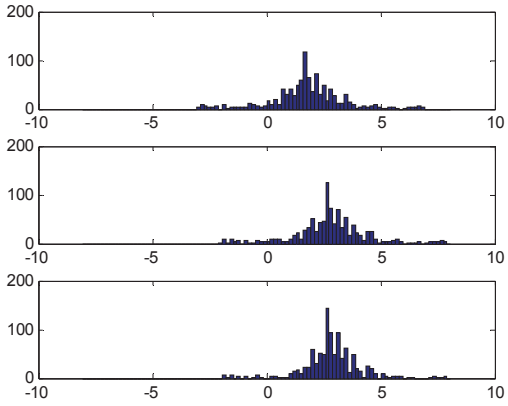

Figure 20: Plot of histograms of $x_{19}^{[m]}$, $x_{u}^{[m]}$ *and* $x_{20}^{[m]}$ *for* $\Delta x = 1$

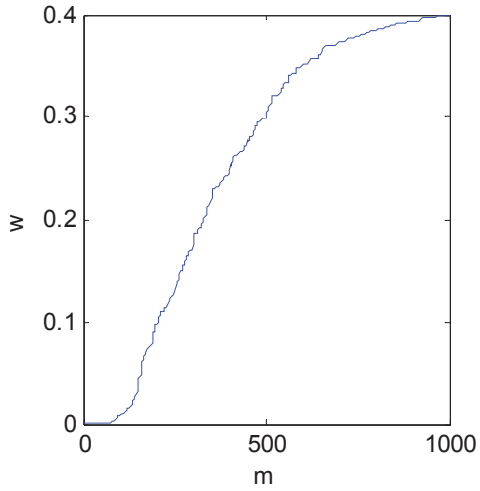

Figure 21: Plot of weights showing some loss of diversity

In this example the UE undergoes a rapid spatial transition from 0 to 2. The plots of Figure 3-5, 3-6 and 3-7 represent the response when the standard deviation of the update Gaussian pdf has values 0.005, 0.02 and 0.06 respectively. The actual displacement is given by the red dashed line and the blue is the conditional mean based on the posterior pdf after each iteration. Note that when the mean is taken of the posterior pdf of $p\left(x_t \mid u_{1:t}, z_{1:t}\right)$ that this implies the conditional mean which is the minimum variance unbiased estimator of x. Also there is an initial error of x=1. As observed the PF does track the actual displacement. The standard deviation is equivalent to that of the UE random motion of each iteration. Also shown is the weights after the last iteration which indicates only a minor loss of diversity. When the variance of the UE motion model decreases then the response time increases significantly. Note that $\sigma = 0.005$ given in Figure 3-5 results in a very sluggish response that does not follow the UE trajectory well. When $\sigma = 0.02$ the UE trajectory is tracked reasonably well and when $\sigma = 0.06$ as plotted in Figure 3-7, the UE is precisely tracked. However as evident is that the penalty of raising σ is that the

spatial spread of the particles increases. This compromise is of course similar to the KF where the Kalman gain is a function of the state transition covariance. Another way of stating this is that the increased variance of the update results in a more rapid spreading of the particles such that the measurements in each iteration have more influence. Plots were generated from P2.m as listed in the appendix A.

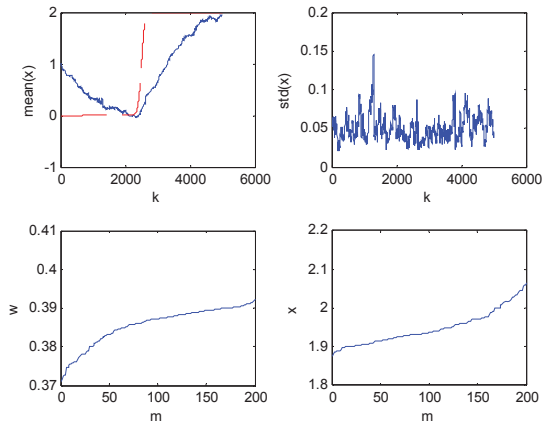

Figure 22: Response of PF when $\sigma = 0.005$

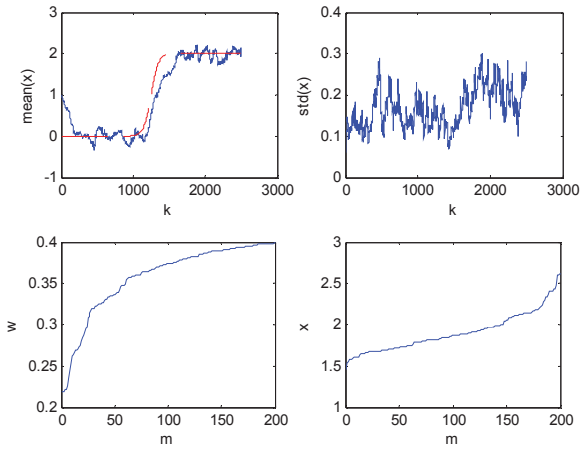

Figure 23: Response of PF when $\sigma = 0.02$

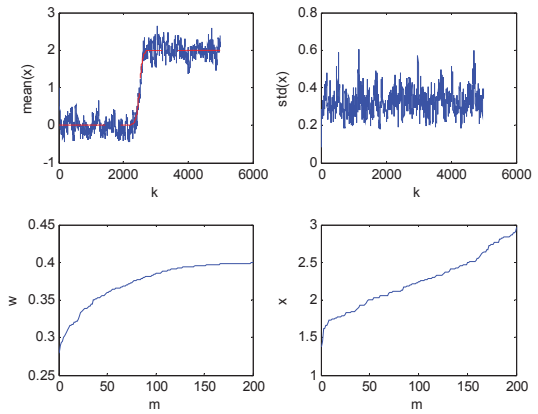

Figure 24: Response of PF when $\sigma = 0.06$

3.3.3 Two dimensional location with the PF

Next consider the AN in a two dimensional rectangular room as shown in Figure 3-8. It is assumed that initially the location of the UE is completely unknown except for the fact that it is in the room. We will use the PF to determine the belief after some observations. Initially assume that the UE does not move. However, there is a UE motion variance applied to each iteration otherwise the initial particles quickly degenerate into one particle. Plot in Figure 3-9 is for the initial particles. The plot in Figure 3-10 is for after 800 iterations. Note that the AN is assumed to be in the origin at x=y=0 which is at the corner of the room. Note that this gives a problem in that there is an annulus of ambiguity as in Figure 3-11 with most of the particles outside of the room. This can be ameliorated with the assumption of side information in that the weight assigned to the particle that leaves the upper right hand quadrant is 0. Results of using side information is given in Figure 3-11. The result with the nulling of the weights outside of the possible room area confines the particles to the first quadrant as desired. Outputs were generated from PF3.m in appendix A.

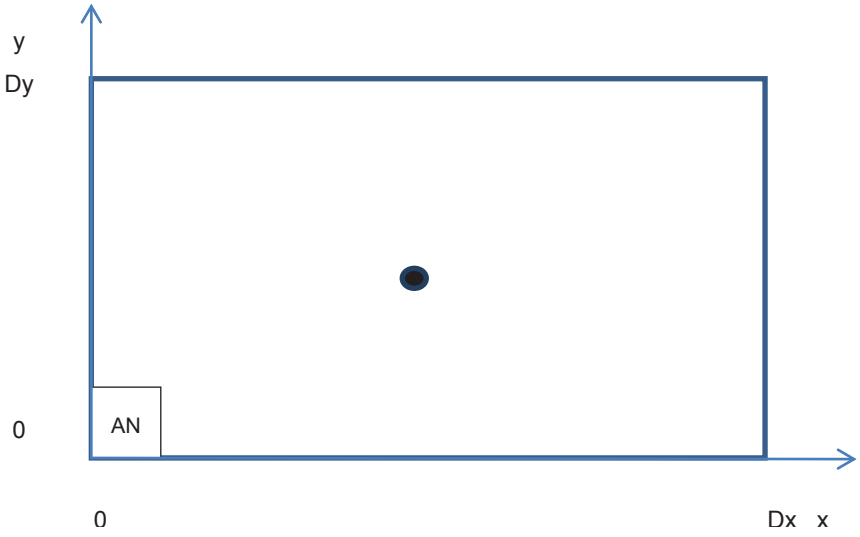

Figure 25: Outline of 2D room with one AN at the origin

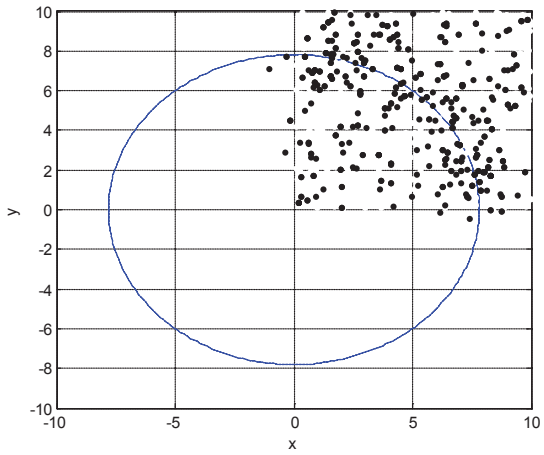

Figure 26: Initial conditions for room location search

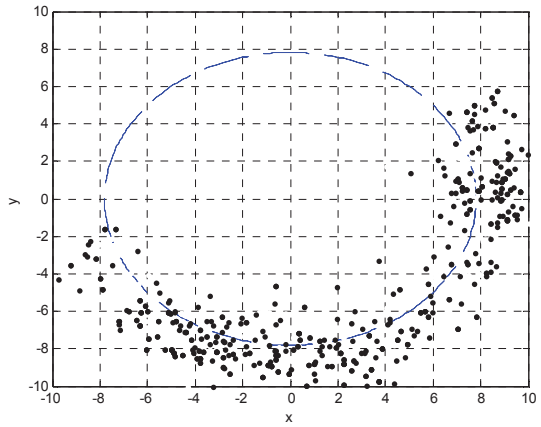

Figure 27: Final particle locations for room search with no wall constraints

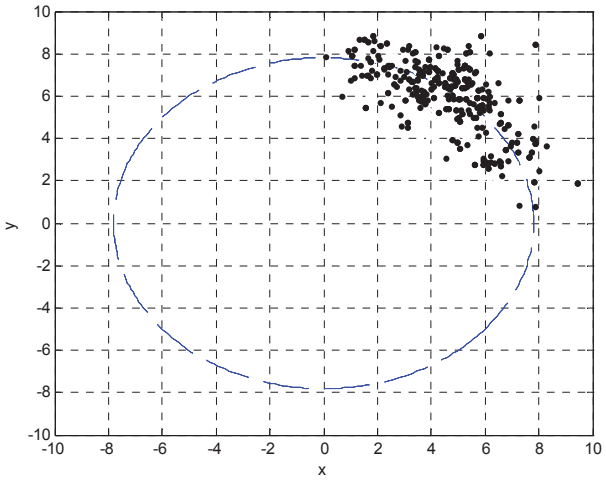

Figure 28: Final particle locations for room search with wall constraints

Next we consider two AN's located at (0,0) as before and an additional one at (0,10). This is shown in Figure 3-12. Convergence with the two AN's is very fast. After 10 iterations we have the particles as shown in Figure 3-13.

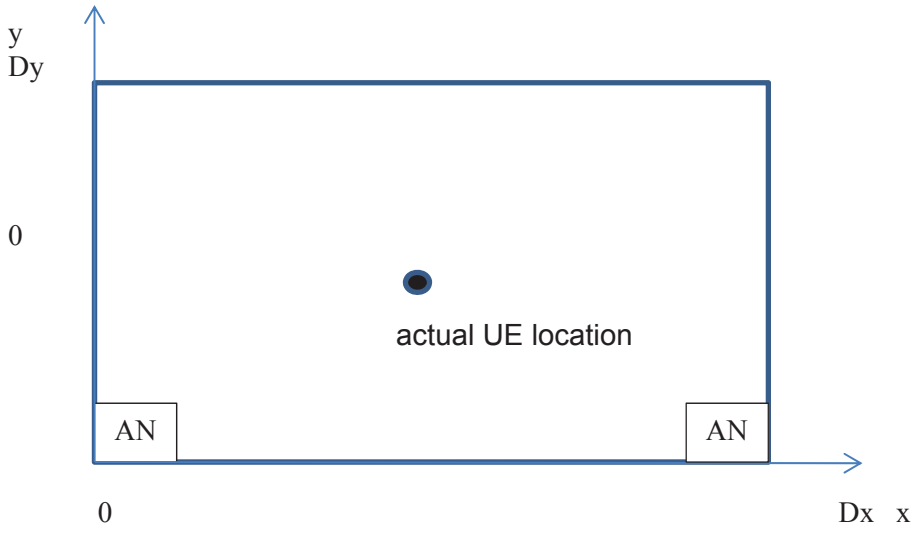

Figure 29: Room with two AN's located at (0,0) and (10,0)

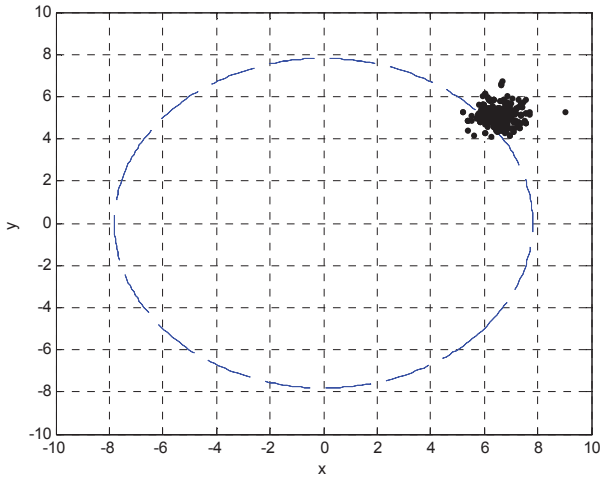

Figure 30: Final particle locations after 10 iterations for room search with wall constraints and two access nodes (pt_7.m)

The measurement is a result of the signals from both AN's as follows. The actual range to the UE from AN_1 and AN_2 is given as

$$z_{o1} = \sqrt{u_x{}^2 + u_y{}^2}$$

$$z_{o2} = \sqrt{(10 - u_x)^2 + u_y{}^2}$$

to which a random measurement uncertain is added of $N\left(0, \sigma_z^2\right)$ such that

$$z_{1,t} \sim N\left(z_{o1}, \sigma_z^2\right)$$
$$z_{2,t} \sim N\left(z_{o2}, \sigma_z^2\right)$$

The distances to each particle is given as

$$z_{1,t}^{[m]} = \sqrt{x_t^{[m]}.x^2 + x_t^{[m]}.y^2}$$
$$z_{2,t}^{[m]} = \sqrt{\left(x_t^{[m]}.x - 10\right)^2 + x_t^{[m]}.y^2}$$

The likelihood of the combined measurement is

$$p\left(z_{1,t}, z_{2,t} \mid x_t^{[m]}\right) = N\left(z_{1,t}, z_{1,t}^{[m]}, \sigma_z^2\right) N\left(z_{2,t}, z_{2,t}^{[m]}, \sigma_z^2\right)$$

The weight assigned to the particle $x_t^{[m]}$ is

$$w_t^{[m]} = \begin{cases} p\left(z_{1,t}, z_{2,t} \mid x_t^{[m]}\right) & 0 \le x_t^{[m]}.x \le 10, 0 \le x_t^{[m]}.y \le 10, \\ 0 & otherwise \end{cases}$$

Finally we have the case where there are 4 AN's with one in each corner of the room. The increased data allows for a sharper measurement kernel which results in faster convergence of the particles. Other than the two additional AN's, the problem geometry is the same as before. The difference is the weights are determined from the conditional measurement probability of

$$p\left(z_{1,t}, z_{2,t} \mid x_t^{[m]}\right) = N\left(z_{1,t}, x_{1,t}^{[m]}, \sigma_z^2\right) N\left(z_{2,t}, x_{2,t}^{[m]}, \sigma_z^2\right) N\left(z_{3,t}, x_{3,t}^{[m]}, \sigma_z^2\right) N\left(z_{4,t}, x_{4,t}^{[m]}, \sigma_z^2\right)$$

The result is a tight cluster of particles around the actual UE location as shown in Figure 3-14.

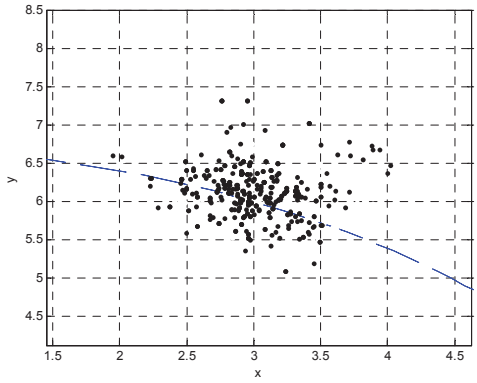

Figure 31: Example of PF for the case where the UE is located at x=3 and y=6

The Matlab program of pt_8 is a PF simulation of the ideal case of 4 AN's in the corners of the room. An observation that will be of relevance later is that of the score of the random variable. We have

$$v\left(x_t^{[m]}.x\right) = \sum_{i=1}^{4} \frac{\partial}{\partial x} \ln f_{z_i;x}\left(z_i; x_t^{[m]}\right)$$

Of emphasis is that the score accumulates as the sum of the individual scores of each measurement. This is true as the measurements are mutually independent.

3.3.4 Unknown receiver clock bias as an additional state variable

Consider the AN's to be perfectly synchronized and that the propagation is LOS. However, let there be an initial bias of the receiver clock which applies equally to all of the range measurements. We can solve for the PF by assuming a state vector of

$$x_t = \begin{bmatrix} x \\ y \\ b \end{bmatrix}$$

where b is the bias. The measurements are therefore modelled with this uncertainty as

$$p\left(z_{i,t} \mid x_t^{[m]}\right) = N\left(z_{i,t}, z_{i,t}^{[m]} + x_t^{[m]}.b, \sigma_z^2\right)$$

where $x_t^{[m]}.b$ is the bias state variable associated with the mth particle and $z_{i,t}^{[m]}$ is the range from the mth particle to the ith AN which is derivable from the state variable vector of the particle and given as

$$z_{i,t}^{[m]} = \sqrt{\left(x_t^{[m]}.x - a.x\right)^2 + \left(x_t^{[m]}.y - a.y\right)^2}$$

The initial distribution of the bias is an issue as the range of b is infinite with no prior knowledge. One possibility is to set the initial pdf of b as a uniform density over the range of $\left\{\min\left[z_{i,t}\right], \max\left[z_{i,t}\right]\right\}$ from which $x_0^{[m]}.b$ is drawn. Of course this can be tempered with prior knowledge of where the UE is initially. The bias will vary with time due to the clock instability of the receiver. Consequently it is reasonable to assume some form of random walk. Initially a wider variance can be assumed for converging the state vector which would be followed by a variance that is commensurate with the Allen deviation of the receiver clock. In terms of physical distance, this is on the order of 50 cm per second.

The following is a simulation of a PF with state variables of $x_t = \begin{bmatrix} x & y & b \end{bmatrix}$ the UE was stationary in this case with a position of x=3 and y=6. The bias term was b=1. Four AN's were assumed with a measurement deviation of 1. Figure 15 shows the results of the simulation demonstrating a fast convergence. The steady state fluctuations of the state variables is due to the markov variance assumed for the UE motion and the bias. Figure 16 shows the location estimation. Matlab program listing is PF4.m given in Appendix A.

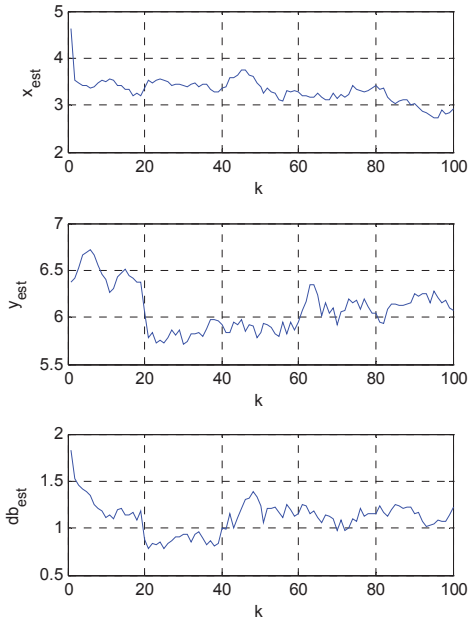

Figure 32: Output of PF for tracking x, y and the clock bias (actual values are x=3,y=6, b=1)

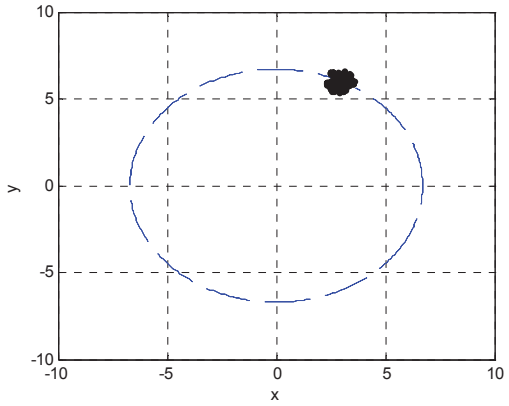

Figure 33: Output of PF for tracking x, y and the clock bias (actual values are x=3,y=6, b=1)

3.3.5 Modelling smooth trajectories for the UE

In the previous cases we looked at a first order markov model for the UE trajectory. Hence the position innovations were given as independent increments at each time step. This results in an unrealistic UE trajectory that is very jittery. Typically the trajectory is much smoother which is side information that we need to take into consideration. The assumption of a smooth trajectory is significant in that there is high correlation between the positions that can be used to filter the otherwise noisy location estimates. However, a first order markov model is required for the PF to be formulated. A first order markov is explicitly assumed in formulating the iterative procedure for determining the current posterior PDF. A PF based on a second or higher order is possible but is significantly more difficult and computationally expensive to implement. Consequently a first order markov will be used but with augmented state variables such that the UE trajectory is effectively modelled as a second order Markov.

Considering first the one dimensional case we can have a state variable vector of

$$x_t = \begin{bmatrix} x \\ v_x \end{bmatrix}$$

where x is the range and v_x is the velocity. For this example it is assumed that the velocity is a random walk with a Gaussian acceleration at each interval. Consider the step of drawing particles from

$$x_u^{[m]} \sim p\left(x_t \mid x_{t-1}^{[m]}, u_t\right)$$

We have

$$x_u^{[m]}.v_x \sim N\left(x_{t-1}^{[m]}.v_x, \sigma_a^2\right)$$

where σ_a^2 is the variance of the acceleration model. For the range we have

$$x_u^{[m]}.x = x_{t-1}^{[m]}.x + x_u^{[m]}.v_x T_s$$

where T_s is the update interval. For simplicity of notation, we will normalize the velocity such that $T_s = 1$. Consequently the single source of entropy is the acceleration.

There are two possibilities for proceeding. In the first procedure we consider the two state variables of r_t and v_t with an observation directly of r_t. The observation will be a noisy sample of the actual range such that

$$z_t \square N\left(x_{a,t}, \sigma_z^2\right)$$

where $x_{a,t}$ is the actual range at the time interval t. The weights are given with regards to the likelihood pdf as

$$w_t^{[m]} = N\left(z_t, x_t^{[m]}.x, \sigma_z^2\right)$$

Note how the variance of the measurement essentially determines the spread of the weights. The disadvantage with this method is that we have to carry a deterministic state variable of the range such that it can be directly compared to the measurement of z_t. Other than the comparison with the measurement, there is no other reason to carry the additional state variable. Note that the trajectory can always be computed from the mean of $x_t^{[m]}.v_x$ for all t. Later when the CV observations are considered, it will be observed that a direct observation of the velocity is possible that can be combined with the range observation from the LTE. An alternate procedure is possible by working with velocity only such that the range state variable does not have to be included. However. the disadvantage is that the range observation of z_t has to be numerically differentiated for a comparison with the velocity. The weights can be given as

$$w_t^{[m]} = N\left(z_t - z_{t-1}, x_t^{[m]}.v, 2\sigma_z^2\right)$$

Note that the assumed variance of the measurement has to be increased by a factor of 2 due to the differentiation operation. This update will work but is not totally correct as the successive velocity observations of $z_t - z_{t-1}$ and $z_{t+1} - z_t$ are now correlated. This mildly violates the Markov assumption made in the application of the PF such that the posterior pdf is incorrect. Hence the variance of the conditional mean will not provide the minimum location variance.

The other approach is to integrate the range of the particle. That is

$$x_t^{[m]}.r = \sum_{k=1}^{t} x_t^{[m]}.v$$

But if we do this then we may as well carry the state vector of range and velocity. Using the velocity only state vector seems to be only advantageous in the case where we have direct independent velocity measurements.

A simulation of the two state formulation is given in Figure 17 with a stationary UE located at the origin. The range measurements have Gaussian noise with variance of $\sigma_z^2 = 1$. M=400, $\sigma_a^2 = 0.01$ and kmax =1400, initial conditions were v=0 and r=0 for all particles

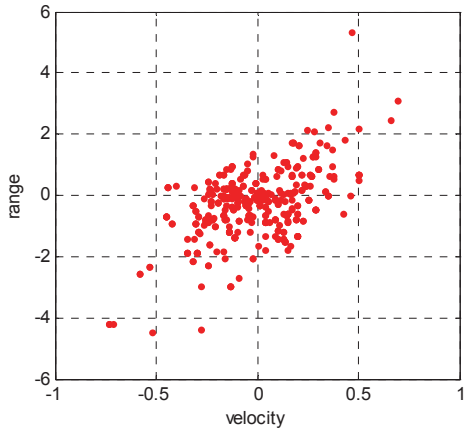

Figure 34: Particle states for stationary UE

It should be reemphasized that the outcome of the PF is the approximation of the posterior pdf and the spread is not indicative of the deviation of the estimate of the state variables. The mean of the posterior pdf is the state estimate and the deviation of this estimate could be lower bounded by the CRLB.

3.3.6 Smooth UE trajectory in two dimensions

Next consider the PF for the more general case where we have five components of the state vector as

$$x_t = \begin{bmatrix} x & y & v_x & v_y & b \end{bmatrix}^T$$

Initially we can assume that the velocities in x and y are given by independent accelerations. However, a better model is probably one that involves the azimuth pose of the UE such as

$$x_t = \begin{bmatrix} x & y & v & \theta & b \end{bmatrix}^T$$

Here θ is the azimuth pose and the velocity is assumed to follow along this bearing with ranges incremented accordingly as

$$r_{x,t} = r_{x,t-1} + v_{t-1}\cos\left(\theta_{t-1}\right)$$
$$r_{y,t} = r_{y,t-1} + v_{t-1}\sin\left(\theta_{t-1}\right)$$

This was tried but a problem that was encountered was that there was a conflict between the solutions of $\left[v,\theta\right]$ and $\left[-v,\theta\pm\pi\right]$. Attempts were made to maintain $v \geq 0$ but this resulted in some sporadic behavior and eventually severe loss of particle diversity. However, the state variables of $x_t = \left[x \quad y \quad v_x \quad v_y \quad b\right]^T$ behaved well and were therefore used. Further investigations are necessary in regards to this point as the handset is moved by a robot or person and hence $x_t^{[m]}.v_x$ and $x_t^{[m]}.v_y$ will be significantly correlated. In the test scenario a rectangular room of 4 AN's in each corner was be considered. The UE will transverse the room in a straight line trajectory as shown in the figure below.

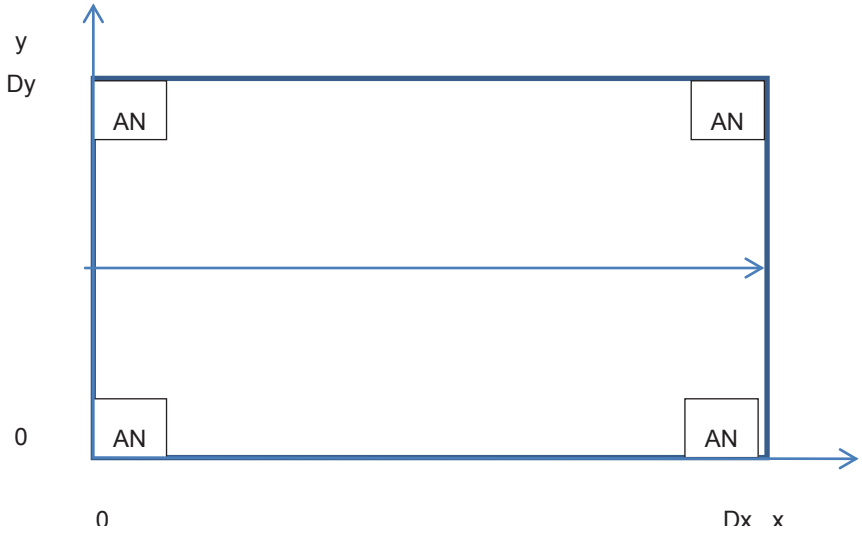

Figure 35: Outline of 2D room with four AN's in each corner

The initial uncertainties from which the initial state particles of x_0 are drawn are given as

$$x \square \delta\left(x - \frac{D_x}{2} \right)$$
$$y \square \pi\left(\frac{y - D_x/2}{D_x} \right)$$
$$v_x \square \pi\left(\frac{v_x - .1}{.1} \right)$$
$$v_y \square \pi\left(\frac{v_x}{.1} \right)$$

The actual trajectory is

$$x_a = v_{xa} t$$
$$y_a = D_y / 2$$
$$v_{xa} = .1$$
$$v_{ya} = .1$$
$$b = 0$$

The model is a random walk for $\{v_x, v_y, b\}$ with variances of

$$\sigma_a^2 = 0.01$$
$$\sigma_b^2 = 0.001$$

The range measurement error from each of the AN's has a variance of

$$\sigma_z^2 = 1$$

and no correlation. This is all the information necessary to implement the PF. Plots of the state variables are given in Figure 3-19.

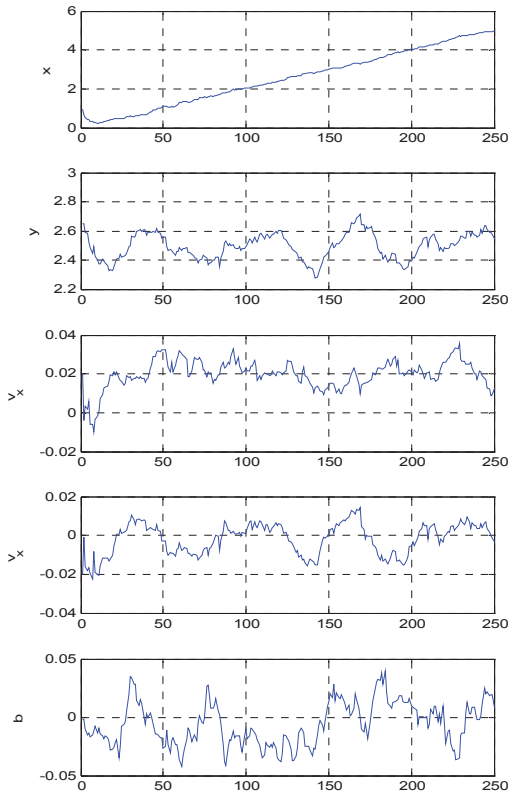

Figure 36: Mean particle states for uniformly moving UE

As observed, all of the state variables converge though they are noisy due to the uncertainty of the dynamic model of the UE motion. The position of the particles in $\{x, y\}$ space are shown below for the final iteration.

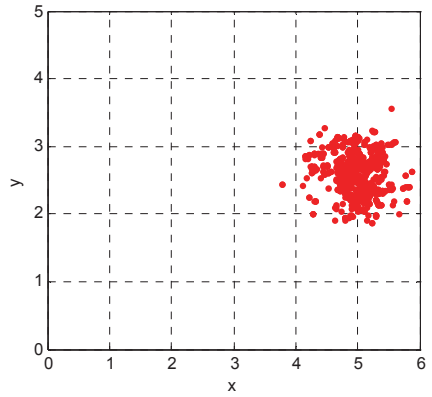

Figure 37: Particles marginalized over the x and y states

The same particles but with the associated weighting factor is shown below. The represented surface is the posterior pdf marginalized over the $\{r_x, r_y\}$ state variables.

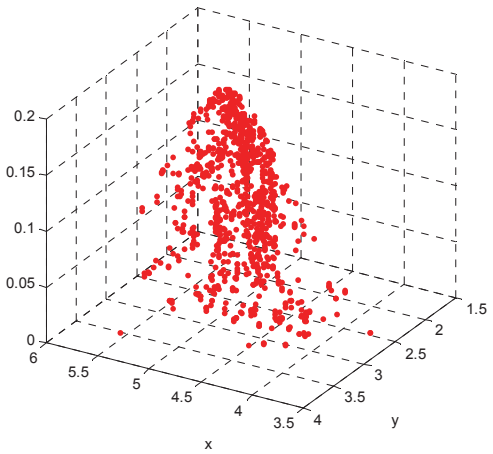

Figure 38: Particles marginalized over the x and y states but with weight indicated (equivalent to the marginalized posterior pdf)

A better means of observing this surface is necessary to develop. The matlab code for this simulation is given in PF5.m as listed in the appendix A. An interesting observation is in watching the movie of the particles in terms of $\{x, y\}$ which reveals an interesting flow away from the peak of the posterior pdf kernel where particles are then annihilated to be reborn as higher probability particles. This recycling is equivalent to scooping up the pdf material at the periphery and dumping at the central region of the kernel. Much like building a sand pile. When there are too few particles then they move in jerks, perhaps in the resampling many new particles get morphed into the few higher probability ones. Even with as few as 50 particles the PF converges but tracks poorly as the conditional means are highly variable.

3.4 Quality and completeness of LTE observables

3.4.1 Overview

Having developed the PF as applied to the SGL problem the next concern is the assessment of the quality and completeness of the set of LTE observables that is used to corral the particles along the actual trajectory of the state variables. The CV inputs will be used to determine the differential update of the UE and will be assessed in the following chapter. In the absence of CV inputs, the UE state variables will be updated based on a first order Markov random walk which is of course significantly weaker than having direct UE update measurements. Ideally the signal received by the UE is subject only to a pure delay of the flight time between the AN and the UE with the additional assumption that the UE and AN's are perfectly synchronized. In this case the measurements of $z_{i,t}$ will correspond directly to the physical distance between the AN and the UE. However, there are the following issues:

1. AN's are not perfectly synchronized and may in fact operate with isolated free running clocks

2. UE receiver clock is free running and not synchronized to the AN's

3. The propagation path from the AN to the UE is subject to an excess delay due to multipath

4. The propagation path is not stationary, and is subject to random transitions between LOS and NLOS propagation

Based on this, each AN to UE path is subject to a random excess delay. If the AN's are synchronized and the multipath all consistently NLOS or LOS for all of the AN-UE paths then we can regard the excess delay as having a mean value that is consistent for all of the AN's which is denoted by the state variable b. As described before, the unsynchronized UE clock is an issue for the initial estimate of b as it can range over $-\infty < b < \infty$. However with the initial set of measurements of $z_{i,t}$ the initial distribution of b can be set to a reasonable range.

If the AN's are not synchronized, which is typically the case for an ad-hoc data communications network, then the SGL becomes more difficult. We will now need to include an individual bias state variable for every AN-UE path. This significantly inflates the number of state variables that must be carried. However, it is possible provided that the UE moves throughout a sizable trajectory.

Multipath excess bias needs to be carefully considered. As mentioned if the paths remain either as LOS or NLOS and the AN's are synchronized then the model reduces to the single state variable b. If the AN's are unsynchronized such that separate b's are required then the difference in multipath propagation for each UE-AN path is of course contained in the separate b's and no additional modelling is required. However, separate bias variables significantly adds to the list of state variables that must be tracked which reduces the robustness and accuracy of the overall SGL tracking. Potentially, instead of having b be a continuous variable it is possible to use a Boolean variable to switch between specific LOS and NLOS models. However, it is not certain that the information imputed by this additional assumed structure will actually result in superior tracking

performance. In the initial work, the standard model will be a separate b variable for each AN source. Calibrated, synchronized AN networks will be considered as a special case. The issue then is that b can have significant variation of up to 100 meters in a moderately large building or even higher in a dense urban area for the excess delay component alone. This does not include the initial arbitrary delay offset. This is where initial UE calibration can be beneficial in that the UE will initially assign reasonable b values to each AN signal based on an approximate knowledge of where it is located. This is implementable by the PF. Bandwidth is an interesting consideration in that the broader the bandwidth, the smaller the variation of the component of b due to variation in the excess propagation delay.

3.4.2 Analysis of the completeness of measurements

The issue of an unknown bias is a problem for SGL that can typically be mitigated by the choice of trajectory. The quality of the information can be determined by the sensitivity of the posterior pdf to changes in the parameter. Hence this can also be determined by the PF. However, a more direct way is to consider the condition of the data matrix. In the following, the relative trajectory is the motion of the UE relative to its start position. Hence the relative trajectory may be known to the receiver but not it's start position nor orientation. Further define N as the number of sets of measurements. That is if there are L AN's then there are L components of each measurement set.

Consider the AN at (0,0) and the trajectory constrained along the x axis. The receiver is subject to an unknown bias. If the relative trajectory is known then there are two unknowns, b and x_o. In this case if $N \geq 2$ then the bias and start position of the trajectory can be resolved. If the trajectory is constrained to the x axis but otherwise unknown then there is a new unknown that is added (ie. x) for every measurement. Hence there will never be sufficient measurements to determine x and b. The best that can be done is to determine x_t and state the trajectory subject to an unknown trajectory offset that is assumed to remain constant.

Note that even if the trajectory is stationary such that $x_t = x_0$ then as b and x_0 depend on the data in exactly the same way then they can never be resolved. This can be expressed as

$$\begin{bmatrix} 1 & 1 \\ 1 & 1 \\ \vdots & \vdots \\ 1 & 1 \end{bmatrix} \begin{bmatrix} x_o \\ b \end{bmatrix} = \begin{bmatrix} z_1 \\ z_2 \\ \vdots \\ z_N \end{bmatrix}$$

Here the data matrix is

$$A = \begin{bmatrix} 1 & 1 \\ 1 & 1 \\ \vdots & \vdots \\ 1 & 1 \end{bmatrix}$$

which clearly only has a rank of 1 and can never resolve both b and x_0 without ambiguity.

Consider next an offset of the AN such that it is at a location of (0,1). We then have

$$z_n = b + \sqrt{1 + x_o^2}$$

Note we can consider a new variable of $c = \sqrt{1 + x_o^2}$ that is directly related to x_0. Hence the rank of A is still 1 regardless of N.

Now consider that the UE undergoes constrained motion along the x axis. As such we have a new unknown for each time step. Let a variable be $c_t = \sqrt{1 + x_t^2}$ and we have a data vector of matrix of $\begin{bmatrix} b & c_0 & \cdots & c_{N-1} \end{bmatrix}^T$ with a data matrix of

$$A = \begin{bmatrix} 1 & 1 & & \\ 1 & & 1 & \\ \vdots & & & \ddots \\ 1 & & & 1 \end{bmatrix}$$

The rank of A is N which is not sufficient for resolving N+1 variables. Suppose that the UE was stationary at one point with a dwell time of two samples. This would lead to A being N by N and N variables. However the matrix will have two repeated rows and again be rank deficient.

Next consider the case where there are two AN's located at (0,-1) and (0,1) with a UE trajectory constrained to run along the x axis then for every new position of the UE there is two measurements. The AN's are synchronized and the unknown is a common bias b. For one measurement set we have

$$\begin{bmatrix} z_1^0 \\ z_2^0 \end{bmatrix} = \begin{bmatrix} b + \sqrt{1 + x_o^2} \\ b + \sqrt{1 + x_o^2} \end{bmatrix}$$

Here the superscript denotes time index.

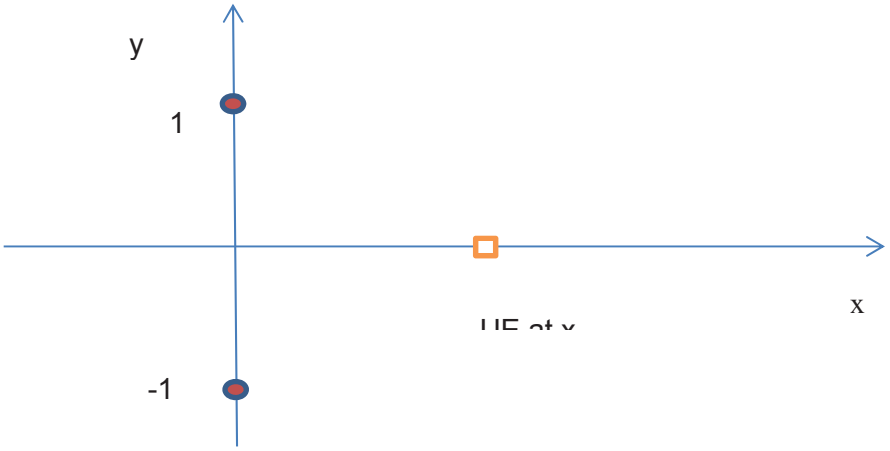

Figure 39: Two AN`s at (0,1) and (0,-1) and UE at x_o

Note the second measurement does not resolve the unknowns due to the symmetry. We need to break this symmetry which can be done by having the AN's at (0,0) and (0,1) resulting in

$$\begin{bmatrix} z_1^0 \\ z_2^0 \end{bmatrix} = \begin{bmatrix} b + x_o \\ b + \sqrt{1 + x_o^2} \end{bmatrix}$$

Now suppose that the initial position is known to within a small offset from x_0. That is $x_0 \to x_0 + \Delta x$ such that

$$\begin{bmatrix} z_1^0 \\ z_2^0 \end{bmatrix} = \begin{bmatrix} b + x_o + \Delta x \\ b + \sqrt{1 + (x_o + \Delta x)^2} \end{bmatrix}$$

Write

$$\begin{aligned} &\sqrt{1 + (x_o + \Delta x)^2} \\ &= \sqrt{1 + x_o{}^2 + 2x_o \Delta x + \Delta x^2} \\ &= \sqrt{1 + x_o{}^2} \sqrt{1 + \frac{2x_o \Delta x + \Delta x^2}{1 + x_o{}^2}} \\ &\approx \sqrt{1 + x_o{}^2} \left(1 + \frac{x_o \Delta x}{1 + x_o{}^2} \right) \\ &= \sqrt{1 + x_o{}^2} + \frac{x_o \Delta x}{\sqrt{1 + x_o{}^2}} \end{aligned}$$

such that

$$\begin{bmatrix} z_1^0 \\ z_2^0 \end{bmatrix} - \begin{bmatrix} x_o \\ b + \sqrt{1 + x_o^{\,2}} \end{bmatrix} = \begin{bmatrix} b + x_o + \Delta x \\ \dfrac{x_o \Delta x}{\sqrt{1 + x_o^{\,2}}} \end{bmatrix}$$

Then we have the modified measurement as

$$\begin{bmatrix} z'^0_1 \\ z'^0_2 \end{bmatrix} = \begin{bmatrix} z_1^0 \\ z_2^0 \end{bmatrix} - \begin{bmatrix} x_o \\ \sqrt{1 + x_o^{\,2}} \end{bmatrix} = \begin{bmatrix} 1 & 1 \\ 1 & \dfrac{x_o}{\sqrt{1 + x_o^{\,2}}} \end{bmatrix} \begin{bmatrix} b \\ \Delta x \end{bmatrix}$$

The rank of A is now 2 such that the variables of $\{b, x_o\}$ can be resolved. However, as x_o becomes large, A will become more singular.

Next consider the case of separate bias offsets for the AN's. We have the following

$$\begin{bmatrix} z_1^0 \\ z_2^0 \end{bmatrix} = \begin{bmatrix} b_1 + x_o \\ b_2 + \sqrt{1 + x_o^2} \end{bmatrix}$$

such that

$$\begin{bmatrix} z'^0_1 \\ z'^0_2 \end{bmatrix} = \begin{bmatrix} z_1^0 \\ z_2^0 \end{bmatrix} - \begin{bmatrix} x_o \\ \sqrt{1 + x_o^{\,2}} \end{bmatrix} = \begin{bmatrix} \Delta z_1^0 \\ \Delta z_2^0 \end{bmatrix} = \begin{bmatrix} 1 & 0 & 1 \\ 0 & 1 & \dfrac{x_o}{\sqrt{1 + x_o^{\,2}}} \end{bmatrix} \begin{bmatrix} b_1 \\ b_2 \\ \Delta x \end{bmatrix}$$

With two sets of measurements, the unknown vector of $\begin{bmatrix} b_1 & b_2 & \Delta x_1 & \Delta x_2 \end{bmatrix}^T$ can be resolved. Hence it is possible to determine the separate biases.

In another scenario the AN's are located at the points of (0,1) and (4,1) meters with an initial offset of $(x_o, 0)$ and the UE moves a distance of Δx. We then have for the first measurement

$$\begin{bmatrix} \Delta z_1^0 \\ \Delta z_2^0 \end{bmatrix} = \begin{bmatrix} 1 & 0 & \dfrac{x_o}{\sqrt{1+(x_o-4)^2}} \\ 0 & 1 & \dfrac{x_o}{\sqrt{1+x_o^2}} \end{bmatrix} \begin{bmatrix} b_1 \\ b_2 \\ \Delta x \end{bmatrix}$$

and for the next measurement

$$\begin{bmatrix} \Delta z_1^1 \\ \Delta z_2^1 \end{bmatrix} = \begin{bmatrix} 1 & 0 & \dfrac{2x_o}{\sqrt{1+(x_o-4)^2}} \\ 0 & 1 & \dfrac{2x_o}{\sqrt{1+x_o^2}} \end{bmatrix} \begin{bmatrix} b_1 \\ b_2 \\ \Delta x \end{bmatrix}$$

For N measurement sets we have an 2N by 3 matrix A of the structure

$$A = \begin{bmatrix} 1 & 0 & \dfrac{x_o}{\sqrt{1+x_o^2}} \\ 0 & 1 & \dfrac{(x_o-4)}{\sqrt{1+(x_o-4)^2}} \\ \vdots & \vdots & \vdots \\ 1 & 0 & \dfrac{Nx_o}{\sqrt{1+x_o^2}} \\ 0 & 1 & \dfrac{N(x_o-4)}{\sqrt{1+(x_o-4)^2}} \end{bmatrix}$$

In the following figure 3.23 the normalized standard deviation of the estimate of the state variables $\{b_1, b_2, \Delta x\}$ is plotted based on N=30 measurement pairs. That is if the measurement has a variance of 1 meter then the standard deviation of the range estimator is about 0.3 meters. The standard deviation of Δx is 0.02 meters such that over the N=30 increments this becomes 0.6 meters.

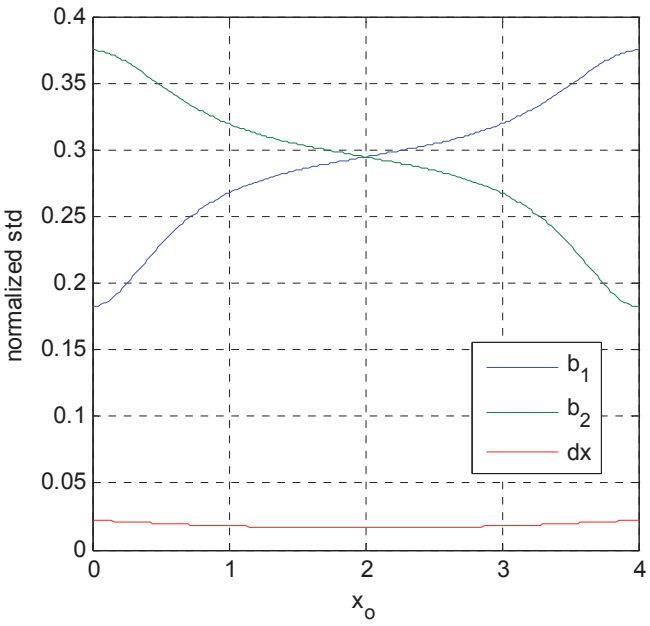

Figure 40: Normalized standard deviation of the estimate of the state variables $\{b_1, b_2, \Delta x\}$ *(see matlab program g1.m)*

It is interesting to contrast this with having just two pairs of measurements. This is the minimum leaving only one redundant equation. The deviations are higher as shown in Figure 3-24.

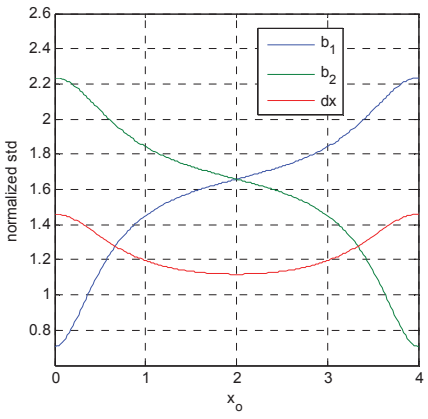

Figure 41: Normalized standard deviation of the estimate of the state variables $\{b_1, b_2, \Delta x\}$

The trend is as expected in that the higher the number of observations for the same number of state variables, the smaller the deviation. However, we still have to justify that the measurement accuracy of 1 meter is reasonable. Note that this is with the multipath bias as a state variable. Hence the question is if the equivalent LOS signal was considered, what would the SNR have to

be for a 1 meter standard deviation? The CRLB is a reasonable guide here with the relation given as (S. Kay volume 1)

$$\sigma_z^2 \geq \frac{c^2}{\rho F}$$

where ρ is the SNR of the measurement, c is the speed of light and F is the mean square bandwidth. For a 10 MHz bandwidth F is given as

$$F = \int_0^1 (2\pi f)^2 df \approx (10^7)^2 = \frac{(2\pi)^2}{3} \approx 10^{14}$$

$$\sigma_z^2 \geq \frac{c^2}{\rho F} = \frac{23}{\rho}$$

Hence ρ must be on the order of 16 dB to resolve the distance to about 1 meter. Unfortunately, this is not the complete issue. At each measurement, the return signal will be spread by the delay spread. Hence not only is there the unknown excess delay parameter b to be considered but there is the delay spread of the signal. In a 10 MHz bandwidth signal with a pulse width of about 200 nsec. Such a pulse is smeared out to be on the order of 400 nsec with the delay spread of the multipath. From the above formulation, this could be construed as being equivalent to halving the bandwidth. As F varies as the square of the bandwidth, this would imply that ρ would have to be increased by an additional 6 dB. Fortunately for indoor environments, SNR is typically not a problem. Also as will be described, the bulk of the experimentation will occur in the laboratory room that is removed from most sources of interference in the ISM band. Where problems will occur will be when the multipath is specular consisting of only a few components such that diffuse multipath of a Gaussian pdf cannot be considered to be an accurate representation.

The next example adds two additional AN's such that there is one in each corner of the 4 meter by 4 meter room. The standard deviation is shown as a surface plot. The state variable vector is given as $s = \begin{bmatrix} b_1 & b_2 & b_3 & b_4 & \Delta x \end{bmatrix}^T$. The component of the A matrix is given as

$$A_i = \begin{bmatrix} 1 & 0 & 0 & 0 & \dfrac{ix_i}{\sqrt{y_o^{\,2} + x_i^{\,2}}} \\ 0 & 1 & 0 & 0 & \dfrac{i(x_i - 4)}{\sqrt{y_o^{\,2} + (x_i - 4)^2}} \\ 0 & 0 & 1 & 0 & \dfrac{i(x_i - 4)}{\sqrt{(y_o - 4)^2 + (x_i - 4)^2}} \\ 0 & 0 & 0 & 1 & \dfrac{ix_i}{\sqrt{(y_o - 4)^2 + x_i^{\,2}}} \end{bmatrix}$$

with $x_i = x_0 + i\Delta x$. In Fig. 3-25 there is a mesh plot of the deviation of estimate of Δx for N=20 and $\Delta x = 0.1$. As noted the deviation exceeds the actual value of Δx. Also the deviation is not very sensitive to the actual UE location. For comparison the plot for the deviation of Δx is given for the case where the biases are all known in Fig. 3-25. Note that the deviation is about 20 dB less. As expected the unknown biases significantly inflate the variation of the estimate of Δx. When a common bias b is unknown then there is a slight increase in the deviation of Δx but it is rather insignificant being only on the order of ten percent. This is calculated by combining a row of ones with the fifth column of A.

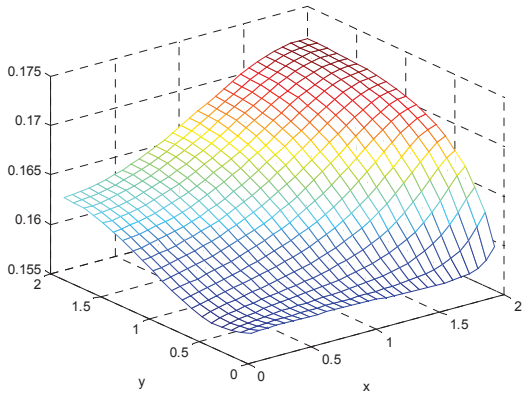

Figure 42: Normalized deviation of the estimate of Δx for N=20 and $\Delta x = 0.1$

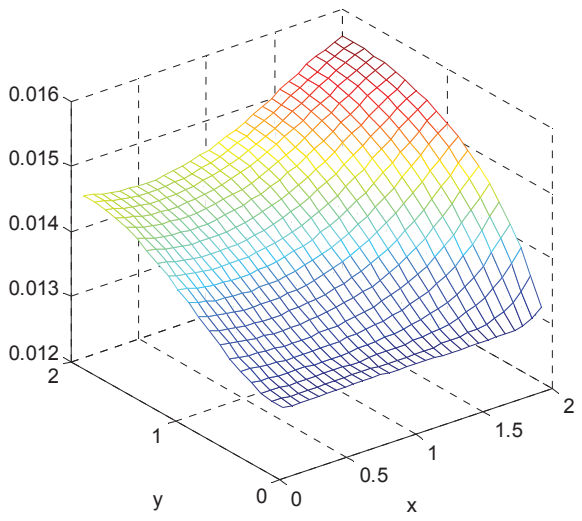

Figure 43: Normalized deviation of case when the biases are known (note the 20 dB reduction in the deviation)

In addition to the multipath bias, there is an uncertainty due to the clock instability between the UE and the rest of the AN system. A reasonable assumption that will be made here is that the network of AN's is tightly synchronized, perhaps locked to a central synchronizing clock or individually to a GPS source. This is a rather benign assumption to make as each AN will have a backhaul connection to a communication hub of sorts. However, the actual signal delay from this central hub to the AN's is difficult to actually control and maintain. Regardless of details, it will be assumed that the AN clocks are perfectly stable and that the clock instability resides with the UE. As the LTE hub is likely based on a higher quality clock than the UE, we can regard the Allen deviation of the UE clock as an indication of the overall clock stability. The Allen deviation of several clock sources is shown in the plot of Figure 3-27.

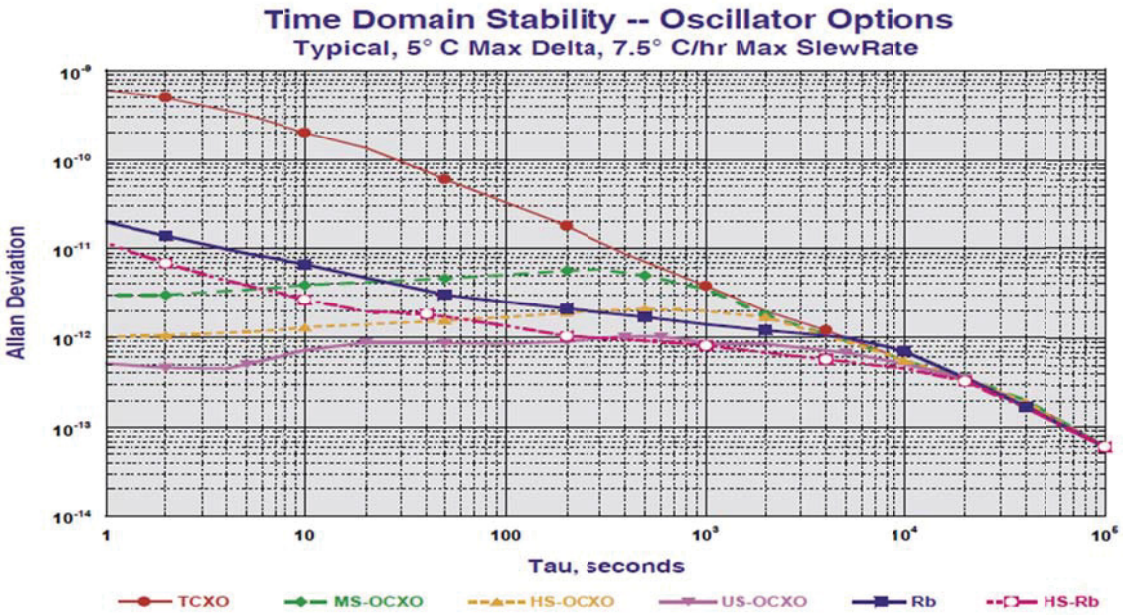

Figure 44: Plot of Allen deviation for various crystal based reference souces taken from http://www.endruntechnologies.com/frequency-standard-oscillators.htm.

Note the stability of the consumer based TCXO is on the order of 0.6×10^{-9}. This implies an instability of about 0.6 nsec per second which is very roughly on the order of 20 cm per second. More elaborate UE receivers could use higher quality oscillators. For instance, from the Allen deviation, it is possible to estimate the instability of b in terms of physical distance. This means that if the scenario consisted of 1UE and 1 AN then if the location was perfectly known at t=0 then that location would drift randomly as a random walk at a deviation of about 20 cm per second. However, as it is a random walk the deviation only increases proportionally to the square root of the time lapse in seconds and not linearly with time. Clearly it is not possible to do the SGL with LTE signals based on a single set of measurements of a stationary UE. The standard deviation of the multipath distance variation for an isolated spatial sample is typically well over 100 meters. The multipath spread can only be reduced by additional spatial samples. However, there is a time lag between these spatial samples that results in additional range errors due to the clock instability. A more significant issue is that it is not known where the spatial samples are taken from. Hence every new position generates a pair of new variables that need to be solved for. If the clock instability is temporarily ignored then there are NL total range measurements and 2N+L total unknowns. If the standard deviation of the range measurements is say 100 meters and we need to reduce the standard deviation of the x and y trajectory positions to about 1 meter then we must have $NL \geq 2N + L$ as a start. But with the DOP requirement of .01 (100 meters to 1 meter) we can approximately state that approximately 100 observation positions are needed (assuming that L is greater than 2).

3.4.3 Fisher Information Assessment of the Amount of Data from LTE samples

A direct quantitative approach to determining the potential accuracy of the trajectory estimation based on the LTE data samples can be formulated from the Fisher Information of the LTE range samples. Start with the sample case of position (x,y) in the area of one AN as shown in Figure 3-28.

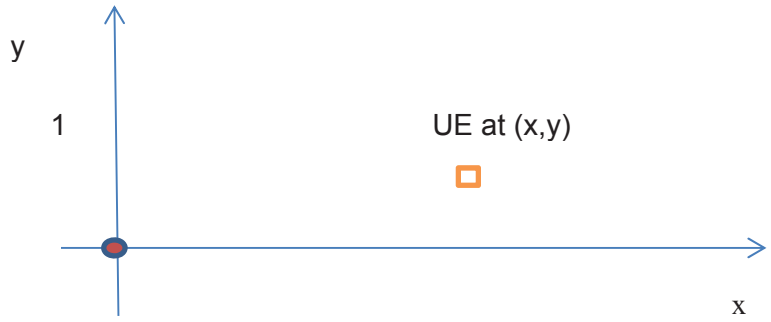

Figure 45: An AN`s at (0,0) and UE at (x,y)

We can determine the quantity of information provided by this single AN even though it by iself cannot determine the three unknowns of $\boldsymbol{\theta} = \begin{bmatrix} x & y & b \end{bmatrix}^T$. The model of the measurement is $z = \sqrt{x^2 + y^2} + b + \eta$

where $\eta \sim N\left(0, \sigma_z^2\right)$. Since $z \sim N\left(\sqrt{x^2 + y^2} + b, \sigma_z^2\right)$ then the Fisher Information is given as

$$\left[\mathbf{J}(\boldsymbol{\theta})\right]_{i,j} = \frac{\partial \mu(\boldsymbol{\theta})^T}{\partial \theta_i} \mathbf{Q}_\mathbf{z} \frac{\partial \mu(\boldsymbol{\theta})}{\partial \theta_j}$$

where $\mu(\boldsymbol{\theta}) = \sqrt{x^2 + y^2} + b$ such that

$$\frac{\partial \mu(\boldsymbol{\theta})}{\partial \theta_i} = \begin{bmatrix} \frac{x}{r} & \frac{y}{r} & 1 \end{bmatrix}$$

with $r = \sqrt{x^2 + y^2}$. Then we have

$$\mathbf{J}(\boldsymbol{\theta}) = \sigma_z^{-2} \frac{\partial \mu(\boldsymbol{\theta})^T}{\partial \theta_i} \frac{\partial \mu(\boldsymbol{\theta})}{\partial \theta_j} = \sigma_z^{-2} \begin{bmatrix} \frac{x^2}{r^2} & \frac{xy}{r^2} & \frac{x}{r} \\ \frac{xy}{r^2} & \frac{y^2}{r^2} & \frac{y}{r} \\ \frac{x}{r} & \frac{y}{r} & 1 \end{bmatrix}$$

Clearly as the rank of $\mathbf{J}(\boldsymbol{\theta})$ is one we cannot invert to get the CRLB of the variables. The measurements of the different AN's are assumed to be independent random variables. This is reasonable as the measurement noise comes from two sources which are the receiver noise and the multipath. The propagation path from the AN's to the UE are statistically independent provided that the AN's are sufficiently separated spatially (which may be violated in the MIMO cases) and that there is no tunnelling propagation or keyhole effect at the receiver. This is generally true. However, in some cases the multipath occurs close to the UE receiver and hence if two AN's are at similar bearings relative to the UE then the multipath will be correlated. This correlation will be ignored in the current analysis. The noise in the receiver is uncorrelated as the RS synchronization signals from the AN's have different spreading codes. Hence the noise subspaces are orthogonal. Consequently the FIM's from additional statistically independent AN signals can simply be added. This is developed through the scenario depicted in Figure 3-29.

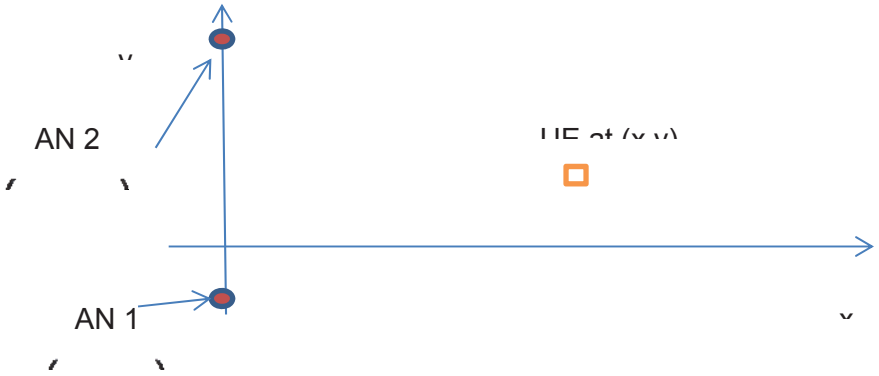

Figure 46: Two AN`s at $(x_{a,1}, y_{a,1})$ *and* $(x_{a,2}, y_{a,2})$ *and UE at (x,y)*

The FIM contributions from each UE is summed as $\mathbf{J}(\boldsymbol{\theta}) = \mathbf{J}_1(\boldsymbol{\theta}) + \mathbf{J}_2(\boldsymbol{\theta})$ with the components given as

$$\mathbf{J}_1(\boldsymbol{\theta}) = \sigma_z^{-2} \frac{\partial \mu_1(\boldsymbol{\theta})^T}{\partial \theta_i} \frac{\partial \mu_1(\boldsymbol{\theta})}{\partial \theta_j}$$

$$\mathbf{J}_2(\boldsymbol{\theta}) = \sigma_z^{-2} \frac{\partial \mu_2(\boldsymbol{\theta})^T}{\partial \theta_i} \frac{\partial \mu_2(\boldsymbol{\theta})}{\partial \theta_j}$$

where $\boldsymbol{\theta} = \begin{bmatrix} x_u & y_u & b_1 & b_2 \end{bmatrix}$

$$\frac{\partial \mu(\boldsymbol{\theta})^T}{\partial \boldsymbol{\theta}} = \begin{bmatrix} \frac{x_u}{r_{u1}} & \frac{y_u}{r_{u1}} & 1 & 0 \end{bmatrix}$$

$$\frac{\partial \mu(\boldsymbol{\theta})^T}{\partial \boldsymbol{\theta}} = \begin{bmatrix} \frac{x_u}{r_{u2}} & \frac{y_u}{r_{u2}} & 0 & 1 \end{bmatrix}$$

This can be extended to L AN nodes as

$$\mathbf{J}(\boldsymbol{\theta}) = \sum_{i=1}^{L} \mathbf{J}_i(\boldsymbol{\theta}) = \sigma_z^2 \sum_{i=1}^{L} \frac{\partial \mu_i(\boldsymbol{\theta})^T}{\partial \boldsymbol{\theta}} \frac{\partial \mu_i(\boldsymbol{\theta})}{\partial \boldsymbol{\theta}}$$

with the components given as

$$\frac{\partial \mu_i(\boldsymbol{\theta})^T}{\partial \boldsymbol{\theta}} = \begin{bmatrix} \frac{x_u}{r_{ui}} & \frac{y_u}{r_{ui}} & 0 & \cdots & 1 & \cdots & 0 \end{bmatrix}$$

Clearly as each AN measurement adds a new bias variable the FIM will never become invertible unless the UE moves spatially and additional samples are added.

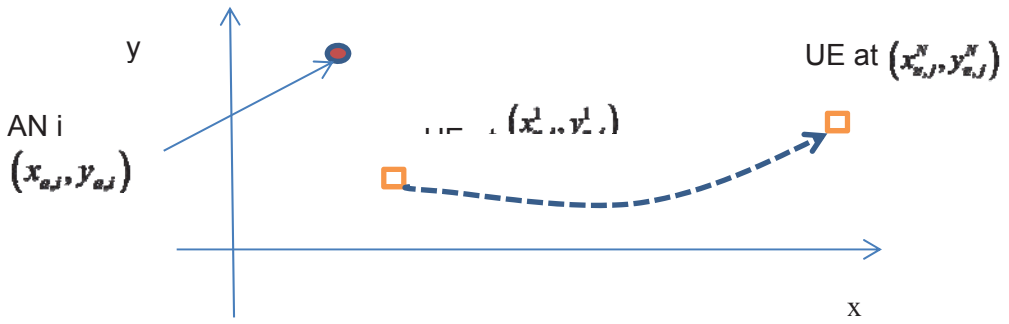

Figure 47: General UE and AN locations

Consider the trajectory consisting of N points as illustrated in Figure 3-31. Suppose that the trajectory was completely unknown such that each new trajectory point of $\left(x^t_{u,j}, y^t_{u,j}\right)$ provided L new range measurements but at the same time added two new UE position variables to be solved for. Note that the variance associated with these position variables would be minimum of σ_z^2/L with ideal geometry and the effect of the L unknown biases ignored. This variance is too high to be of practical interest. Hence we seek a parameterized trajectory of fewer variables.

Consider first the other extreme of a completely known trajectory of N points. The variance of the remaining bias terms will be σ_z^2/N. If the half wavelength of about 10 cm is considered then 10 independent measurements per meter length of the trajectory is possible. With a 5 meter trajectory this would imply that the bias variance is reduced from a 70 meter standard deviation to about 10 meters which is still very large. However, the bias stays relatively constant unless the multipath changes. Hence a longer path is possible. However, the multipath is not stationary. Hence the multipath will dominate a the accuracy. A simple stationarity argument can be posited as follows. Consider a trajectory down a hallway passing AN's along the way. The propagation is going to change from multipath to LOS back to multipath. The segment of distance over which we have stationarity is on the order of 10 meters. Hence 100 independent measurements of the multipath is achievable with a reduction of a factor of 10 of the measurement standard deviation σ_z. Due to multipath, the amount of information of each LTE measurement is very little. Therefore, unless there is a significant ratio of the number of independent multipath samples to DOF of the trajectory, the LTE signals as a source of UE location information will not be sufficient. This reduction in the trajectory DOF can come from the CV measurement.

Consider the extreme where the path is totally correlation but with unknown parameters as the constant velocity straight line path as illustrated in Fig.3-30. A CV system sensor for tracking the short segment behaviour of the trajectory is considered with a couple of outstanding parameters that the CV system cannot resolve with the input of the LTE system. Initially consider the case where the start position of the trajectory is known as well as the localized trajectory itself, say from CV observables. There is only one unknown which is the angle of the trajectory. As the

start position is known as well as the positions of the AN's then the biases of $\{b_1, b_2, b_3, b_4\}$ are measureable. Now suppose that the trajectory is 3 meters and the half wavelength is 10 cm resulting in 30 uncorrelated measurements for each AN. Additionally the AN has a bandwidth of 20 MHz and that the coherence bandwidth is about 10 MHz. This provides the 60 uncorrelated measurements of the trajectory for each AN. Hence the aggregate for the 4 AN's is then 240 measurements. Clearly even if the NLOS multipath has a significant spread then the trajectory angle is easily resolvable to within a meter. This is an indication of the significant advantage of combining wireless LTE based SGL with CV sensors.

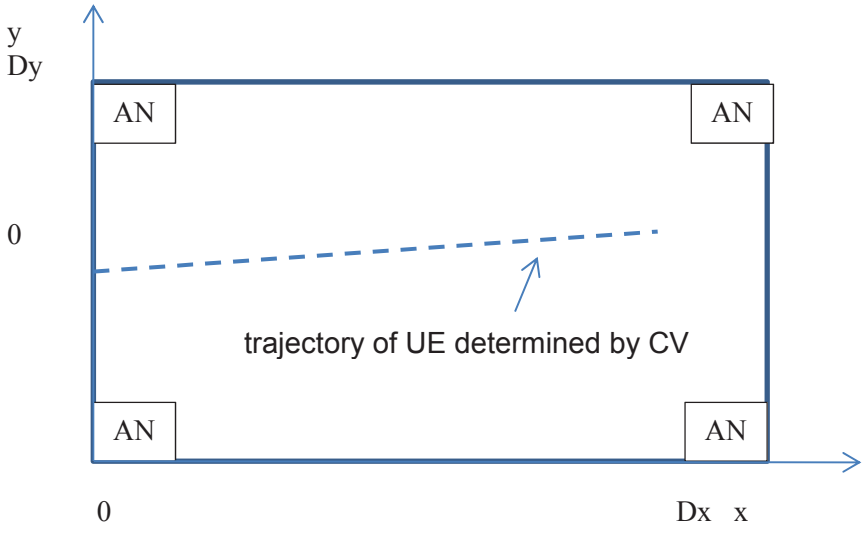

Figure 48: Fixed segment deviations

In this example if one of the AN's was LOS with a much smaller variation then this would be the dominant LTE measurement. However, the PF does not weigh the LOS measurement different than the NLOS measurements unless it is known to be LOS. Note though that since the trajectory is known that it is possible to go back over the measurements made and verify that the AN is a LOS measurement and hence the PF would weigh this contribution much more heavily. Note that this gives significant impetus to implementing the Boolean switch. That is that it is much more significant than the issue of switching between b values.

Next consider the case where the UE oscillator instability is accounted for. Note that if the LOS condition is made for an AN and the trajectory is known based on CV observations then we have a measureable random walk of the oscillator as a function of the trajectory position based on the single AN. We can do a best fit to determining the angle of the trajectory. Note that this is not very precise. If the trajectory takes 10 seconds to traverse, then the deviation of time will be about $0.6\sqrt{10}$ nsec which is about 1 meter. However that is just taking the end sample into account. This will be reduced when all the samples taken every 10 cm are used. Also there are 180 remaining NLOS measurements that can be used which will significantly reduce this distance uncertainty. We can use a BLUE estimator to quickly come up with the variance estimate as

$$\mathbf{x} = \mathbf{H}\theta + \mathbf{w}$$

where $\mathbf{x}$ is the vector of measurements relative to the LOS AN.

$$\mathbf{H} = \begin{bmatrix} 0 & d & \cdots & (N-1)d \end{bmatrix}^T$$

where d is the distance between measurements of 10 cm and N is the number of measurements of 30. The measurement covariance is about

$$\mathbf{C} = \begin{bmatrix} \sigma_m^2 & & & \\ & \sigma_m^2 + 20^2 & & \\ & & \ddots & \\ & & & \sigma_m^2 + (N-1)20^2 \end{bmatrix}$$

where σ_m^2 is the variance of the measurement without oscillator instability which we set at 1000.

The variance of the angle is about

$$\sigma_\theta = \sqrt{\left(\mathbf{H}^T\mathbf{C}^{-1}\mathbf{H}\right)^{-1}} = 0.1 \quad rad$$

Over the 3 meter trajectory we will be out about 0.3 meters.

If the AN propagations are all NLOS and we have 240 measurements total but we do have a clock instability then the precision will be likely within a meter but this depends on the multipath spreading. The LTE signals generate the observables for the PF which are represented by the abstract vector of z_t. As well the conditional pdf of $p\left(z_t \mid x_t^{[m]}\right)$ is required such that the PF weights can be determined. There are two ways of approaching this. The first is that the RS segments of the LTE signal are used as discrete frequency estimates of the channel gain over the operating band of the LTE signal. This then gives an estimate of the transfer function in the frequency domain of the downlink channel from which the bandpass impulse response can be generated. For processing though, it is more direct to correlate the received LTE signal directly with the locally generated replica of the LTE synchronization signal blocks. This gives the correlation peak directly. The location of the first initial peak provides an estimate of the signal arrival time. We refer to this as the TOA of the signal. However it is understood here that the TOA is biased as explained previously and hence it is not the true TOA.

4 Computer Vision Observables

4.1 Overview

The LTE observables as described in the previous section are useful as the wireless signals are generally ubiquitous throughout the indoor environment. The LTE AN's are generally frequency synchronized but may not be time synchronized. The resulting timing biases are a nuisance and degrade the overall performance of the SGL. However the lack of synchronization can be ameliorated through the use of ma multitude of measurements and the assumption of a smooth trajectory. Unfortunately over short trajectory intervals the wireless observables can be highly variable. CV observables, on the other hand, complement the LTE observables in that they provide high accuracy over shorter segments of the trajectory. They also have the very important attribute of being independent of any LTE signalling providing observables where LTE downlink signals are not available or compromised in some way. Wireless signal shadowing, deep fading and jamming from intentional or non-intentional sources are plausible scenarios which compromise the SGL system based on LTE alone. CV represents a very suitable compliment to LTE by providing a mix of passive and active observables based on image processing of a small incidental camera collocated with the UE receiver.

CV provides sensor inputs to determine segments of the trajectory as inputs to the particle filter as illustrated in Figure 5.1. This sensor input will track features on the ground manifold surface updating outputs of the differentials in the pose and the translational motion relative to the ground manifold at the frame rate interval of the camera. Depending on the processing this will be typically 10 to 30 fps. As a result the short term trajectory will be relatively highly accurate but will be subject to longer term drift. Hence this complements the LTE and other wireless signalling observables which provide poor short term accuracy but are not subject to drift.

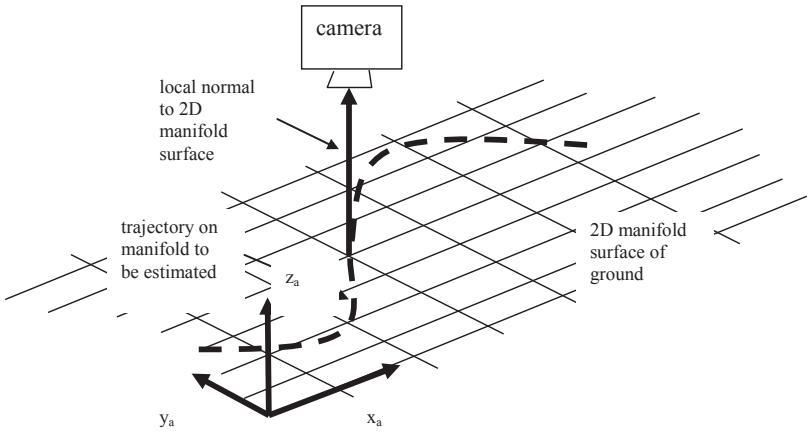

Figure 49: Ego-motion of camera sensor relative to a 2D manifold surface

Ego-motion sensory input from the camera has been considered in significant detail. An issue is that the camera system can accurately determine the trajectory relative to the ground surface coordinate system of $\{x_a, y_a, z_a\}$ provided that there is no camera tilt to be concerned with. If the camera is mounted on a stable cart system and used over a smooth floor surface then tilt angles will be sufficiently small that they can be neglected. However, a hand held device is subject to significant random tilt that must be continuously measured.

After much experimentation with accelerometers as tilt sensors, single camera providing ego-motion estimation over multiple image frames, stereoscopic cameras and tri-scopic cameras, the best system was to use a combination of a small laser projector and IR camera. Such a unit is found in the Microsoft Kinect sensor. The operation is described briefly as follows.

The Kinect uses a small low power laser projector with a diffraction grating that generates approximately 30,000 points over the FOV with high accuracy. A tightly coupled IR camera correlates the grid projection pattern to find the correspondence of the scattering points. As such the $\{x, y, z\}$ coordinates of each of the spatial scattering points can be determined. In essence, the Kinect paints a scattering point texture on the ground manifold which can be estimated in 3D based on the corresponding registration with the IR camera. This is illustrated in figure 4-2.

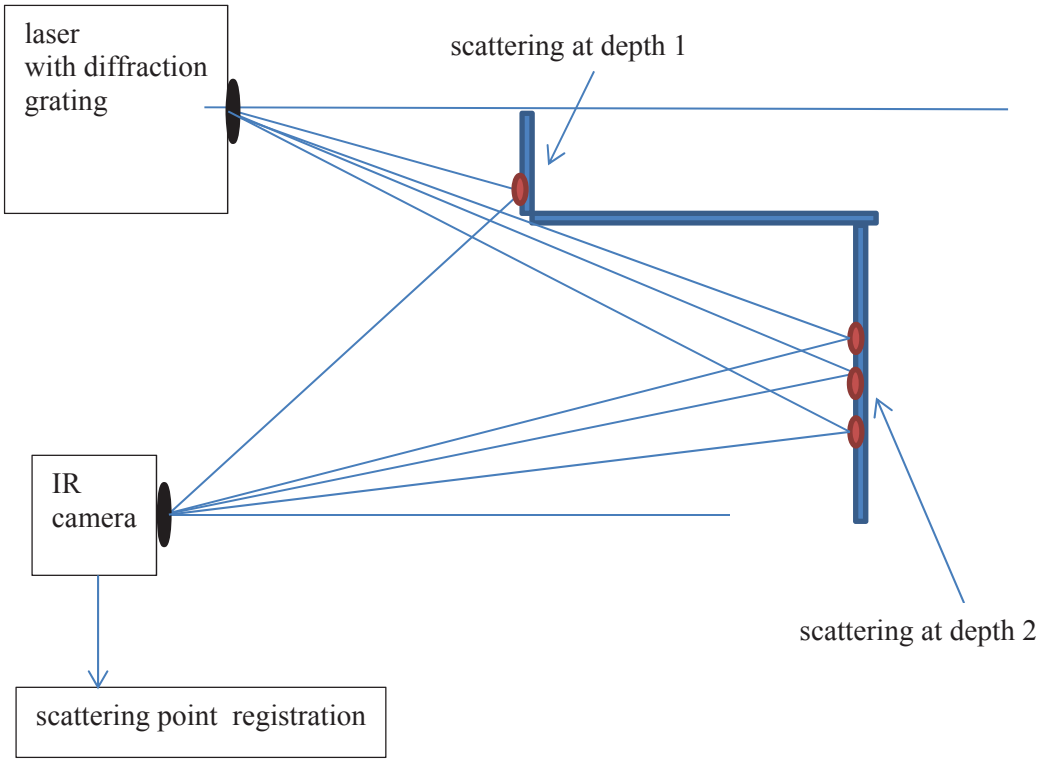

Figure 50: Determination of the 3D spatial coordinates of the scattering points generated by the projector.

As illustrated there will be a point cloud that will correspond to each plane that is in the FOV. For the ground manifold tracking, determining the set of points on the ground plane is straight forward as the image in the FOV is assumed to be uncluttered with the ground surface having a large radius of curvature. This assumption can be waived with further development by grouping the point clouds into different sub-planes. The fundamental issue is then to determine the plane of the local ground manifold in the camera coordinate system. For clarity the following coordinate systems are defined.

system	description
$\{x_a, y_a, z_a\}$	Reference to ground manifold – right hand system
$\{x_b, y_b, z_b\}$	Translated relative to $\{x_a, y_a, z_a\}$ on ground centered directly below the camera center. That is z_b passes through camera center – right hand system
$\{x_c, y_c, z_c\}$	Rotated relative to $\{x_b, y_b, z_b\}$ - right hand system
$\{x_d, y_d, z_d\}$	Azimuth rotated camera centric system with origin at the camera center – left hand system with z_d in the direction of z_c
$\{x_e, y_e, z_e\}$	Camera centric coordinate system referenced to camera with origin at camera center and with two tilt angles relative to the $\{x_e, y_e, z_e\}$ coordinate system – left hand system

Consequently, the ground manifold related systems of $\{x_a, y_a, z_a\}$, $\{x_b, y_b, z_b\}$ and $\{x_c, y_c, z_c\}$ are right hand systems with the z axis collinear with the ground manifold normal vector. The camera centric coordinate systems of $\{x_d, y_d, z_d\}$ and $\{x_e, y_e, z_e\}$ are left hand coordinate systems where the z axis is pointed predominantly vertical into the ground.

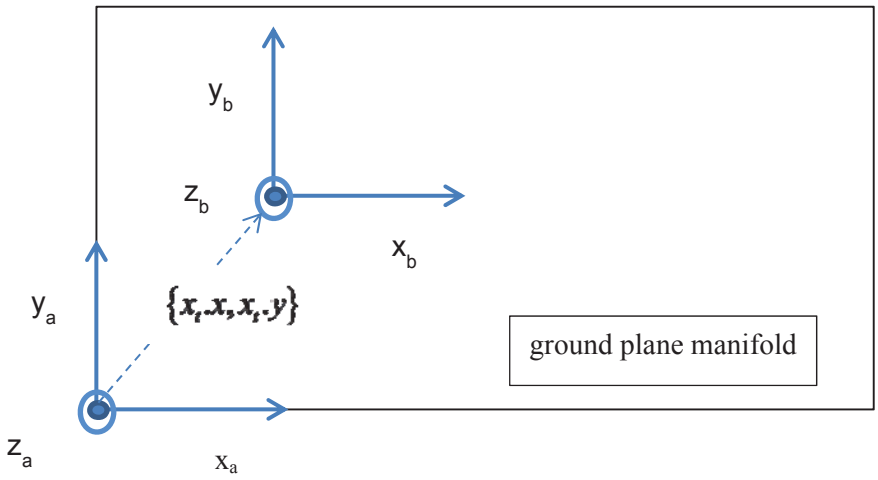

Figure 51: Relation between the coordinate systems $\{x_a, y_a, z_a\}$ *and* $\{x_b, y_b, z_b\}$

Figure 5.3 shows the relation between the coordinate systems of $\{x_a, y_a, z_a\}$ and $\{x_b, y_b, z_b\}$ as a simple translation given by the position of the UE in the ground plane relative to a reference point which is (0,0) in the $\{x_a, y_a, z_a\}$ static ground reference system. The positional offset variables of $\{x_t.x, x_t.y\}$ are part of the PF state vector as the x and y coordinates of the UE. Figure 5.4 shows the relation between the coordinate systems of $\{x_b, y_b, z_b\}$ and $\{x_c, y_c, z_c\}$

as a positive CCW rotation in azimuth about the z axis denoted as $x_t.a_z$. When there is no confusion this is shortened as a_z. A vector in the $\{x_b, y_b, z_b\}$ coordinates can be referenced to the $\{x_c, y_c, z_c\}$ system by the rotation operator of

$$\mathbf{R}_{\mathbf{cb}} = \begin{bmatrix} \cos(a_z) & \sin(a_z) & 0 \\ -\sin(a_z) & \cos(a_z) & 0 \\ 0 & 0 & 1 \end{bmatrix}.$$

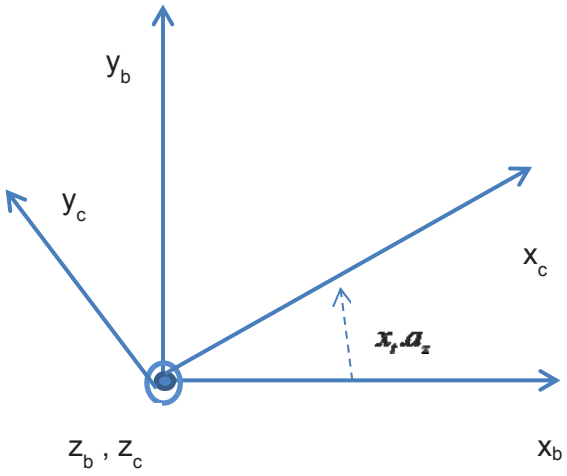

Figure 52: Relation between the coordinate systems $\{x_b, y_b, z_b\}$ *and* $\{x_c, y_c, z_c\}$

Next the relation between the systems of $\{x_c, y_c, z_c\}$ and $\{x_d, y_d, z_d\}$ is shown in Figure 5.5. The height of the UE camera center from the ground plane is h. Note that while $\{x_c, y_c, z_c\}$ is a right hand coordinate system, $\{x_d, y_d, z_d\}$ is a left hand system. The reason for this change is that it is desirable to have the z axis of the camera along the optical axis while maintaining the x and y vectors in the same direction. It is most convenient to express the transformation as an affine operation that is given as

$$\begin{bmatrix} x_d \\ y_d \\ z_d \end{bmatrix} = \begin{bmatrix} 1 & 0 & 0 & 0 \\ 0 & 1 & 0 & 0 \\ 0 & 0 & -1 & h \end{bmatrix} \begin{bmatrix} x_c \\ y_c \\ z_c \\ 1 \end{bmatrix}$$

This transformation takes a vector in $\{x_c, y_c, z_c\}$ relative to the $\{x_d, y_d, z_d\}$ coordinates.

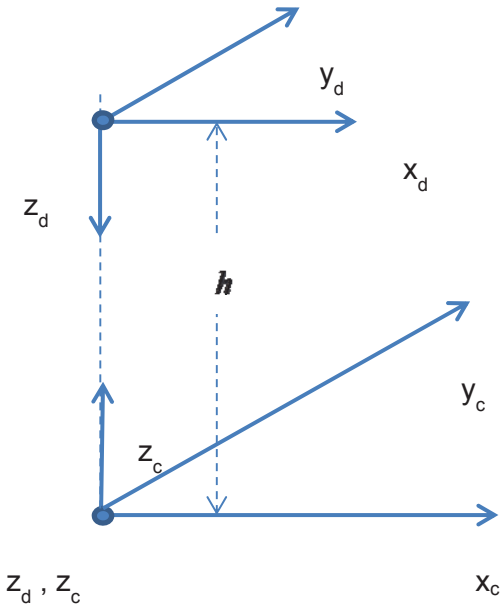

Figure 53: Relation between the coordinate systems $\{x_c, y_c, z_c\}$ *and* $\{x_d, y_d, z_d\}$

Finally we have the transformation between the $\{x_d, y_d, z_d\}$ coordinates and the $\{x_e, y_e, z_e\}$ which accounts for the two tilt angles of the camera which are denoted as a_x and a_y. These are CCW positive rotations about the y_d and z_d coordinate vectors. The order of the rotations is assumed to be a_x followed by a_y. As such a vector in the $\{x_d, y_d, z_d\}$ coordinates is described relative to the $\{x_e, y_e, z_e\}$ coordinates as

$$\begin{bmatrix} x_e \\ y_e \\ z_e \end{bmatrix} = \begin{bmatrix} \cos(a_y) & 0 & \sin(a_y) \\ 0 & 1 & 0 \\ -\sin(a_y) & 0 & \cos(a_y) \end{bmatrix} \begin{bmatrix} 1 & 0 & 0 \\ 0 & \cos(a_x) & -\sin(a_x) \\ 0 & \sin(a_x) & \cos(a_x) \end{bmatrix} \begin{bmatrix} x_d \\ y_d \\ z_d \end{bmatrix}$$

We denote the transformation as

$$\mathbf{R}_{\mathbf{ed}} = \begin{bmatrix} \cos(a_y) & 0 & \sin(a_y) \\ 0 & 1 & 0 \\ -\sin(a_y) & 0 & \cos(a_y) \end{bmatrix} \begin{bmatrix} 1 & 0 & 0 \\ 0 & \cos(a_x) & -\sin(a_x) \\ 0 & \sin(a_x) & \cos(a_x) \end{bmatrix}$$

defined as a vector in $\{x_d, y_d, z_d\}$ is observed in $\{x_e, y_e, z_e\}$ as $\mathbf{R_{ed}}$ multiplied by that vector. Of course this reference can be reversed by using the transpose operator given as $\mathbf{R_{ed}}^T$.

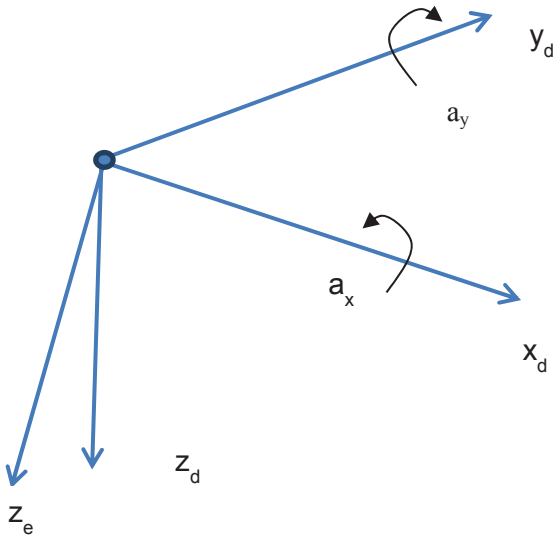

Figure 54: Mapping between the coordinate systems $\{x_d, y_d, z_d\}$ and $\{x_e, y_e, z_e\}$ with positive tilt rotation angles of a_x and a_y

A last complication is that the IR and the RGB cameras are not at the same location but separated by a distance of D_{cam} along the x_e axis. This is not really a problem as the scattering points of the IR and RGB cameras are treated separately. However, there may be reason to consider the relative positions of the sets of scattering points. It is most convenient to consider the RGB camera as being at the center of the $\{x_e, y_e, z_e\}$ frame and the IR camera offset from this by D_{cam} along the x_e axis. Note that the effective height of the IR camera above the ground plane is affected by this.

The scattering point cloud as seen from the IR camera will be registered by the disparity map outcome of the Kinect in the $\{x_f, y_f, z_f\}$ coordinate system. An algorithm based on determining the ground plane with a least squares analysis was developed as follows. Suppose that the points (x_1, y_1, z_1) to (x_N, y_N, z_N) are the projected scattering points of the ground plane surface. The plane equation is given by the linear equation of $Ax + By + Cz + D = 0$ where {A,B,C,D} are coefficients to be determined. We set this up as a matrix as follows:

$$\begin{bmatrix} x_1 & y_1 & z_1 & 1 \\ x_2 & y_2 & z_2 & 1 \\ \vdots & \vdots & \vdots & \vdots \\ x_N & y_N & z_N & 1 \end{bmatrix} \begin{bmatrix} A \\ B \\ C \\ D \end{bmatrix} = \begin{bmatrix} 0 \\ 0 \\ \vdots \\ 0 \end{bmatrix}$$

The solution of the homogeneous over-determined set of equations (assuming N>>4) is determined by using the singular value decomposition (SVD) of the N by 4 model matrix Q defined as

$$Q = \begin{bmatrix} x_1 & y_1 & z_1 & 1 \\ x_2 & y_2 & z_2 & 1 \\ \vdots & \vdots & \vdots & \vdots \\ x_N & y_N & z_N & 1 \end{bmatrix}$$

If the N scattering points perfectly coincided with the ground plane then there would be a single singular value of 0 that corresponds to the solution of the plane coefficients. That is the corresponding right singular vector of Q with the zero singular value gives the [A,B,C,D] coefficients. It is convenient to normalize these coefficients such that the coordinates of the plane normal vector of

$$\mathbf{n_e} = \begin{bmatrix} A \\ B \\ C \end{bmatrix}$$

is such that $\|\mathbf{n_e}\| = 1$. The appropriately scaled value of D gives the negative offset of the plane from the origin along the normal vector. Also there is an ambiguity of the direction of the normal vector which is arbitrarily set to be such that C is positive. Hence the normal will nominally be in a direction that is away from the camera. By definition, the ground surface normal in the $\{x_d, y_d, z_d\}$ system is $\begin{bmatrix} 0 & 0 & -1 \end{bmatrix}^T$. Therefore we have

$$\begin{bmatrix} A \\ B \\ C \end{bmatrix} = \begin{bmatrix} \cos(a_y) & 0 & \sin(a_y) \\ 0 & 1 & 0 \\ -\sin(a_y) & 0 & \cos(a_y) \end{bmatrix} \begin{bmatrix} 1 & 0 & 0 \\ 0 & \cos(a_x) & -\sin(a_x) \\ 0 & \sin(a_x) & \cos(a_x) \end{bmatrix} \begin{bmatrix} 0 \\ 0 \\ -1 \end{bmatrix} = \mathbf{R_{ed}} \begin{bmatrix} 0 \\ 0 \\ -1 \end{bmatrix}$$

From this we can solve for the tilt angles from

$$A = -\sin\left(a_y\right)\cos\left(a_x\right)$$
$$B = \sin\left(a_x\right)$$
$$C = -\cos\left(a_y\right)\cos\left(a_x\right)$$

Note for small tilt angles this is approximately

$$A \approx -a_y$$
$$B \approx a_x$$
$$C \approx -1$$

Clearly due to noise, the singular value corresponding to the homogeneous solution will not be perfectly zero. However, there will generally always be (unless the plane surface is not flat or the data is excessively noisy) a singular value that is much smaller than the other three values. The residual of this singular value relative to the three other larger singular values will give an indication of the quality of the scattering point data. The tilt angles determined for the IR camera are directly applicable for the RGB camera also (provided that they are suitably calibrated).

The plane equation is determined by the IR camera must be transformed to the RGB camera. It is assumed that the RGB camera sits a distance of D_{cam} from the IR camera as illustrated in Figure 5.6. We merely have to translate the ground plane such that it is relative to the RGB camera instead. This is done with the simple transformation of

$$Ax_{IR} + By_{IR} + Cz_{IR} + D = 0$$

Now we have

$$x_{RGB} = x_{IR} - D_{cam}$$
$$y_{RGB} = y_{IR}$$
$$z_{RGB} = z_{IR}$$

such that

$$Ax_{IR} - AD_{cam} + By_{IR} + Cz_{IR} + D + AD_{cam} = 0$$

or

$$Ax_{RGB} + By_{RGB} + Cz_{RGB} + \left(D + AD_{cam}\right) = 0$$

Hence the only change is that of modifying the D coefficient of the plane equation to make it referenced to the RGB camera instead of the IIR camera.

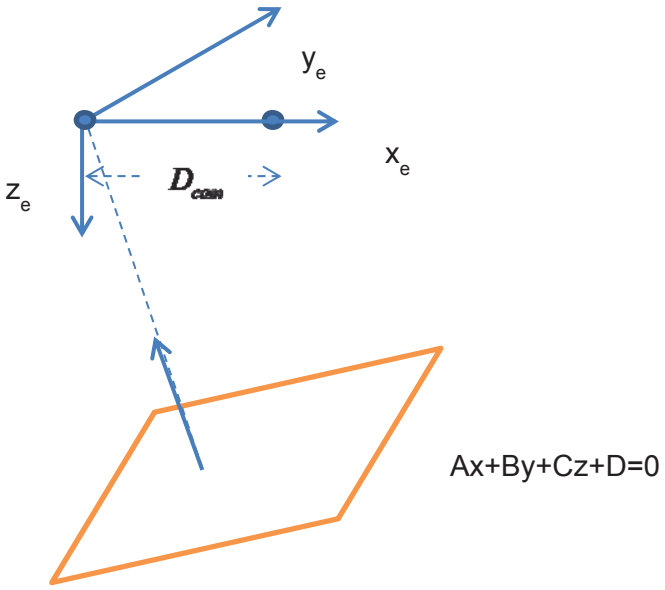

Figure 55: Relation between the IR and the RGB camera and the cloud point plane

As the RGB camera is primary in terms of the projection of the ground fp's the geometry is modified slightly with the RGB camera now at the origin of the $\{x_e, y_e, z_e\}$ frame with the modified plane equation. Next, the projection of the fp's in the image plane onto the ground plane is considered. This is done as shown in Figure 5.7. There are two steps involved. The first is to determine where the fp resides on the ground plane. This is based on a parametric vector. Assume that the fp is in the image plane of $I(x, y)$ with coordinates of i.x and i.y. This corresponds to a focal plane of f such that the vector in the $\{x_e, y_e, z_e\}$ frame passing through the fp is $[i.x, i.y, f]^T$. The interception point of the plane is then simply

$$Ati.x + Bti.y + Ctf + D = 0$$

Find t that satisfies this equation and this gives the point in the plane. The result is the position vector in the $\{x_e, y_e, z_e\}$ frame which is then transformed into the $\{x_c, y_c, z_c\}$ frame. The differential ego-motion will be determined based on these differentials. This is done by

$$\begin{bmatrix} f_x \\ f_y \\ f_z \end{bmatrix} = \mathbf{R}_{ce} \begin{bmatrix} ti.x \\ ti.y \\ tf \end{bmatrix}$$

As a check we can use that f_z=0.

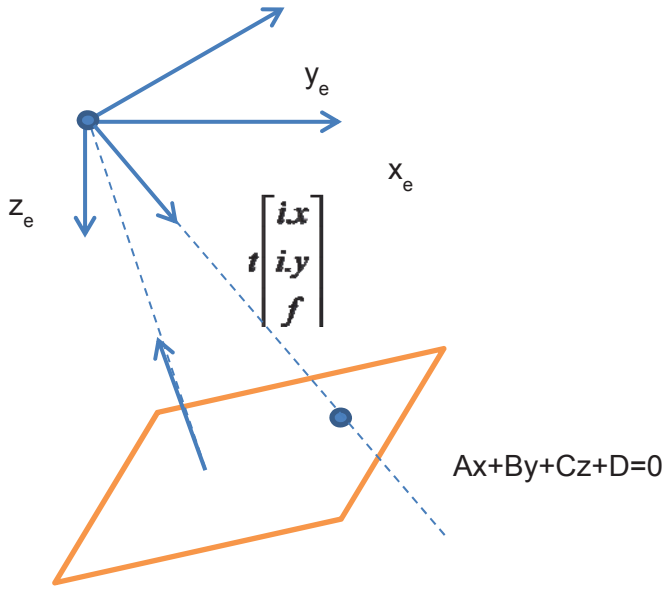

Figure 56: Projection of fp's onto tilted ground plane

The overall procedure is given as the following steps:

1. The IR camera determines the corresponding set of scattering points on the ground manifold.

2. The SVD method is used to determine the singular vector giving the ground plane coefficients of {A,B,C,D} relative to the $\{x_e, y_e, z_e\}$ coordinate system with the IR camera at the origin.

3. The D coefficient is modified as $D \to D + AD_{cam}$ which determines the ground plane with the RGB camera at the origin in the $\{x_e, y_e, z_e\}$ frame.

4. The set of fp's are determined as angles in the FOV of the RGB camera resulting in $[i.x, i.y, f]^T$ for each fp. Here f is a suitable scaling factor such that $[i.x, i.y, f]^T$ is a directional vector in the $\{x_e, y_e, z_e\}$ frame.

5. Find the plane intercept point for each fp by solving $Ati.x + Bti.y + Ctf + D = 0$ for t.

6. Map the vector of $[ti.x, ti.y, tf]^T$ from the $\{x_e, y_e, z_e\}$ frame to the $\{x_c, y_c, z_c\}$ frame.

7. Proceed with computing the differentials in the $\{x_c, y_c, z_c\}$ frame.

when $a_x = a_y = a_z = 0$. Starting with $\{x_f, y_f, z_f\}$ we have a normal in the direction of z_f. Then apply a positive rotation of a_x followed by a positive rotation of a_y such that the ground plane normal vector referenced to the $\{x_f, y_f, z_f\}$ coordinate system is given as

$$\begin{bmatrix} n_{f.x} \\ n_{f.y} \\ n_{f.z} \end{bmatrix} = \begin{bmatrix} \cos(a_y) & 0 & \sin(a_y) \\ 0 & 1 & 0 \\ -\sin(a_y) & 0 & \cos(a_y) \end{bmatrix} \begin{bmatrix} 1 & 0 & 0 \\ 0 & \cos(a_x) & -\sin(a_x) \\ 0 & \sin(a_x) & \cos(a_x) \end{bmatrix} \begin{bmatrix} 0 \\ 0 \\ 1 \end{bmatrix}$$

With this definition we can then determine the normal vector in the $\{x_f, y_f, z_f\}$ coordinate frame and translate to the $\{x_e, y_e, z_e\}$ coordinate frame based on the inverse (transpose) of these operations. Initially we will assume that the trajectory has to be relative to the ground plane such that we are given the above expression. That is we have $\begin{bmatrix} n_{f.x} \\ n_{f.y} \\ n_{f.z} \end{bmatrix}$

Based on these rotations, we can map the position vectors of the feature points observed in the RGB camera which is in the $\{x_f, y_f, z_f\}$ frame to the position vector in the $\{x_e, y_e, z_e\}$ frame. From the height which is given as

$$h_{RGB} = h_{IR} - n_{f.x} d_{IR}^{RGB}$$

we can map the feature points into the azimuth rotated coordinate frame of $\{x_c, y_c, z_c\}$. Here

h_{RGB} - vertical height of RGB camera in $\{x_c, y_c, z_c\}$ frame

h_{IR} - vertical height of IR camera in $\{x_c, y_c, z_c\}$ frame

d_{IR}^{RGB} - distance between IR and RGB camera centers

The camera system relies on two sets of feature points. The active scattering points as generated by the projector laser is one set which essentially establishes the ground plane normal in the tilted camera frame of $\{x_f, y_f, z_f\}$. The other set of feature points are those that reside on the ground plane itself. They are passive and detected by the RGB camera operating in the visible band. These feature points are therefore static relative to the $\{x_c, y_c, z_c\}$ frame. Furthermore they are assumed to be coincident with the ground plane such that the z_c component of each feature point

is assumed to be 0. Then we have a set of K fp's denoted as $\left\{f_{x,k}^{i}, f_{y,k}^{i}\right\}$. Here the index i denotes the image frame, k denotes the feature index and $\{x, y\}$ denote the estimate of the physical location of the feature point on the ground surface consistent with the $\{x_c, y_c, z_c\}$ frame. These feature points are paired with corresponding feature points of the previous frame given as $\left\{f_{x,k}^{i-1}, f_{y,k}^{i-1}\right\}$. If the correspondences cannot be found then the feature point is not used for tracking but stored for the next frame. A feature point track must emerge before it is eligible for use in estimating the ego-motion. In this way many of the sporadic feature points, that would distort the egomotion estimate, can be pruned away.

The motion of the kth feature point from the i-1th to the ith frame is described by the affine transformation in the $\{x_c, y_c, z_c\}$ frame as follows

$$\begin{bmatrix} f_{x,k}^{i} \\ f_{y,k}^{i} \end{bmatrix} = \begin{bmatrix} \cos\left(\Delta a_{z,i}\right) & \sin\left(\Delta a_{z,i}\right) & -\Delta x_i \\ -\sin\left(\Delta a_{z,i}\right) & \cos\left(\Delta a_{z,i}\right) & -\Delta y_i \end{bmatrix} \begin{bmatrix} f_{x,k}^{i-1} \\ f_{y,k}^{i-1} \\ 1 \end{bmatrix}$$

where $\Delta a_{z,i}$ is defined as the incremental CCW rotation of the camera relative to the ground reference frame. That is the incremental azimuthal rotation of $\{x_c, y_c, z_c\}$ relative to $\{x_b, y_b, z_b\}$. This equation can be reorganized into the least squares format for the kth fp as

$$\begin{bmatrix} f_{x,k}^{i} \\ f_{y,k}^{i} \end{bmatrix} = \begin{bmatrix} f_{x,k}^{i-1} & f_{y,k}^{i-1} & -1 & 0 \\ f_{y,k}^{i-1} & -f_{x,k}^{i-1} & 0 & -1 \end{bmatrix} \begin{bmatrix} \cos\left(\Delta a_{z,i}\right) \\ \sin\left(\Delta a_{z,i}\right) \\ \Delta x_i \\ \Delta y_i \end{bmatrix}$$

This is assembled for all of the K fp's and the overdetermined set of relations solved for the parameter vector of $\left[\cos\left(\Delta a_{z,i}\right) \quad \sin\left(\Delta a_{z,i}\right) \quad \Delta x_i \quad \Delta y_i\right]$.

As will be described in the following section the PF accounts for the integration of these differentials into the particle state variables. Hence the outcome of the CV is the differentials only. A problem is that the azimuth angle will drift over time. Hence it would seem that we should add the absolute azimuth angle as a state variable so that the particles can ameliorate the angle drift problem. Hence the state vector of

$$x_t = \begin{bmatrix} x & y & v_x & v_y & a_z \end{bmatrix}^T$$

is necessary. In this case the camera observables map directly into the last three state variables. In summary we have the following processing.

1. From the IR camera we get the plane normal of the ground manifold which provides the variables required for the transformations between the coordinate systems of $\{x_c, y_c, z_c\}$ and $\{x_f, y_f, z_f\}$.

2. The feature points of the RGB camera are then mapped from the $\{x_f, y_f, z_f\}$ frame to the rotated ground frame of $\{x_c, y_c, z_c\}$. As such we get sets of fp's for successive frames that are used in a least squares formulation to extract out the differentials of $\{\Delta x_i, \Delta y_i, \Delta a_{z,i}\}$.

3. Inputs from the LTE observables regarding the delay of each of the transmitted signals from the AN's is input.

4. Each particle is updated statistically based on the presumed dynamics. These updates are combined to update the state variable vectors of each particle from x_{t-1} to x_t.

5. The LTE and camera observables are combined to generate a new weight of each of the particles.

It is interesting that the rotation rate of the CV output is equivalent to a rate gyro if an IMU system was used. Furthermore the velocity components of Δx_i and Δy_i are more useful than the acceleration from potential accelerometers for several reasons:

1. accelerometer outputs of an accelerometer tend to drift significantly. In the CV system there is virtually no drift.

2. There is a loss of accuracy with accelerometers as they must be integrated twice to get the position.

3. The velocity estimates are difficult to get accurately with the LTE or other wireless sources due to the short term deviations of multipath.

Note that the PF state vector will generally have states for the velocities in the x and y directions. The CV outputs can be directly applied. Furthermore it is advantageous to track the pose of the UE as this can be coupled with the probability for the velocity increment. That is the velocity vector is generally correlated with the pose azimuth angle. Of course this depends on how the handheld is actually held.

The PF needs to know the covariance matrix of the estimate of the differentials of $\{\Delta x_i, \Delta y_i, \Delta a_{zi}\}$. At the completion of the LS calculation we then have the estimate of the measurement vector given as $\hat{\mathbf{M}} = \mathbf{A}\hat{\mathbf{P}}$. This resulted in the error vector as

$$\mathbf{e}_i = \mathbf{M}_i - \hat{\mathbf{M}}_i$$

Hence the total square error is given as

$$\varepsilon_i = \mathbf{e}_i^T \mathbf{e}_i = \left(\mathbf{M}_i - \hat{\mathbf{M}}_i\right)^T \left(\mathbf{M}_i - \hat{\mathbf{M}}_i\right)$$

which is minimized by the LS formulation. We can consider the statistical properties of this minimization by examining the Taylor series of ε_i. We write this as a function of the incremental state variables $\mathbf{s_i} = \begin{bmatrix} \Delta x_i & \Delta y_i & \Delta h_i & \Delta\theta_i \end{bmatrix}^T$ and not the direct variables of $\{\Delta x_i, \Delta y_i, C_i, S_i\}$ which captures the mild nonlinear aspects involved.

Let $\mathbf{s_o}$ and $\hat{\mathbf{s}}$ denote the actual and estimated incremental state vector of $\mathbf{s_i}$. The properties of this error function $\varepsilon\left(\hat{\mathbf{s}}, \mathbf{s_o}\right)$, will be explored based on the analysis of the second order Taylor series expansion which is given as

$$\varepsilon\left(\hat{\mathbf{s}}, \mathbf{s_o}\right) = \varepsilon\left(\mathbf{s_o}, \mathbf{s_o}\right) + \nabla\varepsilon\left(\mathbf{s_o}, \mathbf{s_o}\right)\left(\hat{\mathbf{s}} - \mathbf{s_o}\right) + \tfrac{1}{2}\left(\hat{\mathbf{s}} - \mathbf{s_o}\right)^T \nabla^2\varepsilon\left(\mathbf{s_o}, \mathbf{s_o}\right)\left(\hat{\mathbf{s}} - \mathbf{s_o}\right) + H.O.T.$$

By definition of the error we have $\varepsilon\left(\hat{\mathbf{s}}, \mathbf{s_o}\right) = 0$. The gradient is defined as

$$\nabla\varepsilon\left(\mathbf{s_o}, \mathbf{s_o}\right) = \left[\frac{\partial\varepsilon\left(\hat{\mathbf{s}}, \mathbf{s_o}\right)}{\partial s_1} \quad \frac{\partial\varepsilon\left(\hat{\mathbf{s}}, \mathbf{s_o}\right)}{\partial s_2} \quad \cdots \quad \frac{\partial\varepsilon\left(\hat{\mathbf{s}}, \mathbf{s_o}\right)}{\partial s_L}\right]^T \Bigg|_{\hat{\mathbf{s}} = \mathbf{s_o}}$$

where L is the number of state variables which is also zero by the quadrature definition of ε. The Hessian is defined as the outer gradient product of the state variable vector as

$$\nabla^2\varepsilon\left(\mathbf{s_o}, \mathbf{s_o}\right) = \left[\begin{matrix} \frac{\partial^2\varepsilon\left(\hat{\mathbf{s}}, \mathbf{s_o}\right)}{\partial s_1 \partial s_1} & \cdots & \frac{\partial^2\varepsilon\left(\hat{\mathbf{s}}, \mathbf{s_o}\right)}{\partial s_1 \partial s_L} \\ \vdots & \ddots & \vdots \\ \frac{\partial^2\varepsilon\left(\hat{\mathbf{s}}, \mathbf{s_o}\right)}{\partial s_L \partial s_1} & \cdots & \frac{\partial^2\varepsilon\left(\hat{\mathbf{s}}, \mathbf{s_o}\right)}{\partial s_L \partial s_L} \end{matrix}\right] \Bigg| \hat{\mathbf{s}} = \mathbf{s_o}$$

In the LS formulation we can easily determine the Hessian for the estimation variables as $\mathbf{A^T A}$. The curvature in each eigen direction is determined by the eigenvalues of $\mathbf{A^T A}$. The variance of the estimates will be given by

$$\mathbf{Q_P} = \left(\mathbf{A}^T \mathbf{Q_M}^{-1} \mathbf{A}\right)^{-1}$$

The diagonal components are the variance of each of the components as required for the PF. $\mathbf{Q_M}$ is the covariance matrix of the feature point positions in the image plane. This matrix will be a block diagonal matrix with 2x2 blocks for the x and y components of each feature. The fp's themselves are statistically independent as they occur a minimum distance from each other.

4.2 Integration of the particle filter with LTE and CV observables

There are two main types of PF's that can be used to integrate the LTE and CV observables into the SGL estimates. In the first case the state variable of the PF is $x_t = \begin{bmatrix} x & y & b & a_z \end{bmatrix}^T$. The main outputs are the actual UE location variables of $x_t.x$ and $x_t.y$. There are optionally delay parameters for each of the LTE AN's can be included instead of the common $x_t.b$ as developed before. The LTE pseudo-ranges provide observables for combinations of $x_t.x$ $x_t.y$ and $x_t.b$ forming the z_t observables as before. The CV observables, $\{\Delta x, \Delta y, \Delta a_z\}$ are used for the UE position updates. The other main type of PF uses a state variable vector as

$$x_t = \begin{bmatrix} x & y & b & a_z & v_x & v_y \end{bmatrix}^T$$

The velocity components are used such that a smoother trajectory can be implemented. Here the LTE again provides observables for of $x_t.x$ $x_t.y$ and $x_t.b$. But in this case the CV

outputs are used to provide observables for $x_t.v_x$, $x_t.v_y$ and $x_t.a_z$ as opposed to UE updates. While the first type will initially be implemented, this second type will also be considered.

Focusing on the first type, after each CV frame epoch, the IR camera is used to generate the estimate of the current normal of the ground plane. The tilt angles never have to be explicitly determined only $\mathbf{n_t}$. Also generated are the increments to the fp tracks in the ground plane in the system of $\{x_c, y_c, z_c\}$ from the RGB camera. Note that this is the coordinate system that is rotated by a_z relative to the ground. The key is that the CV only provides the differential updates to the PF which updates the UE state vector accordingly. Hence the fp tracks are corrected for

the tilt by mapping the feature points from the $\{x_e, y_e, z_e\}$ frame to the $\{x_c, y_c, z_c\}$ frame. Hence there is no correction made for the rotation and translation relative to the $\{x_a, y_a, z_a\}$ frame. The CV provides observations of

h_t - height

Δaz_t - change of azimuth rotation

Δx_t - velocity in the x direction in $\{x_c, y_c, z_c\}$

Δy_t - velocity in the y direction in $\{x_c, y_c, z_c\}$

The predictive step of the PF is implemented by drawing samples from the conditional pdf of

$p\left(x_t^{[m]} \mid x_{t-1}^{[m]}, u_t\right)$. This update involves the trajectory integration which for now is just the translation as

$$p\left(x_{t.x}^{[m]} \mid x_{t-1.x}^{[m]}, u_t\right) = \delta\left(x_{t.x}^{[m]} - x_{t-1.x}^{[m]} - \cos\left(x_{t-1.az}^{[m]}\right)\Delta x_t - \sin\left(x_{t-1.az}^{[m]}\right)\Delta y_t\right)$$
$$p\left(x_{t.y}^{[m]} \mid x_{t-1.y}^{[m]}, u_t\right) = \delta\left(x_{t.y}^{[m]} - x_{t-1.y}^{[m]} + \sin\left(x_{t-1.az}^{[m]}\right)\Delta x_t - \cos\left(x_{t-1.az}^{[m]}\right)\Delta y_t\right)$$

The azimuth update is given as

$$p\left(x_{t.az}^{[m]} \mid x_{t-1.az}^{[m]}, u_t\right) = \delta\left(x_{t.az}^{[m]} - x_{t-1.az}^{[m]} - \Delta az_t\right)$$

Obviously with the delta functions these are deterministic. As more is learned about the deviations of the RGB camera measurements, a covariance matrix will be supplied such that the particles resulting from the prediction step are not based on deterministic update functions. Note that these are independent updates for x and y directions in $\{x_a, y_a, z_a\}$. As before, the bias term is drawn from a Gaussian PDF that reflects the uncertainty of the clock instability and changes in the multipath delay.

$$p\left(x_{t.b}^{[m]} \mid x_{t-1.b}^{[m]}, u_t\right) = N\left(x_{t-1.b}^{[m]}, \sigma_b^2\right)$$

where σ_b is the standard deviation representing this uncertainty.

The next step is to update the measurement probabilities as conditioned on the previous state vector as $p\left(z_t \mid x_{t-1}, u_t\right)$. There are LTE and CV observables given as

$$z_{LTEi,t}^{[m]} = \sqrt{\left(x_t^{[m]}.x - LTEx_i\right)^2 + \left(x_t^{[m]}.y - LTEy_i\right)^2 + \left(h_t - LTEz_i\right)^2} + x_t^{[m]}.b_i$$

Here h_t is the height of the UE as estimated from the IR camera. Also it is assumed that the location of the i[th] LTE access node is known being located at $\left(LTEx_i, LTEy_i, LTEz_i\right)$. The weights are then determined as

$$w_t^{[m]} = p\left(z_t \mid x_t^{[m]}\right)$$

where z_t is the set of $z_{LTEi,t}^{[m]}$ observables. The pdf of $p\left(z_t \mid x_t^{[m]}\right)$ is assumed to be unbiased as the model includes a bias term. The standard deviation will be determined based on experimental observations.

A shortcoming of this PF type is that it provides no smoothing of the velocity which is basically done by updating the UE state variable with the differentials of $\left\{\Delta x_t, \Delta y_t, \Delta a_{z,t}\right\}$. However, these updates are based on the fp tracks which can be smoothed over several frames.

4.2.1 Generation of CV updates

We start with the placement of the feature points on the ground plane from the projector given the variables $\left\{h, a_x, a_y\right\}$. First compute the transformation from the $\left\{x_d, y_d, z_d\right\}$ to the $\left\{x_e, y_e, z_e\right\}$ coordinate system given as

$$\mathbf{R_{ed}} = \begin{bmatrix} \cos\left(a_y\right) & 0 & \sin\left(a_y\right) \\ 0 & 1 & 0 \\ -\sin\left(a_y\right) & 0 & \cos\left(a_y\right) \end{bmatrix} \begin{bmatrix} 1 & 0 & 0 \\ 0 & \cos\left(a_x\right) & -\sin\left(a_x\right) \\ 0 & \sin\left(a_x\right) & \cos\left(a_x\right) \end{bmatrix}$$

First we have to determine the actual equation of the ground plane as observed in $\left\{x_e, y_e, z_e\right\}$. The equation of the ground plane in $\left\{x_d, y_d, z_d\right\}$ is simply

$$z_d = h$$

Hence the normal of the ground plane relative to $\left\{x_d, y_d, z_d\right\}$ is

$$\mathbf{n_d} = \begin{bmatrix} 0 \\ 0 \\ -1 \end{bmatrix}$$

This is mapped into $\{x_e, y_e, z_e\}$ as

$$\mathbf{n_e} = \mathbf{R_{ed}}\mathbf{n_d} = \mathbf{R_{de}^T}\mathbf{n_d} = \begin{bmatrix} -\sin(a_y)\cos(a_x) \\ \sin(a_x) \\ -\cos(a_x)\cos(a_y) \end{bmatrix}$$

Note that the tilt angles of $\{a_x, a_y\}$ are only required for the simulation aspect. It is not necessary to estimate these angles directly. The plane equation in the $\{x_e, y_e, z_e\}$ frame is given as

$$n_{e.x}x_e + n_{e.y}y_e + n_{e.z}z_e - h = 0$$

The constant $D_e = -h$ results from the point created from –h times the normal must be a point in the plane such that

$$D_e = -h\left(n_{e.x}{}^2 + n_{e.y}{}^2 + n_{e.z}{}^2\right)$$

Suppose we have N_{fsc} points that are projected onto the ground surface from the laser source resulting in randomly placed points that occur on the plane viewed by the camera. To simulate these we assume random projection vectors given as

$$\mathbf{n_{sc,k}} = \begin{bmatrix} n_{sc.x,k} \\ n_{sc.y,k} \\ n_{sc.z,k} \end{bmatrix}$$

The $n_{sc.z,k}$ component is set to a positive constant. The larger it is the narrower the spread of the scattering points. For the current simulation $n_{sc.z,k} = 2$. The points on the plane as determined from the $\{x_e, y_e, z_e\}$ system given as

$$t\left(\mathbf{n_e} \cdot \mathbf{n_{sc,k}}\right) = h$$

which determines the parametric constant t such that the point on the plane will be

$$t\mathbf{n_{sc,k}} = \begin{bmatrix} tn_{sc.x,k} \\ tn_{sc.y,k} \\ tn_{sc.z,k} \end{bmatrix}$$

Next we consider the estimation of the plane using SVD. Look for the singular value of the matrix

$$Q = \begin{bmatrix} t_1 n_{sc.x,1} & t_1 n_{sc.y,1} & t_1 n_{sc.z,1} & 1 \\ t_2 n_{sc.x,2} & t_2 n_{sc.y,2} & t_2 n_{sc.z,2} & 1 \\ \vdots & \vdots & \vdots & \vdots \\ t_N n_{sc.x,N} & t_N n_{sc.y,N} & t_N n_{sc.z,N} & 1 \end{bmatrix}$$

The right singular vector of Q that is associated with the smallest singular value is the vector of the desired coefficients of $\left[n_{e.x}, n_{e.y}, n_{e.z}, h_o \right]$. Note this assumes the appropriate normalization of $n_{e.x}{}^2 + n_{e.y}{}^2 + n_{e.z}{}^2 = 1$.

Next we take and add in the offset to the offset term which is the last term of the vector to obtain the coefficients of

$$\left[n_{e.x}, n_{e.y}, n_{e.z}, h_o + n_{e.x} D_{cam} \right]$$

The output is a variable called plane_coef. As we have the plane in the $\{x_e, y_e, z_e\}$ frame. We now project the fp's in the tilted RGB cameras image plane to the untilted $\{x_d, y_d, z_d\}$ frame. These fp's are then organized into feature point tracks. This involves a significant amount of pruning to remove feature points of low quality (based on corner feature criteria) or which have erratic behaviour. That is if a given feature point in frame t is not in close proximity to a feature point of the previous frame t-1 then it will be flagged as a new potential fp but will not be used as an input to the least squares tracking until it has been in existence for a minimum number of frames. Assume that the result of this fp track filtering results in a set of fp's denoted as f_k^t for frame t and k being the index of the feature point track. Note that the fp track can be filtered with a spline interpolation of sorts to smooth out trajectory fluctuations due to image noise. Such noise is difficult to statistically model as it depends primarily on changes in lighting and shadowing. The fp track selection will be a rather tedious algorithm involving elements of RANSAC also. RANSAC is a method of identifying outliers that can be used to remove fp's that are not behaving in accordance with the nominal optical flow of the camera relative to the ground plane. RANSAC computes residuals from random subsets of fp's used in the least squares calculation of the outputs $\{\Delta x_t, \Delta y_t, \Delta a_{z,t}\}$. Quality metrics are attributed to fp's that consistently provide low residuals. After a number of such calculations, fp's of particularly low quality (consistently high residuals) are rejected. The remaining set of f_k^t is then projected from the image plane to the ground plane determined by the IR camera.

Assume that we have directional vectors for the fp's given as

$$\mathbf{n}_{\mathbf{fp,k}} = \begin{bmatrix} n_{fp.x,k} \\ n_{fp.y,k} \\ n_{fp.z,k} \end{bmatrix}$$

These do not have to be normalized but are based on the scaling of the image plane points and the equivalent of the focal plane distance. However such scaling is arbitrary. Regardless, they are the directional vectors in the $\{x_e, y_e, z_e\}$ system. The points on the ground plane are then determined as

$$t\left(\mathbf{n}_{\mathbf{e}} \square \mathbf{n}_{\mathbf{fp,k}}\right) = h_o + n_{e.x} D_{cam}$$

such that the fp on the ground plane is given as $t\mathbf{n}_{\mathbf{fp,k}}$. These position vectors are mapped into the $\{x_d, y_d, z_d\}$ frame as $\mathbf{R}_{\mathbf{de}} t\mathbf{n}_{\mathbf{fp,k}} = \mathbf{R}_{\mathbf{ed}}^T t\mathbf{n}_{\mathbf{fp,k}}$. The components of x_d and y_d give the coordinates of the fp's on the ground plane in the azimuth rotated frame of $\{x_c, y_c, z_c\}$. The components of $\{f_k^t.x_d, f_k^t.y_d\}$ are then used to determine the least squares estimate of the differentials of $\{\Delta x_t, \Delta y_t, \Delta a_{z,t}\}$. These are subsequently used in the overall PF update of the state vector. Processing of the feature points is described in the following section.

4.2.2 Feature point Processing

After each frame has been processed there is a candidate set of feature points made available denoted as $\{f_{rk}^t.x_d, f_{rk}^t.y_d\}$. Here the index t denotes the frame, k denotes the feature index and $\{x_d, y_d\}$ denote the location of the feature point in the $\{x_d, y_d, z_d\}$ system. The additional subscript of r denotes raw, as opposed to after pruning where the fp's are organized into feature point tracks (fpt). These feature points are paired with corresponding feature points of the previous frame given as $\{f_{r,x,k}^{t-1}, f_{r,y,k}^{t-1}\}$. If the correspondences cannot be found then the feature point is not used for tracking but stored for the next frame. A feature point track must emerge before it is eligible for use in estimating the egomotion. In this way many of the sporadic feature points, that would distort the egomotion estimate, can be pruned away. Erratic fp's will bias the least squares solution of the ego-motion such that spurious behavior will result. The set of pruned fpt's are denoted as $\{f_{x,k}^t, f_{y,k}^t\}$ which are used in the overall estimation of the parameters of the affine transformation which is represented for a pair of fp's (recent segment of the fpt) as

$$\begin{bmatrix} f_{x,k}^i \\ f_{y,k}^i \end{bmatrix} = \begin{bmatrix} C_i & S_i & -\Delta x_i \\ -S_i & C_i & -\Delta y_i \end{bmatrix} \begin{bmatrix} f_{x,k}^{i-1} \\ f_{y,k}^{i-1} \\ 1 \end{bmatrix}$$

where

$$C_i \square \cos\left(\Delta a_{z,t}\right)$$
$$S_i \square \sin\left(\Delta a_{z,t}\right)$$

This assumes that the motion between the two frames remains at the same height. If this height changes then there is a scaling factor that must be considered such that $C_i^2 + S_i^2$ is not constrained to be equal to 1. This can be reorganized into the M=AP format for the k[th] fp as

$$\begin{bmatrix} f_{x,k}^i \\ f_{y,k}^i \end{bmatrix} = \begin{bmatrix} f_{x,k}^{i-1} & f_{y,k}^{i-1} & -1 & 0 \\ f_{y,k}^{i-1} & -f_{x,k}^{i-1} & 0 & -1 \end{bmatrix} \begin{bmatrix} C_i \\ S_i \\ \Delta x_i \\ \Delta y_i \end{bmatrix}$$

This is assembled for all of the K fp's and the over-determined set of relations solved for the parameter vector of $\begin{bmatrix} C_i & S_i & \Delta x_i & \Delta y_i \end{bmatrix}$. The outcome is then $\left\{\Delta a_{z,i} = \text{atan2}\left(S_i, C_i\right), \Delta x_i, \Delta y_i\right\}$ which is passed onto the particle filter. Additionally there is a check on the change in the height which can be expressed as

$$\frac{h_t}{h_{t-1}} = \frac{1}{\sqrt{C_t^2 + S_t^2}}$$

While the height estimate from the IR camera will be more accurate, the estimate of the relative height change in the above relation can be used as a check. Disagreement would imply distortion between the IR and the RGB camera that would make the CV estimation suspect.

The plot in Figure 5-10 is an example of a set of fp's that were picked up by the RGB camera. The image is of a white sheet of paper with ink markings. The green dots are the feature points that were determined based on the corner detection algorithm. Figure 5-11 shows the set of fpt's after trace pruning. The traces appear to be noisy as they were generated by an RGB camera moved by hand with no tilt compensation. The abscissa is the frame index and the ordinate are the $\left\{f_{x,k}^t, f_{y,k}^t\right\}$ displacement. In this case the camera was moved vertically up and then down. The C and Matlab programs for the processing of the fpt's are given in the appendix.

Figure 57: Feature points highlighted by green dots on an image of a white page with ink markings

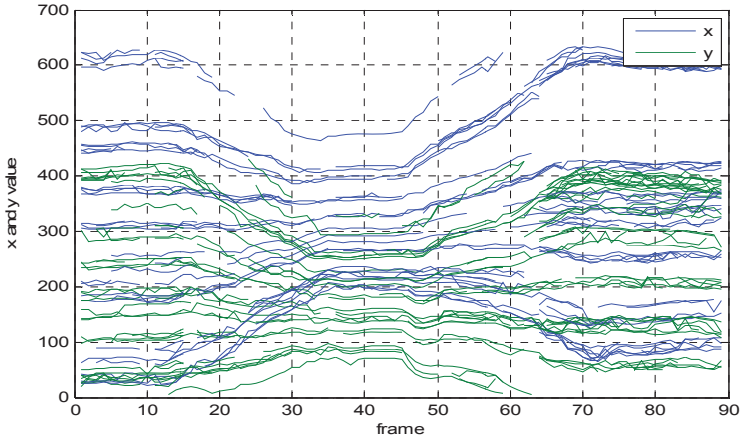

Figure 58: Feature point migration as webcam is raised and then lowered.

4.2.3 Simulation

During phase II a complete detailed simulation of the SGL system with LTE and CV observables. Such a simulation will allow for analysis of different components of the tracking system. It will have provisions for partial experimental data to compliment the simulated responses. This provides a test-bed means for optimizing the algorithms developed. Prior to this, components of the simulation will be constructed some of which at this stage have been partially completed.

These subsystem simulation components that will be rolled into the overall simulation are listed as:

1. Modelling of the LTE downlink signal in a multipath environment for a static location providing observables of $z_{LTEi,t}^{[m]}$.

2. Modelling of the IR and RGB responses to the generation of feature point tracks.

3. Simulation of the generation of the $\{\Delta x_t, \Delta y_t, \Delta a_{z,t}\}$ observables

4. Simulation of the updating of the PF particles based on $\{\Delta x_t, \Delta y_t, \Delta a_{z,t}\}$

5. Simulation of the overall PF.

These subsystems will be developed first followed by an overall integration. Concurrently, the experimental data as described in the following section will be taken. This will eventually lead to the overall experimental/simulation verification of the overall SGL methods as applied to a moving handset UE.

5 Experimental HW design

5.1 Overview

The bulk of the experimental work will be completed in phase II and phase III of this contract. However, due to the contract phasing it was necessary to complete the design, parts procurement and most of the construction of the experimental apparatus in this phase. After review of the requirements, it was concluded that the experimental apparatus needed to operate in two modes:

1. Step frequency mode where the hardware simulated AN's will generate a CW tone that will be transmitted and picked up at the receiver to determine the channel gain at a set of discrete frequencies.

2. Pulse transmission mode where the modulated signal has an instantaneous bandwidth in excess of 20 MHz.

It is necessary to support both of these modes. The discrete CW frequency mode provides accurate coherent channel gain measurements as the receiver is spatially moved which simulates the operation of the synthetic array. Unfortunately, the synthesizers in the transmitter and receiver lose lock every time the frequency changes. Hence the carrier phase undergoes a random increment which is not the same for the receiver and transmitter. This random phase would be difficult and error prone to sort out with post processing. Consequently the step frequency mode can only be used to measure CW channels. The pulse mode uses a pulse generator only in the transmitter that is coherent with the carrier phase. Hence the receiver can sample successive pulses with the assurance that the phase is maintained from pulse to pulse. However, with much less signal energy per frequency component, it is expected that there will be a residual variation of the measured channel gain at a particular frequency. However, the combination of the two modes will provide adequate channel measurement performance.

In both modes, the transmitter can support up to four antennas simulating four spatially distributed AN's. Switching between the CW and pulse mode is done with software control. In the pulse mode, a pulse width of less than 100 nsec will be used that is repeated at a rate of 10 kHz such that a spectral line spectrum will be generated with 10 kHz resolution. This is ample resolution considering that the channel coherency bandwidth for indoor environments is typically on the order of 1 MHz or higher. The receiver will likewise have two modes to mirror the cw and the pulse requirements. The receiver will use a low conversion rate 14 bit ADC that will sample the downconverted and filtered CW signals arriving from the 4 AN's. The transmission of the AN's will be individually switched on and off via a SW controlled switch such that each channel can be measured individually. In the pulse mode, the 20 MHz baseband signal will be sampled and stored by a DSO (digital storage oscilloscope) that will be integrated into the system. A block diagram is as shown in Figure 5-1. Also shown in this diagram is the PC controlled turntable which will be used to move the receiver antenna in a precise fashion for the SA development and testing. Also connected to the PC is the computer vision sensor that will provide additional observables for the particle filter processing. This will be integrated with the LTE wireless signal observables as described in previous section. As described in the previous chapter the CV component will provide direct observables regarding the differential motion and

orientation updates of the UE which will be used to update the particles at each iteration. The particle weights will then be determined by the LTE delay measurements. These delay measurements will be generated from the measurement of the propagated microwave pulse signals from the simulated AN transmit antennas. The four transmit antennas will be initially set up in a large isolated laboratory room at the University of Calgary with the floor plan as sketched in Figure 5.2. The lab is a penthouse on the roof level of a 4th story building and is conveniently removed from most sources of interference in the ISM band used for transmission. Hence the simple pulse modulation is viable for this research. The CV input has the additional advantage in that it will be used to verify the trajectory actually taken by the handheld to provide an assessment of the SGL accuracy based on the LTE signalling.

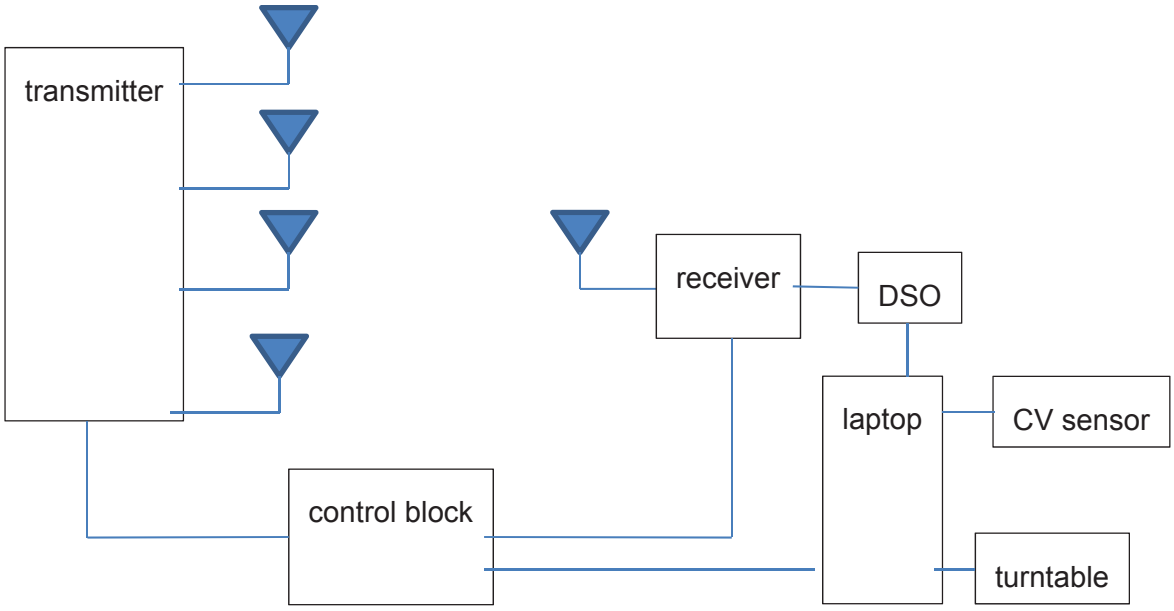

Figure 59: Block diagram of the overall experimental apparatus

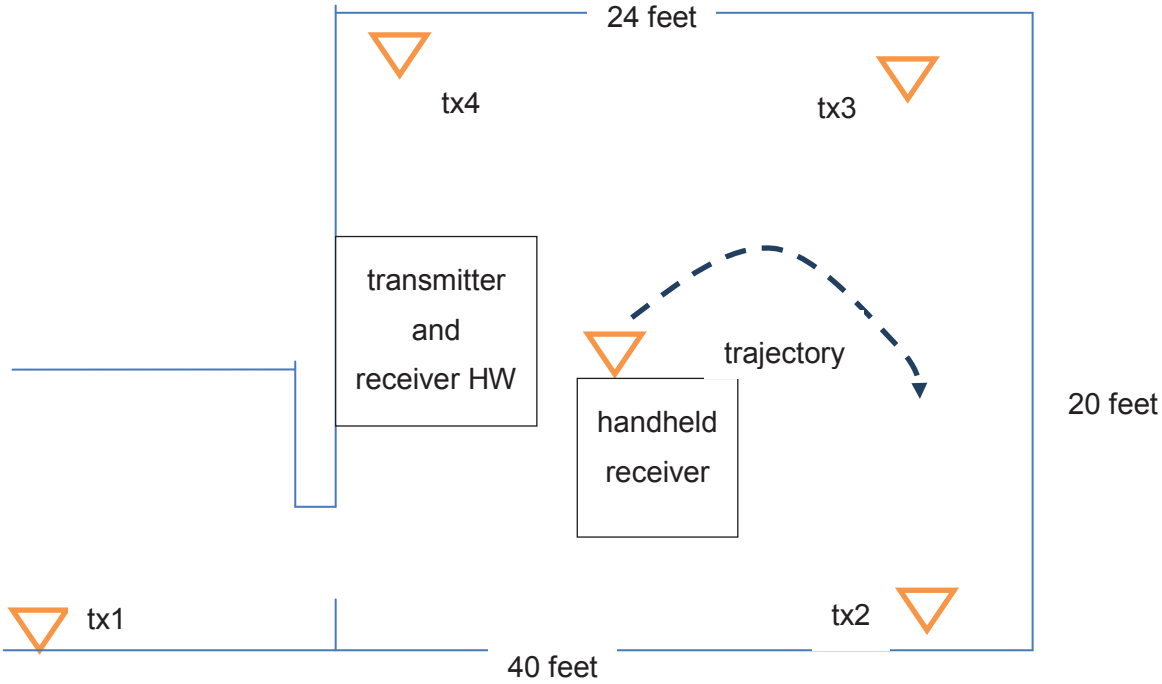

Figure 60: Floor plan layout of the LTE propagation room ENA401 at the University of Calgary

Currently, the receiver and the transmitter are almost complete with the ADC sampling boards completed. The control block and control software will be developed during phase II. A picture of the receiver and transmitter is shown in Figure 5-3. Each of the transmitter and receiver units can support four circuit boards which will contain the electronics. As modifications and inevitable iterations are anticipated, it is necessary to design the units such that the circuitry can evolve.

Figure 61: Almost completed transmitter and receiver units

5.2 Transmitter Design Details

As the objective is to create a transmitter that is portable such that outdoor testing can be done, a synthesizer module is considered for this application. The synthesizer output will be amplified and transmitted in the ISM band antenna shown. The ISM band of 2.45 GHz will be used as it is closer to the typically encountered LTE frequency bands. It is important than an unlicensed band is used as the equipment will be made portable to take into commercial buildings to collect data.

A problem with the CW tone generator is that the synthesizers in the transmitter and the receiver break lock every time the frequency is changed. Hence there will be a phase ambiguity between the received signal and the local receiver signal every time the frequency is changed. Hence while CW is suitable for determining the beam forming aspects as a function of frequency of the SA, it will not provide the desired measurement of the wide band partially resolvable multipath channel that is desired. It is possible to use a frequency ramp but breaking the lock of the synthesizer and sweeping the VCO over a narrow range is not practical as the VCO control is embedded in the synthesizer chip. Another method is to use a spread spectrum PRN coded signal. This was used in the prior TOPS work and aptly extracted the resolvable multipath within the bandwidth of the modelled IS2000 and GPS signals. However, this will then involve despreading in the receiver which requires higher speed baseband signal sampling and FPGA based processing.

A simpler alternative was chosen of just using a narrow pulse modulation. A pulse width of approximately 100 nsec was used which provided a useful bandwidth of about 20 MHz which is adequate for the LTE testing. The block diagram of the LTE transmitter is shown in Figure 5-3. The channel coherence bandwidth is significantly larger than the 10 kHz sub-band bandwidth of the individual LTE OFDM carriers. Hence if the channel is essentially sampled at a 10 kHz interval over the 20 MHz overall modulation bandwidth then this will provide adequate sampling that can be used for the overlay LTE simulation. The transmitter modulation will therefore

simply consist of a periodic signal with a period of 0.1msec that has some pulse like waveform. It is difficult to realize the modulation electronics that will give precise control of the 10 kHz line spacing around the carrier but very simple to construct a modulator that will provide a consistent periodic modulation. Note that any periodic signal can actually be used. It does not have to be a pristine pulse shape as indicated here.

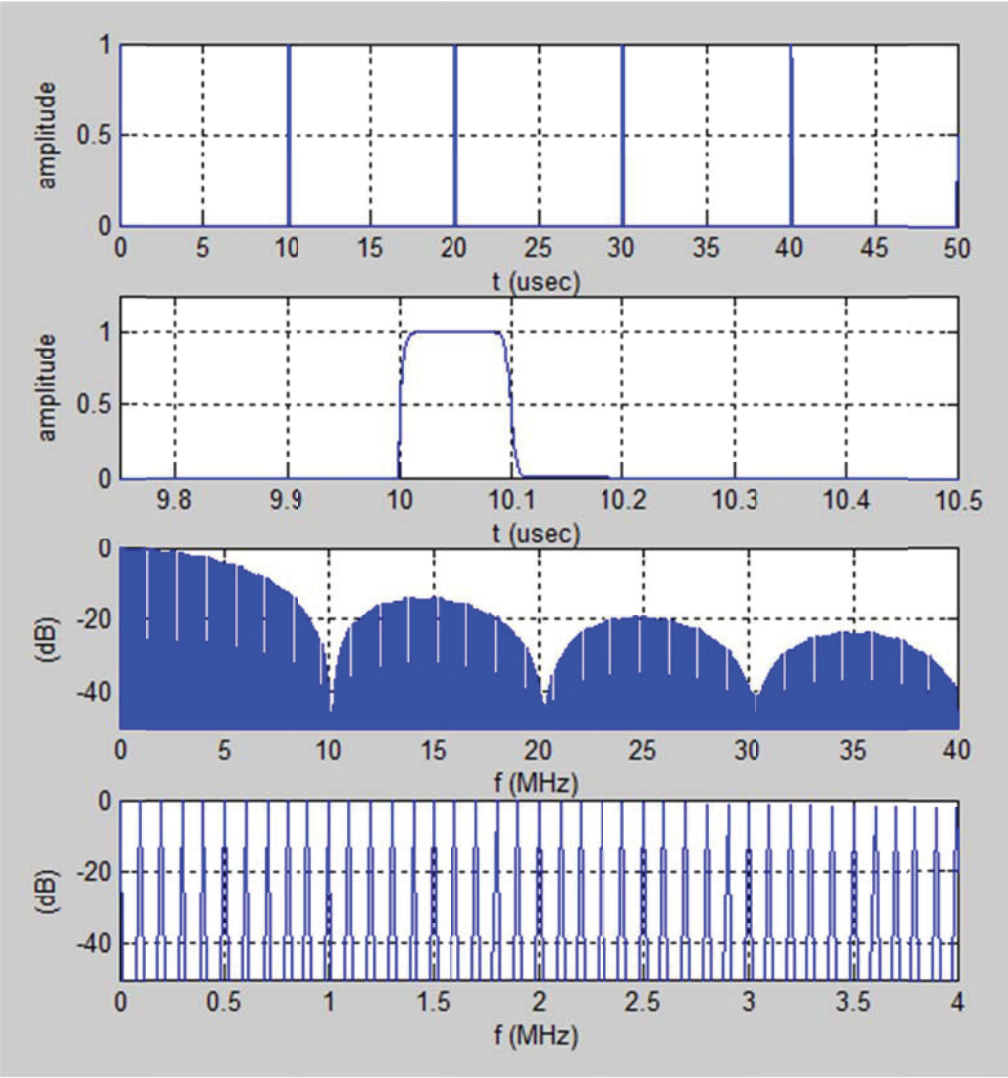

Figure 62: Simple pulse modulation with 100 nsec pulse width signal with period of 10 usec providing 100 kHz frequency spacing (Matlab program g2.m)

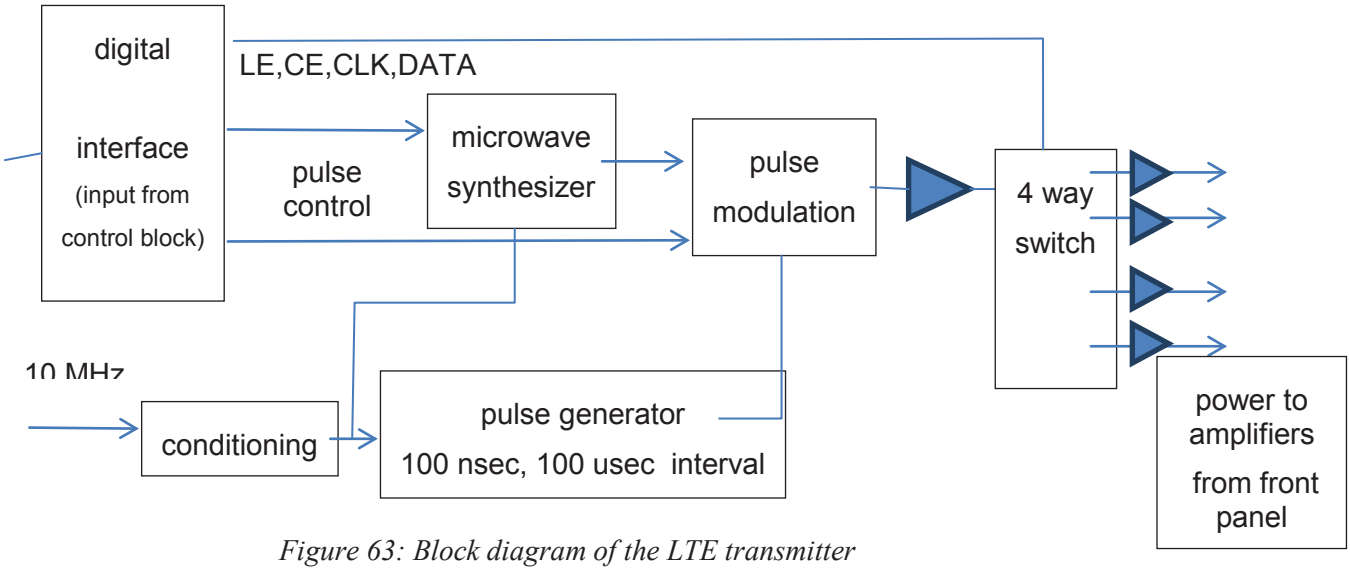

Figure 63: Block diagram of the LTE transmitter

The input interface signals are as follows:

Signal	description
LE,CE,CLK,data	Signals for controlling synthesizer
A1	Enable transmitter port 1
A2	Enable transmitter port 2
A3	Enable transmitter port 3
A4	Enable transmitter port 4
Pulse	Switch between pulse and cw control
Gnd	

The four way switch controls the connection of the signal to each transmitter amplifier input. The power to the amplifier is switched on/off from the front panel switch. This is done to minimize the power drain of the battery.

5.3 Receiver Design Details

The block diagram of the receiver is shown in Figure 5-6.

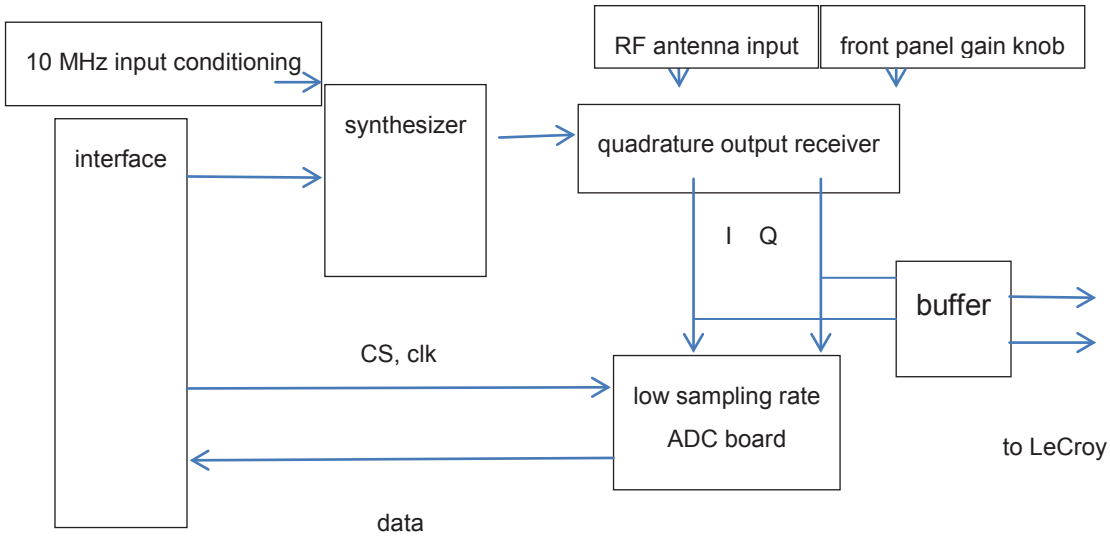

Figure 64: Block diagram of the receiver

The interface signals for the receiver are as follows:

signal	description
LE,CS,CLK,data	Signals for controlling synthesizer
CS,CLK, data	Interface signals for ADC
gnd	

The receiver converts the 2.4 GHz signal into a baseband signal. For the CW application this base band frequency is zero while for the pulse system it is at 20 MHz such that IF sampling in the LeCroy DSO can be used instead of using I and Q channels. This simplifies the data collection.

5.4 Controller Design Details

This block will be developed primarily during phase II. A block diagram of the unit is shown in Figure 5-7. The purpose of this unit is to contain the 10 MHz TCXO clock, interface to the transmitter and the receiver as well as the PC, DSO and turntable.

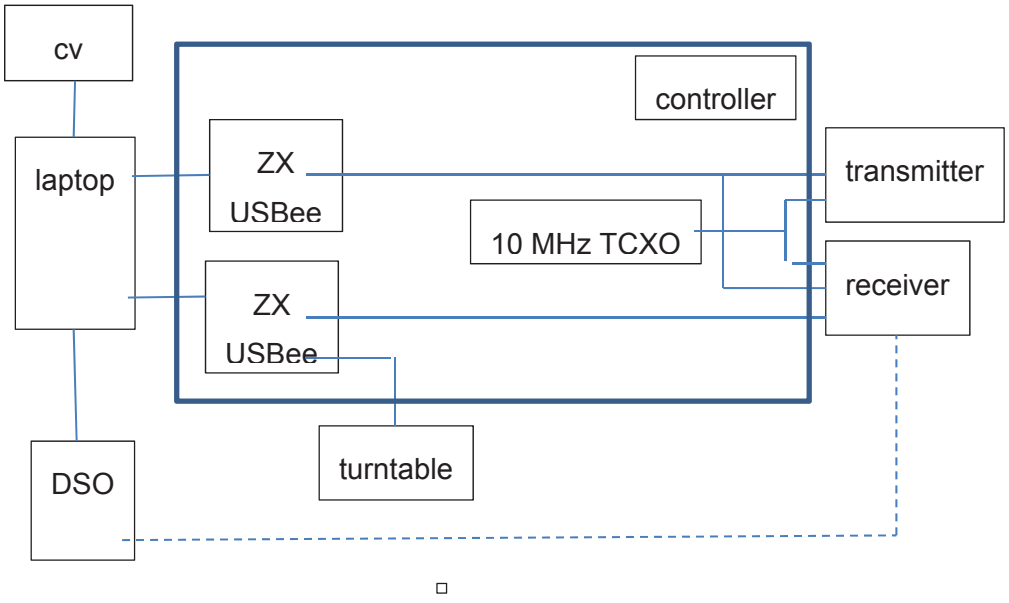

Figure 65: Block diagram of controller

5.5 Software Design Details

5.5.1 Post processing Software

The objective is to record the channel impulse response over a 20 MHz bandwidth from the four transmitters to the receiver for a given receiver antenna trajectory. In the pulse mode, the sampled and averaged pulse signal will be recorded. Simultaneously, the CV data will be recorded. Then in the post processing phase, the LTE channel over variable bandwidths between 1 and 20 MHz can be emulated by applying appropriate filtering to the recorded pulse signal. As the overall system is linear, simulation conditions can be widely varied provided that all of the required channel values fall within the space-frequency envelope of the measured trial results. Once the system is operating satisfactorily it will be setup in various other indoor and outdoor locations such that a suitable statistical sampling of various propagation environments can be made.

5.6 List of Hardware components obtained for the transmitter and receiver construction

Transmitter

component	Cost each	quantity	Total cost
MTS2500-200400 Synergy synthesizer	$1300	1	$1300.00
ZX controller, CWAV	$395	1	$395.00
Coax cable Minicircuits 086-65SMRSM+	$12.15	3	$36.45
Coax cable Minicircuits 086-24SMRSM+	$15.15	2	$30.30
Antennas TBD	$100	2	$200.00
Amplifier wideband Minicircuits ZX60-3011+	$140	1	$140.00
0 degree coupler Mini circuits ZFRSC-42+	$60	1	$60.00
Bandpass filter	$35	2	$70.00

VBF-2435+			
Battery and regulated power supplies (TBD)	$100	1	$100.00
Discrete electronic components			$400.00
Total Transmitter			$2731.75

Receiver

component	Cost each	quantity	Total cost
MTS2500-200400 Synergy synthesizer	$1300	1	$1300
ZX controller, CWAV	$395	1	$395
Coax cable Minicircuits 086-65SMRSM+	$12.15	6	$72.90
Coax cable Minicircuits 086-24SMRSM+	$15.15	4	$60.60
Antennas TBD	$100	2	$200
Amplifier wideband Minicircuits	$140	3	$420

ZX60-3011+			
Mixers, Mini circuits ZEM-4300+	$80	2	$160
90 degree coupler Mini circuits ZAPDQ-4-S	$85	1	$85
0 degree coupler Mini circuits ZFRSC-42+	$60	1	$60
Bandpass filter VBF-2435+	$35	2	$70
Battery and regulated power supplies (TBD)	$100	1	$100
Discrete electronic components			$400
Total receiver			$3323.50

References

[1] "LTE The UMTS Long Term Evolution 2nd edition", Stefanie Sesia, Issam Toufik, Matthew Baker.

[2] 3GPP TS 36.211: "Evolved Universal Terrestrial Radio Access (E-UTRA); Physical channels and modulation".

[3] 3GPP TS 36.212: "Evolved Universal Terrestrial Radio Access (E-UTRA); Multiplexing and channel coding".

[4] 3GPP TS 36.213: "Evolved Universal Terrestrial Radio Access (E-UTRA); Physical layer procedures".

[5] 3GPP TS 36.214: "Evolved Universal Terrestrial Radio Access (E-UTRA); Physical layer – Measurements".

[6] S. Thrun, W. Burgard, D. Fox, "Probabilistic Robotics", MIT press, 2006

[7] M. Arulampalam, S. Maskell, N. Gordon, T. Clapp, " A tutorial on particle filters for online Nonlinear/Non-Gaussian Bayesian tracking", IEEE transactions on signal processing Vol.50, No.2 Feb 2002, pp.174-188

[8]H. VanTrees, "Optimum array processing", John Wiley, 2002

[9] S. Kay, "Fundamental of statistical signal processing – Estimation theory", vol. 1, Prentice Hall 1998

[10] S. Kay, "Fundamental of statistical signal processing – Detection theory", vol. 2, Prentice Hall 1998

[11] http://www.endruntechnologies.com/frequency-standard-oscillators.htm

[12] Pablo Pedregal, "Introduction to optimization", Springer volume 46, 2003

This page intentionally left blank.

Annex A MATLAB code

In this section a listing of the Matlab source codes is provided for future reference.

```
PF1

% number of particles
M = 1000;
% mean increment in x every iteration
Uod = 0;
% var of observation
Ovar = 1;

% initial set of M particles
xo = 10 * rand(M,1)-5;
figure(4);plot(sort(xo),'r'); hold on;
for k=1:20
    if k>1
        xo = x1;
    end

    % deterministic movement
    xu = xo+Uod;
    % measurement result with variance of Ovar resulting in
weights
    z = k*Uod+sqrt(Ovar)*randn(1);
    w = normpdf(z,xu,Ovar);

    % resampling determined by the intervals of W
    W= cumsum(w);
    g1 = W(M)*rand(M,1);
    x1 = zeros(M,1);
    for m=1:M
        [g2,ind]=min(abs(g1(m)-W));
        x1(m)=xu(ind);
    end
     figure(4);plot(sort(x1),'k');
figure(k);
Nbin = 100;
xx = linspace(-8,8,Nbin)';
subplot(311);hist(xo,xx)
subplot(312);hist(xu,xx)
subplot(313);hist(x1,xx)

end


PF2.m

% number of particles
M = 200;
kmax = 2500;
```

```
% actual motion
Uoa = 10*(.1 + .1*tanh(((1:kmax)-kmax/2)/100)); % actual

% mean increment in x every iteration
Uod = 0.0;

% width of initial distribution
xoW = .2;
xob = 1;

% var of observation
Ovar = 1;

% initial set of M particles
xo = xoW * rand(M,1)-xoW/2+xob;
D = zeros(kmax,3);

for k=1:kmax
    if k>1
        xo = x1;
    end
    % deterministic movement
    xu = xo+Uod+ 0.02*randn(M,1);

    % measurement result with variance of Ovar resulting in
weights
    z = Uoa(k)+sqrt(Ovar)*randn(1);
    w = normpdf(z,xu,Ovar);

    % resampling determined by the intervals of W
    W= cumsum(w);
    g1 = W(M)*rand(M,1);
    x1 = zeros(M,1);
    for m=1:M
        [g2,ind]=min(abs(g1(m)-W));
        x1(m)=xu(ind);
    end
    D(k,1) = mean(x1);
    D(k,2) = std(x1);
    D(k,3) = Uoa(k);

end


figure(1);subplot(221);plot(D(:,1));
xlabel('k')
ylabel('mean(x)')
hold on;
plot(D(:,3),'r--');hold off;

subplot(222);plot(D(:,2));
xlabel('k')
ylabel('std(x)')
```

```
subplot(223);plot(sort(w))
xlabel('m')
ylabel('w')


subplot(224);plot(sort(x1))
xlabel('m')
ylabel('x')


PF3.m

% number of particles
M = 500;
kmax = 800;

% actual position
Uoax = 5;
Uoay = 6;
ra = sqrt(Uoax^2+Uoay^2);

% mean increment in x every iteration
Uodx = 0.0;
Uody = 0.0;
xux_std = 0.5;
xuy_std = 0.5;

% width of initial distribution is equivalent to the room size
% room is assumed to be 10 by 10
xoWx = 10;
xobx = 5;
xoWy = 10;
xoby = 5;

% var of observation in range
Ovar = 1;

% initial set of M particles
xox = xoWx * rand(M,1)-xoWx/2+xobx;
xoy = xoWy * rand(M,1)-xoWy/2+xoby;

figure(1);subplot(111);
aa =linspace(0,2*pi,300);
plot(ra * cos(aa),ra * sin(aa),'b--');hold on;
axis([-10,10,-10,10]);


for k=1:kmax


    if k>1
        xox = x1x;
        xoy = x1y;
    end
```

```
    % deterministic movement
    xux = xox+Uodx+ xux_std*randn(M,1);
    xuy = xoy+Uody+ xuy_std*randn(M,1);

    % measurement result with variance of Ovar resulting in
weights
    z = sqrt(Uoax^2+Uoay^2)+sqrt(Ovar)*randn(1);
    w = normpdf(z,sqrt(xux.^2+xuy.^2),Ovar);

    % resampling determined by the intervals of W
    W= cumsum(w);
    g1 = W(M)*rand(M,1);
    x1x = zeros(M,1);
    x1y = zeros(M,1);

    for m=1:M
        [g2,ind]=min(abs(g1(m)-W));
        x1x(m)=xux(ind);
        x1y(m)=xuy(ind);
    end
   if k == kmax
   plot(ra * cos(aa),ra * sin(aa),'b--');
   plot(xox,xoy,'w.');
    plot(x1x,x1y,'k.');
   end
end

hold off;
grid on;
xlabel('x');
ylabel('y');


figure(2);plot(sort(w))
[sx,i] = sort(x1x);
figure(3);plot([sx,x1y(i)])

PF4.m

% number of particles
M = 400;
kmax = 100;

% actual position
Uoax = 3;
Uoay = 6;
ra1 = sqrt(Uoax^2+Uoay^2);
ra2 = sqrt(Uoax^2+(Uoay-10)^2);
ra3 = sqrt((Uoax-10)^2+(Uoay-10)^2);
ra4 = sqrt((Uoax-10)^2+Uoay^2);

% actual delay bias
dba = 1;

% mean increment in x every iteration
```

```
Uodx = 0.0;
Uody = 0.0;
xux_std = 0.1;
xuy_std = 0.1;
xudb_std = 0.1;

% width of initial distribution is equivalent to the room size
% room is assumed to be 10 by 10
xoWx = 10;
xobx = 5;
xoWy = 10;
xoby = 5;
xoWdb = 10;
xobdb = 5;

% var of observation in range
Ovar = 1;

% initial set of M particles
xox = xoWx * rand(M,1)-xoWx/2+xobx;
xoy = xoWy * rand(M,1)-xoWy/2+xoby;
xodb = xoWdb * rand(M,1)-xoWdb/2+xobdb;

figure(1);subplot(111);
aa =linspace(0,2*pi,300);
plot(ra * cos(aa),ra * sin(aa),'b--');hold on;
axis([-10,10,-10,10]);

D = zeros(kmax,3);

for k=1:kmax
    if k>1
        xox = x1x;
        xoy = x1y;
        xodb = x1db;
    end

    % deterministic movement
    xux = xox+Uodx+ xux_std*randn(M,1);
    xuy = xoy+Uody+ xuy_std*randn(M,1);
    xudb = xodb+ xudb_std*randn(M,1);

    % measurement result with variance of Ovar resulting in
weights
    z1 = ra1+dba+sqrt(Ovar)*randn(1);
    z2 = ra2+dba+sqrt(Ovar)*randn(1);
    z3 = ra3+dba+sqrt(Ovar)*randn(1);
    z4 = ra4+dba+sqrt(Ovar)*randn(1);
    w1 = normpdf(z1,sqrt(xux.^2+xuy.^2)+xudb,Ovar);
    w2 = normpdf(z2,sqrt(xux.^2+(10-xuy).^2)+xudb,Ovar);
    w3 = normpdf(z3,sqrt((10-xux).^2+(10-xuy).^2)+xudb,Ovar);
    w4 = normpdf(z4,sqrt((10-xux).^2+xuy.^2)+xudb,Ovar);
    w = w1.*w2 .*w3 .*w4;
    ii = find(xux<0 |xux>10 | xuy<0 |xuy>10);
    w(ii) = zeros(length(ii),1);
```

```
    % resampling determined by the intervals of W
    W= cumsum(w);
    g1 = W(M)*rand(M,1);
    x1x = zeros(M,1);
    x1y = zeros(M,1);
    x1db = zeros(M,1);

    for m=1:M
        [g2,ind]=min(abs(g1(m)-W));
        x1x(m)=xux(ind);
        x1y(m)=xuy(ind);
        x1db(m)=xudb(ind);
    end
   if k == kmax
   plot(ra * cos(aa),ra * sin(aa),'b--');
   plot(xox,xoy,'w.');
    plot(x1x,x1y,'k.');
   end
   D(k,:) = mean([x1x,x1y,x1db]);
end

hold off;
grid on;
xlabel('x');
ylabel('y');


figure(2);plot(sort(w))
[sx,i] = sort(x1x);
figure(3);plot([sx,x1y(i)])

figure(4);subplot(311);plot(D(:,1));
xlabel('k');ylabel('x_{est}');grid on
subplot(312);plot(D(:,2));
xlabel('k');ylabel('y_{est}');grid on;
subplot(313);plot(D(:,3));
xlabel('k');ylabel('db_{est}');grid on;

PF5.m
% same as pt_12 but with vx and vy instead of v and theta
% state vector is [x,y,vx,vy,b]

% parameters
Dx = 6;
Dy = 5;

% number of particles
M = 1000;

% acceleration variance every iteration
var_a = .0001;
var_b = .001;

% var of observation
```

```
Ovar = .6;  % variance of samples used for resampling
stdz = .2;  % actual std of samples

% initial set of M particles
xo_rx = 3*rand(M,1);
xo_ry = Dy/2*ones(M,1)+1.5*randn(M,1);
xo_vx = .011+.2*randn(M,1);
xo_vy = .2*randn(M,1);
xo_b = zeros(M,1);

%iterations
kmax = 100;
D = zeros(kmax,5); % data matrix
for k=1:kmax
    if k>1
        xo_rx = x1_rx;
        xo_ry = x1_ry;
        xo_vx = x1_vx;
        xo_vy = x1_vy;
        xo_b = x1_b;
    end

    % random update
    xu_rx = xo_rx + xo_vx;
    xu_ry = xo_ry + xo_vy;
    xu_vx = xo_vx + sqrt(var_a)*randn(M,1);
    xu_vy = xo_vy + sqrt(var_a)*randn(M,1);
    xu_b = xo_b + sqrt(var_b)*randn(M,1);

    % actual position
    vax = .02;
    rxa = k*vax;
    rya = Dy/2;
    ba= 0;

    % measurement result with variance of Ovar resulting in
weights
    z1 = sqrt(rxa^2 + rya^2) + stdz*randn(1);
    z2 = sqrt((rxa-Dx)^2 + rya^2)+ stdz*randn(1);
    z3 = sqrt((rxa-Dx)^2 + (rya-Dy)^2)+ stdz*randn(1);
    z4 = sqrt(rxa^2 + (rya-Dy)^2)+ stdz*randn(1);

    w1 = normpdf(z1,sqrt(xu_rx.^2 + xu_ry.^2)-xu_b,Ovar);
    w2 = normpdf(z2,sqrt((xu_rx-Dx).^2 + xu_ry.^2)-xu_b,Ovar);
    w3 = normpdf(z3,sqrt((xu_rx-Dx).^2 + (xu_ry-Dy).^2)-
xu_b,Ovar);
    w4 = normpdf(z4,sqrt(xu_rx.^2 + (xu_ry-Dy).^2)-xu_b,Ovar);
    w = w1.* w2.*w3.*w4;
    i = find(xu_rx<0|xu_rx>Dx|xu_ry<0|xu_ry>Dy);
    w(i) = zeros(length(i),1);

    % resampling determined by the intervals of W
    W= cumsum(w);
    g1 = W(M)*rand(M,1);
    x1_rx = zeros(M,1);
```

```
    x1_ry= zeros(M,1);
    x1_vx = zeros(M,1);
    x1_vy = zeros(M,1);
    x1_b = zeros(M,1);

    for m=1:M
        [g2,ind]=min(abs(g1(m)-W));
        x1_rx(m)=xu_rx(ind);
        x1_ry(m)=xu_ry(ind);
        x1_vx(m)=xu_vx(ind);
        x1_vy(m)=xu_vy(ind);
        x1_b(m)=xu_b(ind);
    end
    D(k,:) = mean([x1_rx,x1_ry,x1_vx,x1_vy,x1_b]);
    figure(1);subplot(111);plot(xu_rx,xu_ry,'r.');grid on;
    axis([0,Dx,0,Dy]);
xlabel('x');ylabel('y');pause(.1);
end



figure(4);subplot(111);plot3(xu_rx,xu_ry,w,'r.');grid on;
xlabel('x');ylabel('y');
[ws,i] = sort(w);
figure(2);semilogy([w1(i),w2(i),w3(i),w4(i),w(i)]);
legend('1','2','3','4','w');
figure(3);subplot(511);plot(D(:,1));grid on;
subplot(512);plot(D(:,2));grid on;
subplot(513);plot(D(:,3));grid on;
subplot(514);plot(D(:,4));grid on;
subplot(515);plot(D(:,5));grid on;

C routine to extract feature points from RGB camera
#include <stdio.h>
#include "opencv2\opencv.hpp"


// global variables
const int MAX_CORNERS = 30;  // maximum number of corners
considered in tracking
CvCapture* capture;
IplImage *img,*dst, *grayA, *grayB,*temp,*eig,*fptraj;
double quality = 0.1;
double min_distance = 30;
int corner_count = MAX_CORNERS;
int GFwin = 5;
int gaus_sig =9;
float dist_th = 20.0f;
float bnd_limit = 20;

int main()
{
CvPoint2D32f* cornersA = new CvPoint2D32f[ MAX_CORNERS ];
CvPoint2D32f* cornersB = new CvPoint2D32f[ MAX_CORNERS ];
CvPoint2D32f* pruneA = new CvPoint2D32f[ MAX_CORNERS ];
```

```
CvPoint2D32f* pruneB = new CvPoint2D32f[ MAX_CORNERS ];
char features_found[ MAX_CORNERS ];
float feature_errors[ MAX_CORNERS ];
int win_size=10;
int i1,i2,j1,j2;
float dist,g1,g2;
float *pf;
int i,j,k,Nf,m,ii,prune_flag;
CvSize s;
CvPoint pA,pB;
uchar *p,*pc;

CvCapture* capture1= cvCreateFileCapture



img = cvQueryFrame(capture1);
s=cvGetSize(img);
grayA = cvCreateImage(s,IPL_DEPTH_8U,1);
grayB = cvCreateImage(s,IPL_DEPTH_8U,1);
dst = cvCreateImage(s,IPL_DEPTH_8U,3);
fptraj = cvCreateImage(s,IPL_DEPTH_8U,3);
cvZero(fptraj);

cvNamedWindow( "video", 1 );

// allocate additional image scratchpad for good features
algorithm
CvSize pyr_sz = cvSize( grayA->width+8, grayA->height/3 );
IplImage* pyrA = cvCreateImage( pyr_sz, IPL_DEPTH_32F, 1 );
IplImage* pyrB = cvCreateImage( pyr_sz, IPL_DEPTH_32F, 1 );
eig = cvCreateImage( cvGetSize(grayA), 32, 1 );
temp = cvCreateImage( cvGetSize(grayA), 32, 1 );

// main loop
k=0;
while(1){

//copy image B to image A
cvCopy(grayB,grayA);
cvCopy(pyrB,pyrA);

// find features in grayA
cvGoodFeaturesToTrack(grayA, eig, temp, cornersA,
&corner_count,quality, min_distance, 0, GFwin, 0, 0.04 );

// get new image
if((img = cvQueryFrame(capture1))==0) break;
cvCopy(img,dst);
cvCvtColor(img,grayB,CV_RGB2GRAY);
if(gaus_sig)
cvSmooth(grayB,grayB,CV_GAUSSIAN,gaus_sig,gaus_sig);


// compute LK
```

```
cvCalcOpticalFlowPyrLK(grayA,grayB,pyrA,pyrB,cornersA,cornersB,co
rner_count,
           cvSize( win_size,win_size
),5,features_found,feature_errors,
           cvTermCriteria( CV_TERMCRIT_ITER | CV_TERMCRIT_EPS,
20, .3 ),0);

// Add corners of A and B to figure
for(i=0,ii=0;i<corner_count;i++){
      // pruning of feature points
      prune_flag = 1;
      g1 = cornersA[i].x - cornersB[i].x;
      g2 = cornersA[i].y - cornersB[i].y;
      dist = sqrt(g1*g1+g2*g2);
      if(dist > dist_th)prune_flag = 0;
      if(cornersA[i].x < bnd_limit) prune_flag = 0;
      if(cornersA[i].y < bnd_limit) prune_flag = 0;
    if(s.width-cornersA[i].x < bnd_limit) prune_flag = 0;
    if(s.height-cornersA[i].y < bnd_limit) prune_flag = 0;
      if(cornersB[i].x < bnd_limit) prune_flag = 0;
      if(cornersB[i].y < bnd_limit) prune_flag = 0;
    if(s.width-cornersB[i].x < bnd_limit) prune_flag = 0;
    if(s.height-cornersB[i].y < bnd_limit) prune_flag = 0;


      if(prune_flag){
           pruneA[ii].x = cornersA[i].x;
           pruneA[ii].y = cornersA[i].y;
           pruneB[ii].x = cornersB[i].x;
           pruneB[ii].y = cornersB[i].y;
           pA= cvPoint(cvRound( pruneA[ii].x ),cvRound(
pruneA[ii].y ));
           pB= cvPoint(cvRound( pruneB[ii].x ),cvRound(
pruneB[ii].y ));

           i1 = pA.x-2;
           j1 = pA.y-2;
           i2 = i1+4;
           j2 = j1+4;

      cvRectangle(dst,cvPoint(i1,j1),cvPoint(i2,j2),cvScalar(255,0
,0,0),-1,8,0 );
           cvLine( dst, pA, pB,cvScalar(0,255,0),2 );
           cvCircle(dst,pB,3,cvScalar(0,0,255),2);

      cvRectangle(fptraj,cvPoint(i1,j1),cvPoint(i2,j2),cvScalar(25
5,0,0,0),-1,8,0 );
           cvLine( fptraj, pA, pB,cvScalar(0,255,0),2 );
           cvCircle(fptraj,pB,3,cvScalar(0,0,255),2);
           printf("%d Ax %f  Ay %f  Bx %f  By %f dist
%f\n",ii,pruneA[ii].x,pruneA[ii].y,pruneB[ii].x,pruneB[ii].y,dist
);
ii++;} }
```

```
cvShowImage( "video", dst );
cvShowImage( "traj", fptraj );

cvWaitKey(0);k++;
}
return 1;
}


Matlab file to prune the feature points resulting in feature
point tracks
N = length(fptrack);

% plot feature point trajectories
figure(1);subplot(111);
for i=1:N
    xA = fptrack(i,3);
    yA = fptrack(i,4);
    xB = fptrack(i,5);
    yB = fptrack(i,6);
    line([xA;xB],[yA;yB]);
    hold on;
end
hold off;
xlabel('x (pixels)');
ylabel('y (pixels)');

% plot number of feature points at each segment
% k is the frame index
Nf = max(fptrack(:,1)); % first column is the frame index
Nfp = zeros(Nf,1);

for k=1:Nf
    ii = find(fptrack(:,1) == k);
    Nfp(k) = length(ii);
end
figure(2);stem(Nfp);
xlabel('frame');ylabel('number of feature point pairs');


%calculate the dx,dy cos(da) and sin(da) for each frame increment
P = zeros(Nfp,4);
for k=1:Nf
    ii = find(fptrack(:,1) == k);
    M = length(ii);
    A = zeros(2*M,4);
    B = zeros(2*M,1);
    for j=1:M
        A(2*j-1,1) = fptrack(ii(j),3);
        A(2*j-1,2) = fptrack(ii(j),4);
        A(2*j-1,3) = 1;
        A(2*j,1) = fptrack(ii(j),4);
        A(2*j,2) = -fptrack(ii(j),3);
        A(2*j,4) = 1;
        B(2*j-1)=fptrack(ii(j),5);
```

```
        B(2*j)=fptrack(ii(j),6);
        Nfp(k) = length(ii);
    end
    P(k,:)= (A\B)';
end
figure(3);plot(P);
legend('cos(da)','sin(da)','dx','dy');
xlabel('frame');
ylabel('parameter');



%calculate the trajectory
Tr = zeros(Nfp+1,2);
C = 1;
S = 0;
for k=1:Nf
    C = C*P(k,1)-S*P(k,2);
    S = S*P(k,1)+C*P(k,2);
    Tr(k+1,1) = Tr(k,1) + C*P(k,3)+S*P(k,4);
    Tr(k+1,2) = Tr(k,2) - S*P(k,3)+C*P(k,4);
    ang(k) = (180/pi)*atan2(S,C);
end
figure(4);
plot(Tr(:,1),Tr(:,2));
xlabel('x (pixels)');
ylabel('y (pixels)');

figure(5);
plot(ang);
xlabel('frame');
ylabel('angle (deg)');
```

g1.m

```
% g1.m
% calculation of the standard deviation of the state variables
b1, b2 and dx
N = 30;
A = zeros(2*N,3);
Nx = 200;
xvec = linspace(0,4,Nx)';
zx = zeros(Nx,3);
vx = zeros(Nx,3);
for k=1:Nx
xo = xvec(k);

for i=1:N
    A(2*i-1,1) = 1;
    A(2*i-1,3) = i*xo/sqrt(1+xo^2);
    A(2*i,2) = 1;
    A(2*i,3) = i*(xo-4)/sqrt(1+(xo-4)^2);
end
AA=A'*A;
z = sort(eig(AA));
```

```
z = z/z(3);
zx(k,:) = z';
vx(k,:) = diag(inv(AA))';

end
figure(1);
semilogy(xvec,zx);grid on;
xlabel('x_o');
ylabel('eigenvalues');
figure(2);
plot(xvec,sqrt(vx));grid on;
xlabel('x_o');
ylabel('normalized std');
legend('b_1','b_2','dx');
%g2.m
t = (0:50000)';
tp = mod(t,10000);
tr = 5;

p = 0.5*(tanh((tp)/tr)' - tanh((tp-100)/tr)');

subplot(411);plot(t/1000,p);grid on;
xlabel('t (usec)');
ylabel('amplitude');

subplot(412);plot(t/1000,p);grid on;
xlabel('t (usec)');
ylabel('amplitude');
axis([9.75,10.5,0,1.25]);

P = abs(fft(p));
P = P/max(P);
f = 1000*(0:(length(t)-1))'/length(t);
subplot(413);plot(f,20 * log10(P));grid on;
xlabel('f (MHz)');
ylabel('(dB)');
axis([0,40,-50,0]);

subplot(414);plot(f,20 * log10(P));grid on;
xlabel('f (MHz)');
ylabel('(dB)');
axis([0,4,-50,0]);
```

This page intentionally left blank.

List of symbols/abbreviations/acronyms/initialisms

Acronyms

AN	Access node (eNodeB)
AWGN	Additive White Gaussian Noise
AOA	Angle of Arrival
CSI	Channel state information
CV	Computer Vision
DAOA	Differential Angle of Arrival
FP	Feature point
FPT	Feature point track
LOS	line of sight
LTE	long term integration
LTESA	Long term integration synthetic array
MIMO	Multiple input multiple output
MS	Mobile station (also UE)
NLOS	non line of sight
OFDM	Orthogonal frequency division multiplexing
PAPR	Peak to average power ratio
PF	Particle filter
PI	Principle investigator
PSS	Primary sync series
RB	Resource block
RFP	Request for proposal
RN	reference node (also called anchor point in the literature)
RS	Reference signal
RSS	Receiver signal strength

RTT	Round trip time
SA	synthetic array
SGL	Self Geo-Location
SVD	Singular Value Decomposition
SSS	Secondary sync series
TDOA	Time difference of arrival
TOA	Time of arrival
TOF	Time of flight
UE	User equipment (also MS)
3G, 4G	Third and fourth generation – referring to wireless communications standards

Variables used

variable	**description**
$bel(x_{0:t})$	Posterior pdf of the particles over the complete time interval from 0 to tT_s
$N(x,\mu,\sigma^2)$	Normal pdf of a random variable x with a mean of μ and a variance of σ^2
$p(\ )$	General pdf form
$\pi(x)$	Uniform pdf from -1/2 to ½
T_s	Sampling time interval
$u_{1:t}$	Deterministic updates of the particle base on known dynamics
$x_t^{[m]}$	Particle from the PF formulation where t denotes the time index and m denotes the particle index. Specification of a particular state variable

	associated with the particle is indicated as $x_t^{[m]}.x$ for the "x" spatial displacement.
$z_{1:t}$	Vector of measurements available for the first to tth time interval.

DOCUMENT CONTROL DATA

(Security classification of title, body of abstract and indexing annotation must be entered when the overall document is classified)

1. ORIGINATOR (The name and address of the organization preparing the document. Organizations for whom the document was prepared, e.g. Centre sponsoring a contractor's report, or tasking agency, are entered in section 8.)

John Nielsen
Department of Electrical Engineering
The University of Calgary
2500 University Dr., NW
Calgary, AB T2N1N4

2. SECURITY CLASSIFICATION (Overall security classification of the document including special warning terms if applicable.)

UNCLASSIFIED
(NON-CONTROLLED GOODS)
DMC A
REVIEW: GCEC JUNE 2010

3. TITLE (The complete document title as indicated on the title page. Its classification should be indicated by the appropriate abbreviation (S, C or U) in parentheses after the title.)

LTE Handheld Synthetic Array: Interim Report I

4. AUTHORS (last name, followed by initials – ranks, titles, etc. not to be used)

Neilsen, J

5. DATE OF PUBLICATION (Month and year of publication of document.)	6a. NO. OF PAGES (Total containing information, including Annexes, Appendices, etc.)	6b. NO. OF REFS (Total cited in document.)
December 2012	134	12

7. DESCRIPTIVE NOTES (The category of the document, e.g. technical report, technical note or memorandum. If appropriate, enter the type of report, e.g. interim, progress, summary, annual or final. Give the inclusive dates when a specific reporting period is covered.)

Contract Report

8. SPONSORING ACTIVITY (The name of the department project office or laboratory sponsoring the research and development – include address.)

Defence R&D Canada – Ottawa
3701 Carling Avenue
Ottawa, Ontario K1A 0Z4

9a. PROJECT OR GRANT NO. (If appropriate, the applicable research and development project or grant number under which the document was written. Please specify whether project or grant.)	9b. CONTRACT NO. (If appropriate, the applicable number under which the document was written.)
15DR	W7714-115195

10a. ORIGINATOR'S DOCUMENT NUMBER (The official document number by which the document is identified by the originating activity. This number must be unique to this document.)	10b. OTHER DOCUMENT NO(s). (Any other numbers which may be assigned this document either by the originator or by the sponsor.)
	DRDC Ottawa CR 2012-141

11. DOCUMENT AVAILABILITY (Any limitations on further dissemination of the document, other than those imposed by security classification.)

Unlimited

12. DOCUMENT ANNOUNCEMENT (Any limitation to the bibliographic announcement of this document. This will normally correspond to the Document Availability (11). However, where further distribution (beyond the audience specified in (11) is possible, a wider announcement audience may be selected.))

Unlimited

13. ABSTRACT (A brief and factual summary of the document. It may also appear elsewhere in the body of the document itself. It is highly desirable that the abstract of classified documents be unclassified. Each paragraph of the abstract shall begin with an indication of the security classification of the information in the paragraph (unless the document itself is unclassified) represented as (S), (C), (R), or (U). It is not necessary to include here abstracts in both official languages unless the text is bilingual.)

In the LTE, a 4th-generation cellular communications standard, downlink synchronization signalling is provided via its access nodes (ANs). This downlink signalling could provide the opportunity for the user equipment (UE) to self geo-locate with no assistance from network location processing or GPS. The proposed self geo-location approach is based on the particle filter; a general method Bayesian filtering used when the statistics of the movement model and observations are non-Gaussian. The novel aspect of the work is the creation of a synthetic array as the handset is moved, and the objective of the research is to combine the LTE downlink processing with the synthetic array processing in order to extract measurements which enhance the self-geolocation result. The performance enhancement that is afforded by the synthetic array processing relative to traditional geo-location methodology will be quantified.

Dans le domaine de la technologie d'évolution à long terme (Long Term Evolution — LTE), soit une norme de communication cellulaire de 4e génération, la signalisation de synchronisation descendante est assurée par les nœuds d'accès. La signalisation descendante pourrait permettre l'autogéolocalisation d'un équipement utilisateur, sans l'appui d'un traitement de positionnement de réseau ou d'un système de positionnement à couverture mondiale (Global Positioning System — GPS). Dans le présent rapport, on propose une approche d'autogéolocalisation qui repose sur un filtre à particules et qui constitue une méthode de filtrage générale bayésienne utilisée lorsque les statistiques d'un modèle de déplacement et d'observations ne sont pas de type gaussien. Les travaux ont revêtis un nouvel aspect, à savoir une antenne dont le réseau synthétique se développe à mesure qu'un dispositif est déplacé, et visaient à combiner le traitement descendant de la LTE et celui de l'antenne réseau synthétique, afin d'extraire des mesures qui permettraient d'améliorer l'autogéolocalisation. Dans le présent rapport, on quantifie l'amélioration du rendement obtenue par un traitement d'antenne réseau synthétique par rapport à celle obtenue par géolocalisation classique.

14. KEYWORDS, DESCRIPTORS or IDENTIFIERS (Technically meaningful terms or short phrases that characterize a document and could be helpful in cataloguing the document. They should be selected so that no security classification is required. Identifiers, such as equipment model designation, trade name, military project code name, geographic location may also be included. If possible keywords should be selected from a published thesaurus, e.g. Thesaurus of Engineering and Scientific Terms (TEST) and that thesaurus identified. If it is not possible to select indexing terms which are Unclassified, the classification of each should be indicated as with the title.)

geo-location; self positioning; cellular networks

Defence R&D Canada

Canada's leader in Defence
and National Security
Science and Technology

R & D pour la défense Canada

Chef de file au Canada en matière
de science et de technologie pour
la défense et la sécurité nationale

www.drdc-rddc.gc.ca